ABSTRACT

Title of Document: CO-SOLVENT ASSISTED SPRAY PYROLYSIS FOR THE PREPARATION OF METAL MICROPARTILCE.

Kai Zhong, Doctor of Philosophy, 2012

Directed By: Professor Sheryl H. Ehrman,

Department of Chemical and Biomolecular Engineering

Metal and bimetallic particles play an important role in catalytic, medical and electronic applications. Various techniques have been developed for the preparation of metal particles, including vaporization techniques, sonochemical, polyol method, mechanical alloying and spray pyrolysis. Compared with the other preparation techniques, the spray pyrolysis process has the advantages of easy scale up in industry, tunable particle size and controllable particle composition. Sometimes hydrogen was used in the process to promote the formation of metallic phase in a lower temperature, but it also created a potential safety problem. In order to eliminate the use of hydrogen, a cosolvent assisted ultrasonic spray pyrolysis process was developed, and ethanol (ET) and ethylene glycol

(EG) are used as the cosolvent. In this study, the cosolvent assisted ultrasonic spray pyrolysis process was used for the generation of various oxide free oxide particles, and the reaction mechanism was shown.

In the first part of this study, properties of ultrasonic droplet generator were investigated. Precursor solutions were atomized by a 1.7 MHz ultrasonic nebulizer. The droplet size distribution and atomization rate were measured. Relationship between droplet diameters and the physical properties were revealed by statistic tools. Bimodal droplets distribution was observed during the experiment.

Then copper particles were generated by the spray pyrolysis process. Copper nitrate aqueous solution was used as the precursor and either ET or EG was used as cosolvent. Oxide free particles were generated at temperature from 400 $^{\circ}$C to 1000 $^{\circ}$C. It was noticed that particles morphology and formation process was strong affected by the properties of the cosolvents.

In the following study, the spray pyrolysis process was successfully used for the generation of AgNi, CuNi and AgCu bi-components particles. Various particle structures were observed, and the structures were mainly determined by the thermodynamic properties of the particles components.

In the last part of this dissertation, efforts mainly focused on the mechanism of AgCu particle generation. Reaction intermediates were collected. Reaction process from nitrates to pure metal and the phase separation behavior between Cu and Ag was demonstrated.

CO-SOLVENT ASSISTED SPRAY PYROLYSIS FOR THE PREPARATION OF
METAL MICROPARTILCE

By

Kai Zhong

Dissertation submitted to the Faculty of the Graduate School of the
University of Maryland, College Park in partial fulfillment
of the requirements for the degree of
Doctor of Philosophy
2012

Advisory Committee:

Professor Sheryl Ehrman, Committee Chair

Professor André W. Marshall

Professor Chunsheng Wang

Dr. Howard D Glicksman

Professor Michael Zachariah

Professor Raymond A. Adomaitis

Acknowledgement

Table of Contents

List of Tables

List of Figures

Chapter 1: Introduction and Overview

This dissertation is focused on the preparation of single component and bi-component micron sized metal particles by cosolvent assisted ultrasonic spray pyrolysis process. In this chapter, overall problems and research approaches are outlined.

1.1 PROBLEM DESCRIPTION AND MOTIVATION

Metal and bimetallic particles are of remarkable importance in catalytic, medical and electronic applications (Sheppard 1993; Lewis 1993; Link and EI-Sayed 1999; Watari et al. 2004; Wu et al. 2007; Liu, Li and Zeng 2010; Kim, Stach and Handwerker 2010; Yim et al. 2010). Ag, Ni Fe and Pt powders have been widely used as catalysts for oil refinement, ammonia synthesis and hydrogenation/dehydrogenation of organic compounds. Typically a large surface area and small crystal size is desired to obtain a better catalytic activity (Sheppard 1993; Lewis 1993). Metal particles have vast potential for application in many areas of biomedicine from diagnostics to treatment of diseases (Link and EI-Sayed 1999; Sonvico et al. 2005). Applications of metal powders for electronics have been largely expanded in recent years. Ag, Cu and Ni particles have been used as ingredients of thick film conductive pastes, in hybrid integrated circuitry and as electromagnetic shielding enclosure materials (Kim et al. 2003; Wu et al. 2007; Yim et al. 2010).

The spray pyrolysis process is an effective way to produce metal particles with the advantages of easy scale up in industry, tunable particle size and controllable composition, compared with other particle generation techniques, such as sonochemical, polyol method, vaporization techniques and mechanical alloying. Bench scale spray

pyrolysis systems are typically based off of a single ultrasonic atomizer, used to generate precursor droplets with diameters around 5 microns. However in industrial applications, the scaling up may involve more than a hundred ultrasonic transducers combined together in a matrix to allow the atomization of solutions on a larger scale. Particle size and composition is controlled by the composition of the precursor solution. Various metal oxides have been synthesized from metal nitrates, chlorides and acetates. Sometimes an addition of 10 vol% hydrogen was used to promote the formation of oxide free particles (Gurav et al. 1993), but hydrogen is a potential safety problem because of its lower explosive concentration limit, which is defined as the smallest concentration in the air that leads to explosion after ignition. In recent years, a cosolvent spray pyrolysis method was proposed to improve the safety of pyrolysis processes. In the new method, hydrogen is replaced by a cosolvent, such as ethanol or ethylene glycol. The cosolvent is added into the precursor solution and decomposes to hydrogen and carbon monoxide with concentrations much lower than the explosion limit in a high temperature. Cosolvent spray pyrolysis has been reported for the generation of copper particles with a cosolvent of ethanol. However, the flash point of ET is 14 ^{o}C, which makes ET a National Fire Protection Association (NFPA) class 3 flammable material. For industrial applications, ethylene glycol (EG), a NFPA class 1 flammable material with a flash point of 111 ^{o}C, is potentially a better choice for the cosolvent.

In order to make particles with desired composition and morphology, experimental conditions, such as cosolvent, cosolvent volume ratio, precursor concentration, furnaces temperature and the carrier gas flow rate should be carefully selected. Reaction process from nitrate precursor to metal particles should be investigated.

2

1.2 RESEARCH APROACHES AND OBJECTIVES

In this dissertation, work will focus on the investigation of ultrasonic atomizer properties, single component metal particle generation, two component metal particle preparation and the particles formation mechanisms.

1.2.1. Properties of the ultrasonic atomizer

The precursor solution will be atomized to droplets by a 1.7 MHz ultrasonic generator. Product particles size was dominated by the droplet size and salt concentration. A narrow size distribution of droplets, which leads to a narrow size distribution of particles, is preferred for industry applications. High atomization efficiency of the generator is also required, because it determines particles yield rate. In the Chapter 3, copper nitrate/water/ethanol and copper nitrate/water/ethylene glycol precursor solutions were atomized by a 1.7 MHz ultrasonic nebulizer. The droplet size distribution was measured using Malvern light scattering system, and atomization rate were measured by the change of the mass change. Relationship between solution properties and droplet size/atomization rate are revealed.

1.2.2. Single component metal particle generation

Cosovlent spray pray pyrolysis process is designed for the generation of oxide free metal particles. Hydrogen is replaced by cosolvent, so the safety of the system is improved. In Chapter 4, I showed the properties of copper particles generated by this technology. Different cosolvents were used. Effects of experimental conditions on the particles morphology were systematically investigated. XRD and SEM were used for the

characterization of the particles. Effect of experiment conditions on particles density and morphology were investigated.

1.2.3. Two component metal particle preparation

Cosolvent spray pyrolysis process is also a potential patchy particle generation method. In Chapter 5, AgNi, CuNi and AgCu bimetallic particles were generated by this process in the lab. Various patchy structures of the AgNi and AgCu particles were shown, and their formation mechanisms were discussed.

1.2.4. Particle formation mechanism investigation

Understanding the particles formation mechanism will be very helpful for the generation of particles with desired composition and morphology. Spray pyrolysis is a single step process. All the reactions happened in the hot furnaces, so it is hard to investigate the reaction process directly. Short residence time experiment method is developed to solve this problem. In the experiment, residence times were reduced from several seconds to hundreds millisecond by reducing hot zone length and increasing carrier gas flow rate, therefore, transitional reaction product could be collected. In chapter 6, AgCu particles formation process was investigated by short residence time experiments. Effects of different cosolvent and the phase separation behavior between Ag and Cu were discussed.

Chapter 2: Background Information

A review of various particles generation method with their advantages and disadvantages were described in this chapter. Details of particle prepared by spray pyrolysis were also discussed.

2.1 METAL PARTICLE PREPARATION METHOD

Various methods have been developed for the generation of metal particles with diameters ranging from several nanometers to several microns. For example, controlled chemical reduction (K. L. Tsai and Dye 1991; Hirai, Nakao, and Toshima 1978; Kalidindi, Sanyal and Jagirdar 2011), sonochemical method (Okitsu, Mizukoshi, et al. 1996; Okitsu, Bandow, et al. 1996; Nagata et al. 1996), radiation-chemical reduction (Kraeutler and Bard 1978; Koudelka, Sanchez, and Augustynski 1982; Yonezava et al. 1991; Torigoe and Esumi 1993; Yingjie et al. 1995), polyol method (Silvert et al. 1996; Kurihara, Chow, and Schoen 1995; Fievet et al. 1993; Gaceur et al. 2012), vaporization techniques (Cardenas-Trivino, Klabunde and Dale 1987; Satoh and Kimura 1989), mechanical alloying (Benjamin 1970; Koch et al. 1983; Aymard et al. 1996; Pabi and Murty 1996a, 1996b; Pabi, Joardar, and Murty 1996; Murty and Ranganathan 1998; Murty 1993) and spray pyrolysis (A. Gurav et al. 1993a; Nagashima, Morimitsu, and Kato 1987; Stopic, Ilic and Uskokovic 1996a; Pluym et al. 1993; Okuyama and Wuled Lenggoro 2003; Jian et al. 2007; Choa et al. 2003; Ahn, Hyun and Kim 2012; Rudin, Wegner and Pratsinis 2011).

The controlled chemical reduction method developed by Tsai (Tsai and Dye 1991) was based on the homogenous reduction dissolved alkalides or electrides in an aprotic solvent

such as dimethyl ether or tetrahydrofuran. Single component chloride salts of Ni. Fe, Zn, Ga, Si, Mo, W, In, Sn, and Sb were used as precursors. Metal and metal oxide particles were prepared depending on the materials. When the mixed salt solutions were used as precursors, preparation of Au-Zn, Au-Cu, Cu-Te, and Zn-Te binary alloys or compounds was allowed.

The sonochemical method use ultrasonic irradiation to activate the reduction reaction of the metal ion in aqueous solution. Okitsu reported the preparation of Ag, Pd, Au, Pt and Rh particles with small diameters around several nanometers (Okitsu, Mizukoshi, et al. 1996). Additionally when certain organic additives such as surfactants, water-soluble polymers and aliphatic alcohols were added, it was discovered the reaction was effectively accelerated. The particle sizes were mainly determined by the initial concentration and protective agent as illustrated below (Okitsu, Bandow, et al. 1996).

The radiation-chemical reduction employed electromagnetic radiation to enhance the reduction reaction in metallic salt solution. 253.7 nm UV light was used in the preparation of colloidal silver solution by Yonezawa (Yonezawa et al. 1991). A sharp and intense absorption band of colloidal silver was observed after a period of reaction time depending on different precursor solution. Two years later, bimetallic silver-palladium colloids with average particle diameters ranging from 3 to 11 nm in the poly(vinylpyrrolidone) were prepared with the radiation of UV (Torigoe and Esumi 1993). UV light has been used for the preparation of nano Ag, Au and Pt particles (Esumi et al. 1998), but stronger radiation was required if the radiation-chemical reduction method was applied to Cu particle preparation. In 1995, Ag-Cu alloy particles with

diameters of 25 nm were synthesized from the solution containing $Ag(NH_3)_2^+$ and $Cu(NH_3)_4^{2-}$ complex ions by γ radiation (Yingjie et al. 1995).

The polyol method for metal particles preparation was first reported by Fievet in 1989 (Fievet et al. 1989). A metallic salt or oxide was dissolved in ethylene glycol, and then heated to 120 °C-200 °C for several hours, leading to formation of metal particles. Particles with different composition, including Fe, Co, Ni, Cu, Ru, Rh, Pd, Ag, Sn, Re, W, Pt, Fe-Cu, Co-Ni and Ni-Cu, were synthesized by other research groups (Silvert et al. 1996; Kurihara et al. 1995; Fievet et al. 1993, 1989), and particles size ranged from several nanometers to several microns. In order to generate nano size particles, the addition of polymer was used to avoid the sintering of the primary particles.

The vaporization method, also named as the gas flow cold trap method was first proposed by Keisaku Kimura (Kimura and Bandow 1983) for the preparation of colloidal metal particles, and was illustrated in Figure 2.1. Pure metals were heated up and evaporated. The vapor was then sent into cold vacuum chamber and condensed to form particles with diameters from 10 nm to 50 nm. Replacing the chamber with a cold solvent, Kimura prepared colloid solutions with different kinds of metal particles including Ag, Au, Cu, In, Al, Ca, Sn and Pb. Stability of the colloid was determined by the particles material. Naoki Satoh's experiment showed that the stability could be improved by the addition of certain surfactant[22], such as dimethyl dioctadecyl ammonium chloride (DOAC).
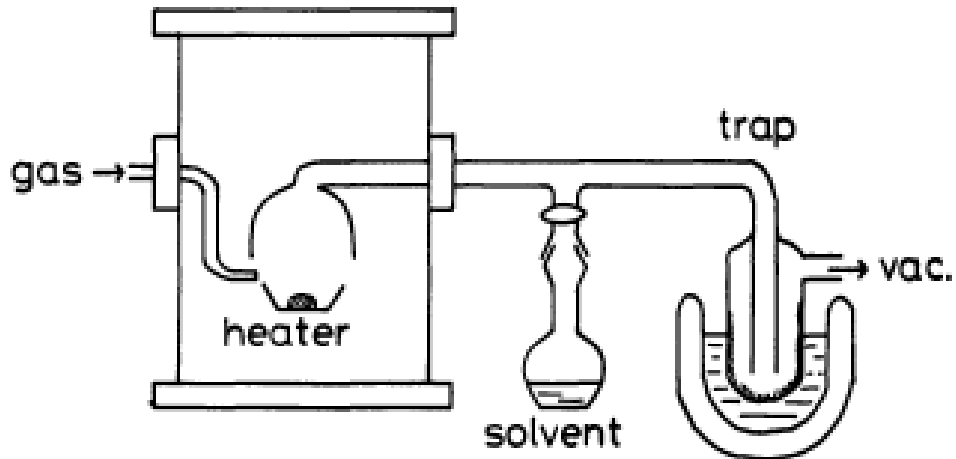
Gas flow - Cold trap

Figure 2.1. The apparatus for the gas flow cold trap method adapted from literature (Kimura and Bandow 1983).

Mechanical alloying (MA) was proposed by Benjamin and his co-workers (Benjamin 1970) aiming at coating the oxide particles with Ni, and this technology was greatly developed in the following twenty years. Ni-, Fe- and Al-based alloys were synthesized around 1980 by MA. In 1983, Koch reported the formation of amorphous phase in the Ni-Nb alloy synthesized by MA (Koch et al. 1983). After that MA was widely researched and applied to various alloys. All these works were summarized by Murty in 1998 (Murty and Ranganathan 1998). Most recent work about morphology Sn-Ag-Cu particles synthesis was reported by Kao (Kao and Duh 2004). The particle size of the SnAgCu solder decreased from 1 mm down to 10-100 μm by doping the Cu_6Sn_5 nanoparticle during the AM process.

The spray pyrolysis method has been widely researched for more than thirty years (Gurav et al. 1993; Messing, Zhang and Jayanthi 1993). The process is composed of different stages, including solution spraying, drying process and the reaction in tube furnace or

8

flame. Metal particles of Ag and Pt could be directly synthesized from metal nitrate aqueous solution, but other material, such as Cu and Ni, are easier to form oxide, and were usually generated by the assistant of hydrogen (Gurav et al. 1993). The morphology of the particles was determined by the residence time and the properties of the precursor solution (Jain, Skamser and Kodas 1997). Particle size is tunable according to the different types of droplet generators and the concentration of the precursor solution. Take copper particle generation as an example, ultrasonic atomization generates droplets with diameters around 5 μm, and if the concentration of copper nitrate in the precursor solution is 1 M, the dense copper particle diameter should be around 1 um.

Some properties of reported preparation method are summarized in Table 2.1. From the table it is interesting to observe that in most of the techniques, particles were generated during the liquid to solid transition, such as the controlled chemical reduction method, sonochemical method and radiation-chemical reduction methods. The gas to solid reaction is used in the vaporization method and limited to single component metal particle preparation. Because the different vapor pressure of materials, generation of multicomponent metal particles by the vaporization method will lead to a deviation from the desired stoichiometric composition. The MA method produces alloys by a solid to solid transition, but it is nearly impossible to reduce the particles size to below one micron and keep a spherical morphology of the particles.

Compared with the alternatives, spray pyrolysis exhibits the advantages of tunable particle diameter from nanometer to micronmeter and controllable particle composition. Most metal particles can be synthesized with only simple equipment required, which means easy to scale up in industry. Kim improved the safety of the spray pyrolysis

technique by replacing hydrogen with a co-solvent, such as ethanol, and this improvement indicates a promising future of the spray pyrolysis technique (Kim et al. 2003). More details of spray pyrolysis technique will be reviewed in the following paragraphs.

Table 2.1. Summary of metal particles preparation methods

Method	Phase change	Reduction	Reported composition	Reported particles size	Source
Controlled chemical reduction method	Liquid to solid	Alkalides, electrides	Ni. Fe, Zn, Ga, Si, Mo, W, In, Sn, Au-Zn, Au-Cu, Cu-Te, and Zn-Te	3nm – 15 nm	(Hirai et al. 1978; K. L. Tsai and Dye 1991)
Sonochemical method	Liquid to solid	Ultrasonic	Ag, Pd, Au, Pt and Rh	5nm – 110 nm	(Okitsu, Mizukoshi, et al. 1996; Okitsu, Bandow, et al. 1996; Nagata et al. 1996)
Radiation-chemical reduction	Liquid to solid	UV light, γ radiation	Ag, Au, Pt and Ag-Cu	25nm	(Kraeutler and Bard 1978; Torigoe and Esumi 1993; Yingjie et al. 1995)
Polyol method	Liquid to solid	Glycol	Fe, Co, Ni, Cu, Ru, Rh, Pd, Ag, Sn, Re, W, Pt, Fe-Cu, Co-Ni and Ni-Cu	7nm – 14nm 0.5 μm – 4 μm	(Silvert et al. 1996; Kurihara et al. 1995; Fievet et al. 1993)
Vaporization techniques	Gas to solid	--------	Ag, Au, Cu, In, Al, Ca, Sn and Pb	10 nm- 50 nm	(Cardenas-Trivino et al. 1987; Kimura and Bandow

					1983)
Mechanical alloying	Solid to solid	--------	Most of the alloys were included	Above 1micronmeter,usually 10-100 μm	(Benjamin 1970; Pabi and Murty 1996a, 1996b; Murty and Ranganathan 1998; Murty 1993)
Spray pyrolysis	Liquid to solid	Hydrogen	Ag, Ni, Co, Cu, Ag-Ni, Ag-Cu, Co-Ni and CuNi	20 nm – 1 μm	(Gurav et al. 1993a; Nagashima et al. 1987; Okuyama and Lenggoro 2003; Choa et al. 2003; Jian et al. 2007)

2.2 METAL PARTICLE PREPARATION BY SPRAY

2.2.1 Ag and Ag composite particle preparation

Because of special conductivity and magnetic traits of Ag particles, they are widely used in electromagnetic shielding enclosure materials, antibiotic products, conductive inks, paste, and various electronic devices. As early as 1985, Ag powder preparation by spray pyrolysis was reported by Kato (Kato, Takayama, and Morimitsu 1985). Solid Ag particles were formed from $AgNO_3$ and water/ethanol solution, and dense particles were obtained only when the temperature was above the melting point of 961 ^{o}C. Pluym repeated the experiment using $AgNO_3$ aqueous solution as precursor. Dense and pure phase Ag particles were obtained at and above 600 $^{\circ}$C using N2 carrier gas, and at and above 900 ℃ using air as the carrier gas (Pluym et al. 1993). The dense silver particle

11

preparation temperature could be further reduced to 400 ^{o}C based on Kieda's report when AgNO$_3$–NH$_4$HCO$_3$ solution was used as precursor (Kieda and Messing 1998). Kieda also pointed out that the morphology and size of the final particles was not only determined by the condensing process but also related to the drying process. In another work, the morphology was affected by both the decomposition reaction from AgNO$_3$ to Ag and the precipitating of the AgNO$_3$ when solvent was evaporated. Solutions of Ag$_2$CO$_3$, Ag$_2$O, and AgNO$_3$ with NH$_4$HCO$_3$ were used separately in the test with a short residence time of drying process, and then significantly different morphologies were observed in the product Ag particles (Kieda and Messing 1998).

After 1999, more research was focused on the Ag-metal oxide composite particles, such as Ag-ZnO, Ag-TiO$_2$ and Ag-CuO. Oxide composite particles could be obtained by using precursor solutions containing both oxide nanoparticles and nitrate salt. Ag-ZnO particles were designed for electrical contact materials, and prepared by AgNO$_3$ aqueous solution containing nano size ZnO particles (Kang and Park 1999). The product micron particles were composed of several submicron particles and had rough surfaces, which were attributed to the heterogeneous precipitation of silver nitrate salts on the surface of nanometer ZnO particles. Ag-TiO$_2$ was usually used in photocatalysis application and was prepared in similar method by Lee (Lee, Jung, and Park 1999). The crystallite size of Ag was 10–20 nm and the crystallinity of TiO$_2$ was the same as initial oxide particles in the precursor. Ag-TiO$_2$ particle structure was further determined by transmission electron microscopy and three-dimensional electron tomography, and supported the conclusion that the TiO$_2$–Ag nanocomposite particle consisted of well-dispersed Ag and TiO$_2$ nanoparticles.

Researchers also tried another way to achieve composite Ag-metal oxide particles by using mixtures of nitrate in solution, but it made the structure of the particles more unpredictable because of the complicated behavior of co-precipitation and reaction. For example, composite Ag/CuO powders were synthesized from mixtures of soluble precursors of aqueous silver and copper nitrates (Majumdar, Glicksman, and Kodas 2000). The author presented a reaction process and believed that copper nitrate decomposed first, and then $AgNO_3$ melting, and finally the silver filled the voidage of a porous copper oxide shell at $1000^{o}C$. By the same method, Ag/MgO composite powder was fabricated from silver nitrate and magnesium nitrate around $750^{o}C$. Nanosized silver particles were observed in the MgO matrix, and silver nanoparticles were obtained by removing MgO (X. Shi et al. 2008). More complicated Ag-metal oxide particles were reported in recent years, such as Ag-Bi-based superconductor and silver-glass systems, and multicomponent nitrate salts solutions were required (Mancic et al. 2004; Jung, Koo, and Kang 2010; Kim, Park and Kim 2008).

2.2.2 Cu and Cu composite particle preparation

Cu has similar conductivity as Ag but a lower price, and micrometer- or nanometer-size copper particles have various applications such as electrode materials and electromagnetic interference shielding materials. A few papers have been found about the pyrolysis preparation of pure copper from copper nitrate aqueous solution. Unlike $AgNO_3$, which decomposes to pure Ag at temperatures higher than $400\ ^{o}C$, $Cu(NO_3)_2$ has a more complicated decomposition behavior (Nagashima et al. 1990; Majumdar et al. 1996; Firmansyah et al. 2009a).

K Ca Na Mg Al Zn Fe(II) Sn Pb (H) Cu(II) Hg Ag Pt Ag

Decreasing metal activity

Figure 2.2. Activity of different metal materials, decreasing from left to right.

Field analyzed the physical and chemical properties of most metal nitrates, and found the thermal decomposition reaction has different product based on different materials (Field and Hardy 1964). It is believed that the decomposition reaction is composed of several steps, beginning with the loss of oxygen with the formation of metal nitrite. If the metal nitrite is stable at the reaction temperature, decomposition will stop and nitrite will be obtained. For example, decomposition of alkali-metal nitrates at temperature below 750^oC:

$$2MNO_3 = 2MNO_2 + O_2,$$

where M is Li, Na, K, Rb and Cs. If the nitrite is unstable at a given temperature, the nitrite will further decompose to oxide of metal and nitrogen. For $Ba(NO_3)_2$ at $600\ ^oC$:

$$Ba(NO_3)_2 = Ba(NO_2)_2 + O_2$$

$$Ba(NO_2)_2 = BaO + NO + NO_2$$

Most metal nitrates, such as Ca, Ba, Mg, Al, Zn, Fe, Sn, Pb and Cu, will decompose to metal oxide as $Ba(NO_3)_2$ does, but for some metals which have a thermally unstable oxide at a given temperature, pure metal will be produced:

$$AgNO_3 = Ag + NO_2 + 1/2O_2$$
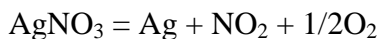
The nitrates of Pt and Au have similar decomposition reactions, with final product of pure Pt and Au. Simple rules can be used for the estimation of the decomposition product based on the metal activity series (Figure 2.2). Metals with high activity prefer to

decompose to nitrite. Upon increasing temperature to higher than 1000, further decomposition will happen. Most metal nitrates will decompose to oxide. For the low activity metals which have an unstable oxide, pure metal will be produced. In Field's report, it was also mentioned that these rules are oversimplified, and other reactions are known to proceed simultaneously for many nitrates (Field and Hardy 1964). Two radically different (crystal shattering and gasification) reaction mechanisms were proposed to explain the change in the thermal decomposition reaction (Jackson, Fonseca, and Holcombe 1995; Lvov and Novichikhin 1995a). The "gasification mechanism" suggests that metal nitrates decompose in a single step to produce $MO(g)$, O_2 and NO_2 in the gas phase, but crystal shattering hypothesis believes the decomposition is governed by the kinetics of the process and happens when the liquid presents on the surface. Detailed research indicated that the decomposition of hydrated copper nitrate is quite complicated with a metastable intermediate of $Cu_2(OH)_3(NO_3)$. Some of the results were summarized in Table 2.2.

Table 2.2. Thermal decomposition of $Cu(NO_3)_2*3H_2O$ adapted from literature (Ryu, Lee and Park 2004).

Temp. (°C)	40-80	80-110	116-152	120-150	167-205	199-217	200-250	247-260	263-310
(Mu and Perlmutter 1981)			Melting to Cu(NO$_3$)$_2$			Cu$_2$(OH)$_3$(NO$_3$)			CuO
(Taylor, Dollimore, and Gamlen 1986)	3Cu(NO$_3$)$_2$ Cu (OH)$_2$					182~312 CuO			
(Lvov and Novichikhin 1995a)						Cu$_2$(OH)$_3$(NO$_3$)		CuO	
(Morozov et al. 2003)	Cu(NO$_3$)$_2$*2.5H$_2$O Cu(NO$_3$)$_2$*H$_2$O	Melting to Cu(NO$_3$)$_2$		Sublimation			CuO		
(Ryu, Lee and Park 2004)		80~150 melting 105 Cu$_2$(OH)$_3$(NO$_3$)			Cu$_2$(OH)$_3$(NO$_3$)	CuO/ Cu$_2$O			

16

In 1990, Nagashima prepared fine, spherical Cu particles from copper nitrate by spray pyrolysis (Nagashima et al. 1990). In 1996, D. Majumdar repeated the experiment (Lvov and Novichikhin 1995). The results showed that in an inert (nitrogen) atmosphere spray pyrolysis of copper nitrate solutions over a range of temperatures (400–1300 ^{o}C) and residence times (3–7 s) produce only copper oxide, however, if 7% hydrogen was added into the carrier gas, copper particles were generated at 500–700 ^{o}C. Another interesting observation is the bimodal size distribution of the particles, prepared at 1200 ^{o}C in nitrogen. Beside the primary copper oxide particles with diameters around 1 micron, many small particles were detected on the surface of the primary particles. These ultrafine particles were attributed to two possible mechanisms. One is the bursting of droplets during the drying process, and the other could be the volatility of copper nitrate trihydrate. Copper nitrate volatilized and then decomposed in the gas phase to generate small oxide particles by homogeneous nucleation. Though hydrogen facilitated the reduction from copper oxide to pure copper, the required concentration of hydrogen, which is usually higher than the explosion limit, brought another safety challenge. Kim proposed a simple idea of generation of H_2 from cosolvent during the pyrolysis process rather than using hydrogen/inert mixture gas. He demonstrates the preparation of copper particles at 450 – 1000 ^{o}C from copper nitrate and copper acetate. 10 percent ethanol was used as cosolvent and added into the aqueous solution before atomization. The author hypothesized " cosolvent decomposition creates a strong reducing atmosphere during spray pyrolysis via in situ production of hydrogen and carbon monoxide" (Kim et al. 2003). Firmansyah's work revealed that the reduction of copper oxide will happen in different ways at different reaction temperatures (Firmansyah et al. 2009a). At a

temperature lower than 525 ^{o}C, Cu$_2$O was oxidized to CuO and then decompose to Cu. At a higher temperature, the Cu was formed directly from Cu$_2$O.

2.2.3 Ni and Ni composite particle preparation

Ni is another metal which is of wide interest because of its application as electrode and catalyst materials. Nagashima and Takashima reported the preparation of Ni particles from nickel nitrate aqueous solution by spray pyrolysis process in N$_2$/H$_2$ mixture atmosphere separately (Nagashima, Wada and Kato 1990; Che et al. 1999). According to their report, Ni(NO$_3$)$_2$ decomposed to hollow NiO particles in drying droplets, and then was reduced to Ni at temperatures above 300 ^{o}C. Pure nickel particles were obtained at 600 ^{o}C , but densification of the hollow nickel particles required a relatively long residence time and a temperature higher than 1000°C because of the high melting point of Ni, which is about 1453 ^{o}C. Without hydrogen, only hollow NiO particles were generated even after increasing the temperature to 1200 ^{o}C. In the following ten years, adjustment of precursor solution and change of furnace temperature were suggested to improve the morphology of the Ni particles (Stopic et al. 1999; Kang, S. G. Kim, and H. S. Kim 2004; K. N. Kim and S. G. Kim 2004). Stopic and his co-workers reported the preparation of Ni particles from NiCl$_2$ aqueous solution using N$_2$/H$_2$ mixture atmosphere at 900 ^{o}C. 0.1 mass% of Pd, Cu, or Ni was added into precursor solution to promote the completed reduction of nitrate and improve the morphology of the particles. TGA and DTA data indicated that the reduction temperature was reduced because of the additives, which also affected the surface roughness of the particles. A co solvent spray pyrolysis technique was used for the Ni preparation in 2003, and submicron Ni particles were prepared with co-solvent of 10vol% ethanol. Ni aqueous solution containing ammonia was reported to

be another kind of precursor used for the generation of Ni in an inert atmosphere (Xia, Lenggoro and Okuyama 2000; Park et al. 2003; Forsman et al. 2008). Ammonia was supplied by additives of chemical reagents, such as ammonium bicarbonate, ethylenediaminetetraacetic acid (EDTA) and urea. Ammonia was found to be an effective reduction reagent for the NiO to Ni transition, and Ni particles were obtained in the absence of H_2 when additives were used. The size distribution and morphology were also significantly affected by the additives of EDTA and urea. Additives accelerated the densification of the particles and led to a smoother surface. Ultrafine particles with diameters smaller than 100 nm were also detected when micron Ni particles were prepared (Jung et al. 2007). Jung believed that $Ni(NO_3)_2$ evaporated at the entrance of the reactor because of the high temperature of the furnace, and the vapor of $Ni(NO_3)_2$ was turned to NiO and Ni in gas phase. Finally the ultrafine Ni particles were formed from the nucleation of Ni vapor. In order to eliminate the ultrafine particles, a temperature gradient from low to high was used to promote the completely transition from nitrate to oxide before the evaporation of nitrate. Another effective ways to suppress the evaporation of the nickel nitrate were to slow down the carrier gas and additives of copper. Reducing the carrier flow rate from 100 L/min to 50 L/min allowed a longer time for the nitrate to oxide decomposition, and copper acetate would precipitated out as a solid shell which stopped the evaporation of copper nitrate.

2.2.4 Alloy particle

Different kinds of alloy particles have been prepared by spray pyrolysis process since 1995 with the advantage of controllable size and composition. Diameters of alloy particles changed from hundred nanometers to several microns depending on the

concentration of solution, and sometimes were affected by the given temperature and residence time. Metal salt solutions, including metal nitrate, metal chloride and metal acetate, were used as precursor solutions, and the ratio of each component within the particles could be adjusted by changing the concentration of each metal salt in solution. Varying amounts of hydrogen were used in some cases to promote the reduction of metal oxide. Details of various alloy particle generation by spray pyrolysis are shown in Table 2.3.

Table 2.3. Preparation of alloy particles by spray pyrolysis.

author	alloy	precursor	carrier gas	reaction temperature (^{o}C)	particles morphology
(Eroglu, Zhang, and Messing 1996)	70wt.% Ni-30 wt.% Fe	1 g $(C_2H_5)_2Ni$ and 0.5g $(C_2N_5)_2Fe$ dissolved in 0.125L 2-methoxyethanol	N_2	750 - 950	single phase, nanocrystalline, bimodal size distribution, spherical particles composed of 70 to 80 nm and smaller than 10 nm particle
(Gurmen et al. 2009)	$Ni_{0.5}Fe_{0.5}$	$FeCl_2/NiCl_2$ aqueous solution with total concentrations between 0.05 and 0.4 M	H_2	900	single phase, nanocrystalline particles with diameters changed from 80 nm to 500 nm
(Pluym et al. 1995; Aoyagi et al. 2003)	$Ag_{0.7}Pb_{0.3}$	$AgNO_3$ and $Pb(NO_3)_2$ aqueous solution	N_2	700 and above	single phase, nanocrystalline and sub micron particles

(Aoyagi et al. 2003)	$Cu_{0.7}Ni_{0.3}$	0.07M $Cu(NO_3)_2$ and 0.03M $Ni(NO_3)_2$ aqueous solution	$Ar/4\%H_2$	800	single phase, nanocrystalline and diameters of 1.5 micron
(Yang, Kim, and Kim 2008)	$Ag_0.5Ni_{0.5}$	0.25M $AgNO_3$ and 0.25M $Ni(NO_3)_2$ aqueous solution	$N_2/10\%H_2$	1000	separated Ag and Ni phase, nanostalline and diameters of 0.8 micron
(Jang, Ju and Kang 2009)	$Co_{0.5}Ni_{0.5}$	$Co(NO_3)_2/Ni(NO_3)_2$ aqueous solution with toatle concentration of 0.5M	$N_2/10\%H_2$	1000-1400	single phase, hollow particles with diameters of 0.8 micrion at 1200 ^{o}C, dense particles with diameter of 0.69 micron at 1400 ^{o}C

2.3 Morphology and structure control during the pyrolysis process

Size distribution and morphology of the metal particles were required to be controlled for the final application in the industry. As an example, for Ag in the production of microcircuit materials, oxide free and dense Ag particles with narrow distributed diameters around one micron are required for the formation of highly conductive lines. However in the spray pyrolysis reaction, hollow particles with bimodal size distribution were reported everywhere (Jain et al. 1997a; Majumdar et al. 1996; Stopic et al. 1999; Park et al. 2003; Kang et al. 2004).

Hollow particles were formed due to the concentration and temperature gradient in the droplet during solvent evaporation. If characteristic time of evaporation τ_e is larger than τ_d which represent the diffusion time of metal salt in the droplets, a salt shell will be formed on the surface of the droplet. Conversely, a solid salt particle is more likely to be observed. Then at a higher temperature, during the decomposition of metal salt, for example copper nitrate to copper oxide, solid particles may have another chance to become hollow because of the lower density of oxide. After reduction in a hydrogen atmosphere, hollow metal particles are generated from hollow oxide particles. Theoretically speaking, hollow particles could be eliminated when given temperature higher than their melting point and enough residence time.

Bimodal size distributions were usually reported because of the observation of ultrafine particles with diameter ranging from tens of nanometers to submicron in size. Droplet bursting and chemical vapor deposition (CVD) was proposed to explain the formation of ultrafine particles. In an ideal situation, one primary particle comes from one droplet, but sometimes because of rapid evaporation of solvent, droplets burst into small pieces,

22

which changed to ultrafine particles post reactions. Small oxide pieces and metal pieces were also probably formed after nitrate to oxide and oxide to metal reaction. CVD was used to explain the formation of CuO, Ni and Sn ultrafine particles based on the high vapor pressure of $Cu(NO_3)_2$, $Ni(NO_3)_2$ and $SnCl_2$ (Majumdar et al. 1996; Jung et al. 2007; Ju et al. 2009). The metal salt evaporated at the beginning of heating process, decomposed to oxide at a higher temperature and then condensed to nanoparticles by homogenous nucleation as illustrated in Figure 2.3.

Crystallite size is another important characteristic of metal particles, and affects the catalyst activity and magnetic properties of materials. The evolution of interparticle crystal structure was summarized for oxide particles by Gurav (Gurav et al. 1993a). For single component oxide particles formation, salt precipitates after the evaporation of solvent, and then amorphous oxide is formed from the decomposition of the metal salt. Particles with nanophase structure are observed with increasing temperature and residence time. Further densification and grain growth lead to the polycrystalline structure of the particles. A similar evolution process was observed in single component metal particles generation, but one more step, the reduction from oxide to metal needs to be considered. Crystallize processes during the formation of alloy particles, such as AgCu particles, are more complicated than the single component particle, and more details will be discussed on this in this thesis.
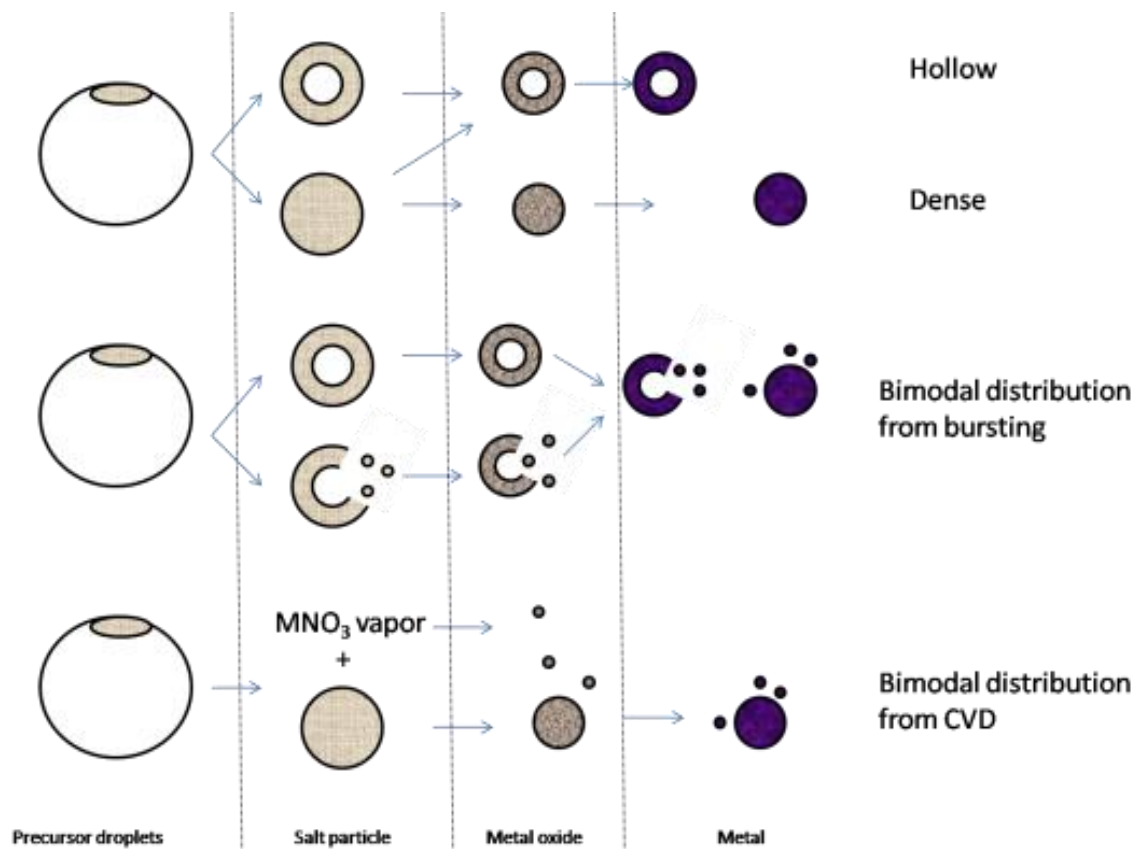
Figure 2.3. Formation of metal particles with hollow and bimodal size distribution.

Chapter 3: Atomization Behavior of Copper Nitrate Solution in 1.7 MHz Ultrasonic Nebulizer

3.1. ABSTRACT

Ultrasonic nebulizers are commonly used as the droplet source for particle generation by spray pyrolysis. Product particle diameters are greatly affected by both the precursor concentration and droplet diameter in addition to pyrolysis operating conditions. In this report, copper nitrate/water/ethanol and copper nitrate/water/ethylene glycol precursor solutions were atomized by a 1.7 MHz ultrasonic nebulizer. The droplet size distribution and atomization rate were measured. The effects of nitrate concentration, cosolvent volume ratio and carrier gas flow rate on the droplet diameter and atomization rate were investigated. Results indicated that increasing either the concentration or the cosolvent volume ratio increased the viscosity and the droplet diameter, and at the same time decreased the atomization rate. Increasing the carrier gas flow rate increased the atomization rate, and had a limited effect on the droplet diameter. Droplets with D50 around 5 μm were observed with a solution viscosity lower than 3 mm^2/s, and a linear behavior of log(D) vs. log(Ω) indicated the generation of droplets from the regular surface fluctuations. As the viscosity became larger than 3 mm^2/s, a bimodal droplet size distribution was observed with the first peak around 5 μm and the second one around 70 μm. Formation of large droplets with diameters of around 70 μm was detected from breakup of the filaments by the shadowgraphy experiment.

3.2. INTRODUCTION

Ultrasonic atomization is an effective method to produce droplets(Lierke 1998) for applications including drug delivery, analytical chemistry, industrial cleaning and precursor droplet generation in the pyrolysis process. (Usmani 2005; LaVan, McGuire and Langer 2003; Suh and Suslick 2005; Taniguchi 2005; Capote and Castro 2006; Laurell, Petersson and Nilsson 2007; Gurav et al. 1993a; Biskos et al. 2008) When used as the droplet source for spray pyrolysis particle generation, ultrasonic atomization is advantageous in the generation of droplets with a relatively narrow size distribution and also is relatively straightforward to scale up compared with other atomization methods, such as the two-fluid nozzle method. Because spray pyrolysis is a one droplet - one particle process, narrow size distribution of droplets leads to a narrow size distribution of particles, which is preferred for applications involving compaction and sintering (Okuyama and Lenggoro 2003). Atomization efficiency, usually characterized by the mass of the liquid atomized in a unit time, can be promoted by using transducers in a matrix configuration for the large scale application in the industry. Generation of Cu particles is one of important applications of ultrasonic spray pyrolysis (Kim et al. 2003). Mixtures of copper nitrate, water and a cosolvent of either ethanol (ET) or ethylene glycol (EG) were used as the precursor solutions. Solutions were atomized to droplets and sent into the tube reactor, where copper nitrate was reduced to Cu in a reducing atmosphere created by the cosolvent.

The mechanism of droplet formation via ultrasonic generation has been widely studied (Lang 1962, 1962; Peskin and Raco 1963; Goodridge et al. 1997; Yule and Al - Suleimani 2000; Rajan and Pandit 2001; Barreras, Amaveda and Lozano 2002; Dobre

and Bolle 2002; Donnelly et al. 2004; Avvaru et al. 2006; J. Ju et al. 2008; Wang et al. 2008; Hamai et al. 2009; Tsai et al. 2009). Two major hypotheses have been proposed to explain the mechanism of liquid disintegration during ultrasonic atomization, namely the capillary wave hypothesis and the cavitation hypothesis.(Lang 1962; Strutt 2009) Researchers have also tried to combine these two hypotheses together into a "conjunction theory", according to which the cavitation and capillary waves interact with each other and excite the formation of droplets (Ya and Eknadiosyants 1969). Based on the capillary wave hypothesis, the droplet diameter should be of the same order of the capillary wave length which is a function of the solution density, surface tension and the ultrasonic frequency. Lang proposed the following Lang's equation (Lang 1962):

$$d_d = 0.34 \left(\frac{8\pi\sigma}{\rho f^2} \right)^{1/3} \ldots\ldots\ldots\ldots\ldots\ldots\ldots\ldots\ldots\ldots\ldots\ldots\ldots\ldots\ldots\ldots\ldots\ldots \text{(3.1)}$$

where σ is surface tension, ρ is liquid density and f is the ultrasonic frequency. 0.34 is an experimentally determined coefficient. Because the above equation is not dependent on viscosity, in contrast to what is usually observed in experiments, Rajan proposed an empirical correlation considering the dependence on almost all physicochemical properties of the liquid atomized as follows:(Rajan and Pandit 2001)

$$d_d = A * (f)^{-0.66} (Q)^{0.207} (\sigma)^{0.11} (\rho)^{-0.274} (\eta)^{0.166} \ldots\ldots\ldots\ldots\ldots\ldots\ldots \text{(3.2)}$$

where A is a constant, η is liquid viscosity, and Q is the liquid flow rate. Similar equations were proposed in the last several decades to describe droplet formation process via ultrasonic activation (Ju et al. 2008). Dimensional analysis is another way to describe the relationship between droplet size and precursor properties. Considering the capillary

27

wave as a Faraday excitation problem (Faraday 1831), Donnelly nondimensionalized the fluid parameters (Donnelly et al. 2004): the unique frequency v_*, length scale l_*, and mass m_*. They are constructed as:

$$\omega_* = \frac{(\sigma/\rho)^2}{\gamma^3} \dots\dots\dots\dots\dots\dots\dots\dots\dots\dots\dots\dots\dots\dots\dots\dots\dots\dots\dots(3.3)$$

$$l_* = \frac{(\gamma)^2}{\sigma/\rho} \quad \dots\dots\dots\dots\dots\dots\dots\dots\dots\dots\dots\dots\dots\dots\dots\dots\dots\dots(3.4)$$

$$m_* = \rho l_*^3 \dots\dots\dots\dots\dots\dots\dots\dots\dots\dots\dots\dots\dots\dots\dots\dots\dots\dots\dots(3.5)$$

where σ is surface tension with a unit of mass/(time)^2, γ is kinematic viscosity with a unit of (length)^2/time and ρ is density with a unit of mass/(length)^3. The dimensionless droplet diameter and frequency are defined:

$$\Omega = \omega/\omega_* \dots\dots\dots\dots\dots\dots\dots\dots\dots\dots\dots\dots\dots\dots\dots\dots\dots\dots\dots(3.6)$$

$$D = d/l_* \quad \dots\dots\dots\dots\dots\dots\dots\dots\dots\dots\dots\dots\dots\dots\dots\dots\dots\dots(3.7)$$

where d is the dimensional diameter, and ω is the frequency of the atomizer. When $\Omega \gg 1$ ($\omega \gg \omega_*$), viscous effects can be neglected and the relationship between droplet size and D, similar to Lang's equation, can be expressed as:

$$D \propto \Omega^{-2/3} \rightarrow d \propto (\sigma/\rho)^{1/3}\omega^{-2/3}\dots\dots\dots\dots\dots\dots\dots\dots\dots\dots\dots(3.8)$$

which can be rearranged to the form of Lang's equation (Equation 3.1).

If $\Omega \ll 1$ ($\omega \ll \omega_*$), viscous effects will be dominant:

$$D \propto \Omega^{-1/2} \rightarrow d \propto \gamma^{1/3}\omega^{-1/2}\dots\dots\dots\dots\dots\dots\dots\dots\dots\dots\dots\dots(3.9)$$

Similar analyses can be found in other articles (Goodridge et al. 1997; Donnelly et al. 2005).

Formation of a bimodal droplet size distribution during ultrasonic atomization was reported by both Wang (Wang et al. 2008) and Barreras (Barreras et al. 2002). Wang sprayed pure water using a 1.7 MHz ultrasonic generator, and obtained a bimodal distribution with two peaks, both ranging from 1 to 20 microns. He hypothesized that the big droplets are formed from coagulation of small ones. According to Barreras's experiment, when the fluid was placed directly on the transducer and not replenished, the liquid film thinned during the last few seconds of the spray process. When the water over the transducer is almost depleted, droplets emerged from breakup of discrete filaments rather than from the surface waves as occurred when there was sufficient water on the transducer. The droplet diameter distribution changed from unimodal to bimodal with one peak around 9 μm and the other at around 50 μm (Barreras et al. 2002).

Atomization efficiency is another important property to be considered in industrial applications. Though atomization efficiency can be increased by using multiple transducers, it is also affected by atomization power, precursor temperature, and carrier gas flow rates according to Wang's report (Wang et al. 2008). In Wang's experiments, precursor solutions with viscosity larger than 2.0×10^{-3} Ns/m^2 (about 2 mm^2/s) cannot be atomized, but increasing temperature could improve the atomization efficiency by decreasing the solution viscosity.

In this work, precursors used for the generation of copper particles by spray pyrolysis, copper nitrate/water/ethanol and copper nitrate/water/ethylene glycol solution systems,

were selected as research targets. A 2^k design of experiment (DOE), with k = 3, was used to develop the experimental plan. The effects of concentration, cosolvent volume ratio and carrier gas flow rate on the droplet size were investigated, and the relationship between atomization rate, the solution properties and the operating conditions were also explored. The formation process of the droplets was analyzed by shadowgraphy.

3.3. EXPERIMENT

3.3.1. Ultrasonic atomization system

The ultrasonic nebulizer consists of a cylindrical chamber with a height of 20 cm and a diameter of 10 cm (Figure 3.1). The nebulizer is separated into two parts by a cellophane film located 5 cm above the bottom. Below the film, there is a piezoelectric transducer and recycled cooling water. A peristaltic pump is used to circulate the water, maintained at 25 ^{o}C using a temperature controlled bath. The transducer operates at a fixed frequency of 1.7 MHz with input power of 50 W. Precursor solution is circulated to keep the liquid level constant and solution well mixed in the chamber above the film. Solution flows into the reservoir and is sprayed to droplets by the ultrasonic nebulizer. Nitrogen was used as the carrier gas with flow rate controlled between 1 L/min to 4 L/min. The total mass of the solution and reservoir was recorded every ten minutes, and the atomization rate of the solution was calculated by the mass change. Copper nitrate/water/ET and copper nitrate/water/EG systems were selected as my research targets.
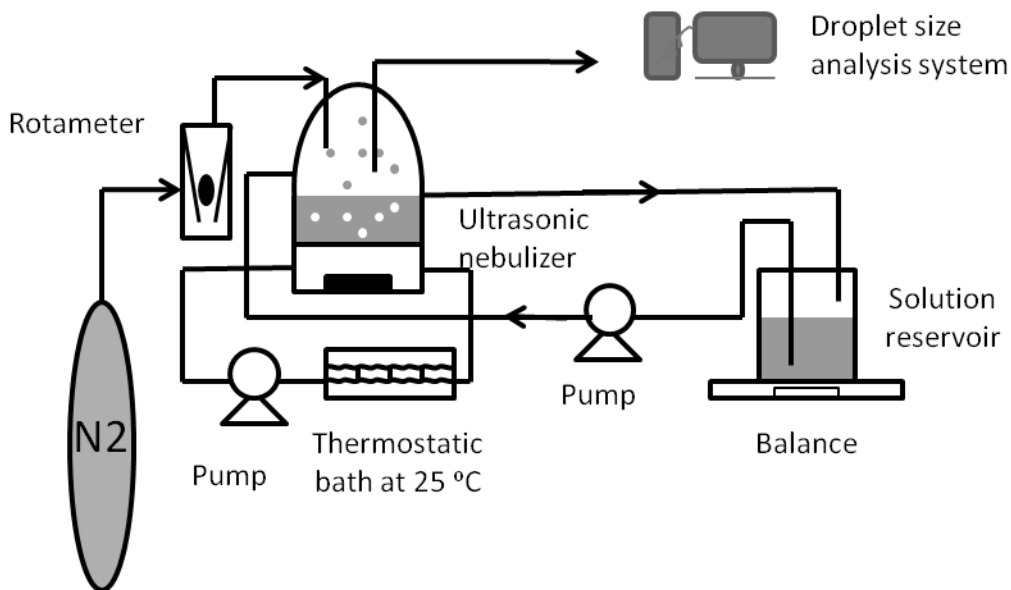
Figure 3.1. Schematic ofhe ultrasonic droplet generator system.

3.3.2. Droplet size analysis.

A droplet size analysis system (Spraytec, Malvern Instruments Ltd., Malvern, U.K.) was used for droplet size distribution measurements. The measurement is based on the light scattering behavior of the droplets. In this system, laser light is scattered by droplets, and then passes through the focus lens. A detector behind the lens is used to record the light signal. The droplet diameter resolution depends on the laser wavelength and the lens focal length. In my experiment, a 670 nm laser and a 450 nm focal length were used, and the droplet diameter detected ranged from 0.1 μm to 150 μm. All the measurements were carried out in a dark room to eliminate the influence of natural light. The droplet size distribution was described based on volume ratio. The median value D50, the diameter which splits the droplet size distribution with half above and half below it based on the volume, was used for the characterization of the droplet diameter.

31

3.3.3. Physical property measurement

Surface tension, viscosity and density of each solution were measured. Surface tension was obtained by the pendant droplet method. A pendant droplet was first generated on the tip of the needle, and the droplet was shaped as gravity and the surface tension reach the balance. The shape of the droplet was photographed, and the surface tension between the solution and air was calculated.(FORDHAM 1948) Viscosity was measured by the Cannon-Fenske routine viscometer. For the density, the mass of every solution of fixed volume was obtained by an electronic analytical balance, and density was calculated by dividing the mass over the volume.

3.3.4. Shadowgraphy image analysis

The ultrasonic spray process was recorded by a shadowgraphy image system (LAVISION, ParticleMaster shadow). Frequency doubled Nd:YAG laser (wavelength of 532 nm) combined with a diffuser was used as the back lighting illumination. A long distance microscope working range of 560 mm to 1520 mm with a SVGA camera was used as a detector, theoretically resolving particles down to 5 μm in diameter. In the experiment, particles smaller than 10 μm were hard to resolve from the image because of the high concentration of droplets.

3.3.5. Statistical analysis

The statistical software package Minitab 15 was used for the 2^3 full factorial experiment design and analysis of results (Montgomery and Runger 2006). The relationship between the covariance, either the droplet diameter or atomization efficiency, and possible effect factors was investigated. For both copper nitrate/water/ET and copper nitrate/water/EG system, copper nitrate concentration, cosolvent (ET/EG) volume ratio and flow rate were

designed as possible main factors. High/low level was 0.5 M / 2 M, 0 vol% / 40 vol% and 1 L/min / 4 L/min separately. These are the most common conditions for copper particle generation. Each test was repeated, and three center points were added. For each solution system, there were 19 samples tested including repeated ones and center point ones, so that were 38 samples for two solution system. Additional three copper nitrate/EG/water solutions were made to investigate the correlation between the bimodal distribution and the solution viscosity.

3.4. RESULTS AND DISCUSSION

3.4.1. Droplet size distribution of copper nitrate /EG/water system

Compositions and physical properties of the 19 sample solutions are listed in Table 3.1. Experiments were run in a random order to to avoid introducing bias into the results. Copper nitrate concentration, EG volume ratio and carrier gas flow rate were changed between high/low levels. Densities of solutions varied from 1.1 g/ml to 1.4 g/ml, and increased with either increasing concentration or the volume of EG. Surface tension was increased from 59 mN/m to 80.7 mN/m by either increasing the concentration of nitrate or decreasing the volume ratio of EG. Viscosity, ranging from 7.06 mm^2/s to 1.09 mm^2/s, was positively related to both concentration and EG volume ratio. Atomization rate varied from a low of 0.05 ml/min to a high of 1.46 ml/min. Most of solutions had D50 around 5 μm; however, D50 around 80 μm was detected in some cases because of a bimodal droplet size distribution, as I will discuss later.

Table 3.1. 2^3 design of experiment. Copper nitrate concentration, EG volume ratio and carrier gas flow rate, considered to be possible important factors, are shown in the table. Density, surface tension and viscosity of each solution are also listed.

Run order	Concentration (M)	Co solvent volume (vol %)	Carrier flow rate (L/min)	Density (g/ml)	Surface tension (mN/m)	Viscosity (mm^2/s)	D50 (μm)	Atomization rate (ml/min)
1	2	0	1	1.4	80.7	1.72	5.7	0.28
2	1.25	20	2.5	1.3	70.2	2.21	5.6	0.57
3	2	40	1	1.4	66	7.00	87.2	0.05
4	0.5	40	1	1.1	59	3.31	6.7	0.14
5	0.5	0	1	1.1	72.9	1.10	6.2	0.43
6	1.25	20	2.5	1.3	67.6	2.24	6.6	0.43
7	2	0	4	1.4	81.6	1.69	5.5	0.87
8	0.5	0	1	1.1	73.3	1.09	6.2	0.43
9	0.5	40	4	1.1	60.1	3.25	6.3	0.28
10	2	0	1	1.4	82	1.66	5.3	0.31
11	2	0	4	1.4	80.2	1.71	5.4	1.03
12	2	40	1	1.4	65.5	7.06	88.4	0.05
13	0.5	40	4	1.1	59.3	3.19	8.1	0.21
14	0.5	0	4	1.1	73.5	1.10	4.8	1.46
15	1.25	20	2.5	1.3	66.9	2.35	4.9	0.45
16	2	40	4	1.4	66.1	6.89	72.2	0.08
17	0.5	0	4	1.1	73.3	1.09	4.2	1.48
18	0.5	40	1	1.1	60.6	3.03	5.3	0.17
19	2	40	4	1.4	65.9	6.46	79.7	0.10

Droplet size distributions of copper nitrate /EG/water solutions are shown in Figure 3.2. The typical solution produced a lognormal distribution with droplet diameters ranging from 0.1 μm to 15 μm, but bimodal size distributions were observed when the solution contained 2 M nitrate and 40 vol% EG. The first mode had lower intensity and ranged from 0.1 μm to 30 μm, followed by the second one from 30 μm to 150 μm. The onset of formation of a bimodal size distribution led to a dramatic change of the droplet diameter, and in the second test with the same solution composition and carrier gas flow rate, the

frequency at diameter of 75 μm varied from highest 0.35 to lowest 0.05, indicating the second mode is not quite stable.
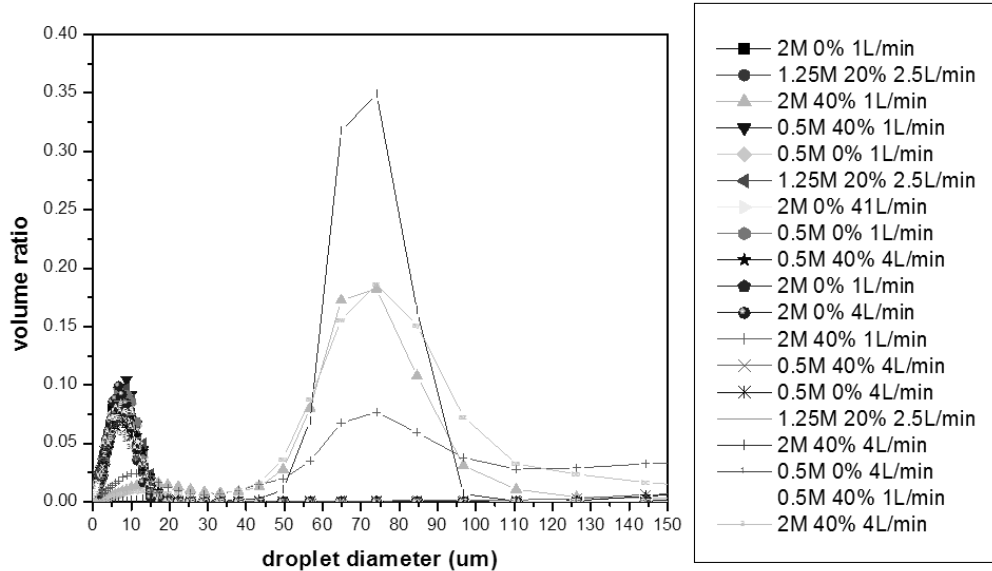
Figure 3.2. Copper nitrate/EG/water droplet size distributions.

Software (Minitab) was used to fit the data and calculate the coefficients (β), which represent the effect of the factor on the variables such as D50 and the atomization rate. (As detailed in the supplement). A coefficient equal to 0 means the factor is not important for the change of D50 or the atomization rate. The P value is defined as the probability of β equaling to 0. When P is smaller than 0.05, the factor has a significant effect on the variable at the 95% confidence level. The standard deviations of coefficients and P values are listed in the Table 2 and Table 3 when Y is the droplet diameter D50 and the atomization rate respectively. The corresponding coefficients of determination (R-squared), which represent the quality of the fit, are 99.8 and 99.2 respectively.

35

In Table 3.2, concentration, EG ratio and flow rate have P values smaller than 0.05, indicating that these three factors are significant factors for the change of the diameter. A positive concentration coefficient of 18.85 indicated the particle diameter increased with increasing concentration. The droplet diameters D50 are plotted against nitrate concentration in Figure 3.3 a. Lines were used to connect the diameters measured at high/low concentration levels with volume ratio and flow rate fixed. Each condition experiment was repeated, and an average value of two measurements was used as the start point and end point of the lines. There was an obvious increase observed when solution contained 40 vol% EG, in which case a bimodal droplet size distribution was detected. At the lower level of EG volume ratio (20 vol%), the change of droplet size is not very significant. EG volume ratio also has a positive coefficient of 19.41. Figure 3.3 b shows droplet diameter versus EG volume ratio, and it showed the significant increase of droplet size happened only when concentration was 2 M. The coefficient for the carrier gas flow rate is 1.55, and the p value is 0.007. From Figure 3.3 c, a very slight decrease in diameters was observed in the conditions of 0.5 M concentration/0 vol% EG, 2 M concentration/0 vol% EG and 2 M concentration/40 vol% EG respectively. But for the case of 0.5 M concentration/40 vol% EG, the change in diameters was insignificant. In conclusion, the droplet diameter increases with both increasing concentration and EG volume ratio, mostly because of the formation of bimodal distribution. Increasing flow rate slightly decreases droplet size in most cases, but it is not necessarily true when solution contains 40 vol% EG and concentration was 0.5 M.

Table 3.2. Effects of concentration, EG volume ratio and carrier gas flow rate on droplet diameter D50, coefficients (β) represent how much the factor will change the variables. SE is the standard error of the coefficients. The P value is defined as the probability of β equaling to 0.

Term	Coef (β)	SE Coef	P
constant	24.82	0.46	0
concentration	18.85	0.46	0
volume ratio	19.41	0.46	0
flow rate	-1.55	0.46	0.007
concentration*volume ratio	18.78	0.46	0
concentration*flow rate	-1.42	0.46	0.011
volume ratio *flow rate	-1.11	0.46	0.036
concentration*volume ratio*flow rate	-1.83	0.46	0.003
Ct Pt	-19.11	1.15	0

$R^2 = 99.82\%$

Table 3.3 lists effect parameters for concentration, EG volume ratio and carrier gas flow rate on atomization rate. A negative coefficient of -0.11 and -0.33 indicated that either increasing concentration or increasing EG volume ratio decreased the atomization rate, but increasing carrier gas increased the atomization rate, indicated by a positive coefficient of 0.23. Graphs of atomization rate vs. concentration, EG volume ratio and flow rate are shown in Figure 3.3 d-f. A significant change in atomization rate could be observed with concentration. A negative correlation between atomization rate and concentration/volume ratio and a positive correlation between atomization rate and flow rate were observed.

Table 3.3. Effects of concentration, EG volume ratio and carrier gas flow rate on atomization rate.

Term	Coef	SE Coef	P
constant	0.46	0.01	0
concentration	-0.11	0.01	0
volume ratio	-0.33	0.01	0
flow rate	0.23	0.01	0
concentration*volume ratio	0.05	0.01	0.004
concentration*flow rate	-0.05	0.01	0.002
volume ratio *flow rate	-0.19	0.01	0
concentration*volume ratio*flow rate	0.04	0.01	0.012
Ct Pt	0.02	0.03	0.517

$R^2 = 99.17\%$

a

b

c

d

e   f
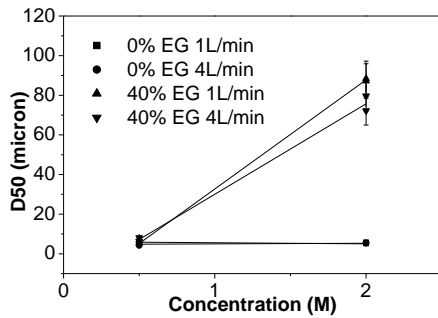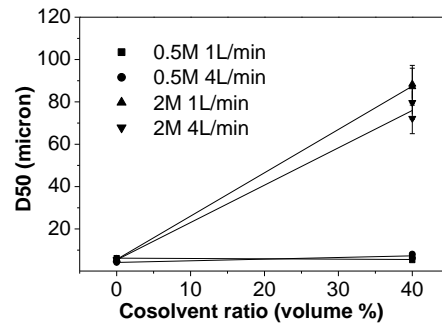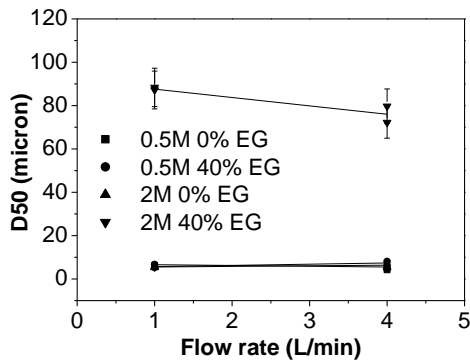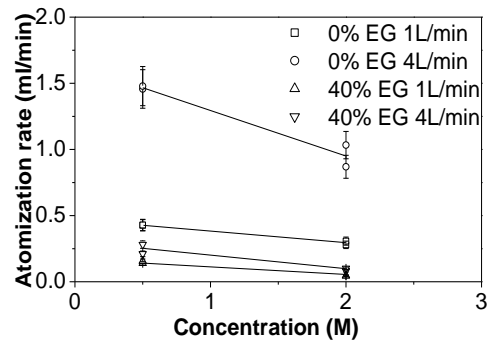
Figure 3.3. Interaction of concentration/EG volume ratio/carrier gas flow rate and droplet diameter/atomization rate.

3.4.2. Droplet size distribution of copper nitrate/ET/water system

A similar design of experiment and analysis process was applied to the copper nitrate/ET/water system. Solution properties, droplet diameters and atomization rates are listed in Table 3.4. Both density and surface tension increased with increasing copper nitrate concentration, but decreased by adding more ET. Because viscosity was positive depending on concentration and ET volume ratio, the greatest viscosity of 4.53 mm^2/s was obtained at a high level of copper nitrate concentration (2 M) and high level of ET volume ratio (40 vol%). The atomization rate changed from 0.11 ml/min to 1.63 ml/min. Droplet size distributions are shown in Figure 3.4. D50 was typically around 5 μm, but became very large when the bimodal distributions were observed. Bimodal distributions were observed at high concentration/high volume ratio conditions.

39

Table 3.4. 2^3 design of experiment. Copper nitrate concentration, ET volume ratio and carrier gas flow rate, considered to be possible important factors, are shown in the table. Density, surface tension and viscosity of each solution are also listed.

Run order	Concentration (M)	Co solvent volume (vol %)	Carrier flow rate (L/min)	Density (g/ml)	Surface tension (mN/m)	Viscosity (mm^2/s)	D50 (μm)	Atomization rate (ml/min)
1	2	0	1	1.4	80.0	1.55	4.9	0.39
2	1.25	20	2.5	1.2	40.2	1.96	5.0	0.51
3	2	40	1	1.3	34.8	4.42	28.5	0.11
4	0.5	40	1	1.0	33.1	2.60	3.6	0.18
5	0.5	0	1	1.1	74.8	0.99	3.8	0.41
6	1.25	20	2.5	1.2	42.9	2.09	4.5	0.45
7	2	0	4	1.4	80.7	1.53	4.2	0.97
8	0.5	0	1	1.1	75.1	1.00	4.7	0.44
9	0.5	40	4	1.0	31.9	2.53	4.4	0.43
10	2	0	1	1.4	81.0	1.51	5.0	0.37
11	2	0	4	1.4	81.4	1.46	3.7	0.81
12	2	40	1	1.3	35.2	4.13	62.4	0.15
13	0.5	40	4	1.0	32.6	2.59	4.9	0.57
14	0.5	0	4	1.1	75.4	1.00	5.5	1.40
15	1.25	20	2.5	1.4	43.0	2.10	4.8	0.45
16	2	40	4	1.2	35.5	4.42	54.7	0.32
17	0.5	0	4	1.3	74.8	1.06	4.8	1.63
18	0.5	40	1	1.0	32.4	2.75	4.8	0.13
19	2	40	4	1.1	35.0	4.53	95.8	0.35
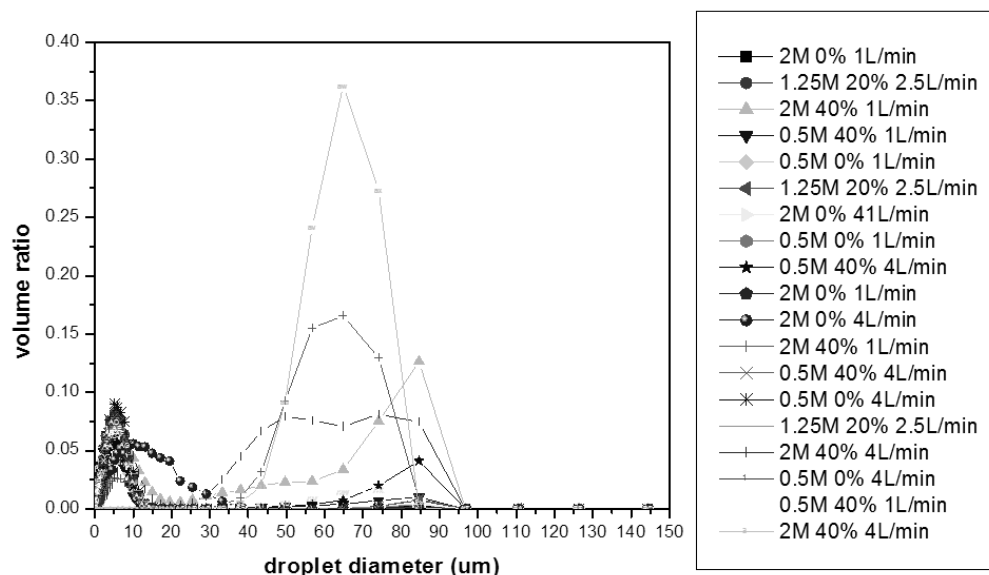
Figure 3.4. Copper nitrate/ET/water droplet size distributions.

Statistical analysis results are listed in Table 3.5. Considering the droplet diameter D50 as the variable, P values of nitrate concentration, ET volume ratio and carrier gas flow rate are 0.001, 0.001 and 0.234 respectively, indicating that droplet size was not significantly changed by carrier gas flow rate, but was positively correlated with nitrate concentration and ET volume ratio. Plots of droplet diameter D50 vs. concentration, volume ratio and flow rate are shown in Figure 3.5 a-c. The result is quite similar to the case when EG was used as a cosolvent. Droplet diameter increased with increasing concentration when 40 vol% ET was used, but with 0 vol% ET, diameter change is not significant (Figure 3.5 a). Droplet diameter increased with increasing volume ratio with a high concentration level of 2 M (Figure 3.5 b). At low concentration levels of 0.5 M, diameter even slightly decreased. No obvious relationship can be found from Figure 5 c.

41

The analysis process was applied for the atomization rate. Both results of the P value calculation (Table 3.6) and plots of atomization rate vs. nitrate concentration, ET volume ratio and carrier gas flow rate (Figure 3.5 d-f) showed clear negative correlation between atomization rate, concentration and ET volume ratio, and positive correlation between atomization rate and carrier gas flow rate.

Table 3.5. Effects of concentration, ET volume ratio and carrier gas flow rate on droplet diameter D50.

| Term	Coef	SE Coef	P
constant	18.48	2.98	0
concentration	13.91	2.98	0.001
volume ratio	13.92	2.98	0.001
flow rate	3.78	2.98	0.234
concentration*volume ratio	14.04	2.98	0.001
concentration*flow rate	3.43	2.98	0.277
volume ratio *flow rate	3.78	2.98	0.234
concentration*volume ratio*flow rate	3.92	2.98	0.218
Ct Pt	-13.7	7.51	0.098

$R^2 = 88.27\%$

Table 3.6. Effects of concentration, ET volume ratio and carrier gas flow rate on atomization rate.

| Term	Coef	SE Coef	P
constant	0.54	0.02	0
concentration	-0.11	0.02	0
volume ratio	-0.26	0.02	0
flow rate	0.27	0.02	0
concentration*volume ratio	0.06	0.02	0.009
concentration*flow rate	-0.09	0.02	0.001
volume ratio *flow rate	-0.13	0.02	0
concentration*volume ratio*flow rate	0.06	0.02	0.015
Ct Pt	-0.07	0.05	0.152

$R^2 = 98.13\%$
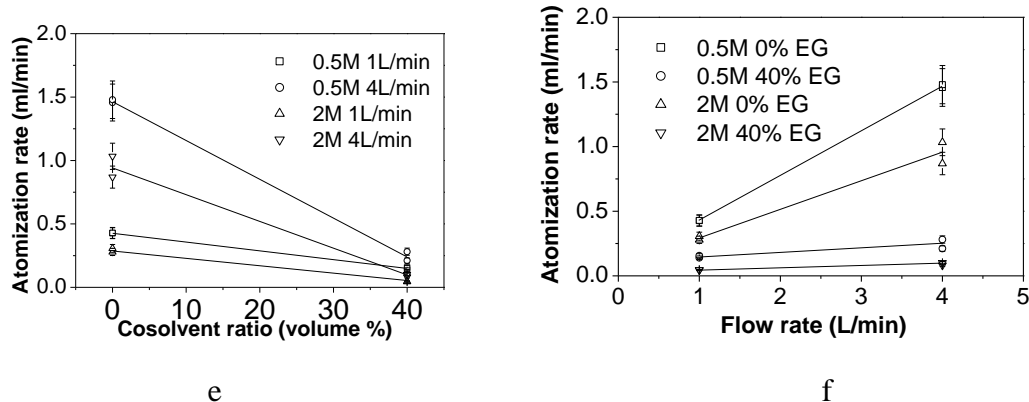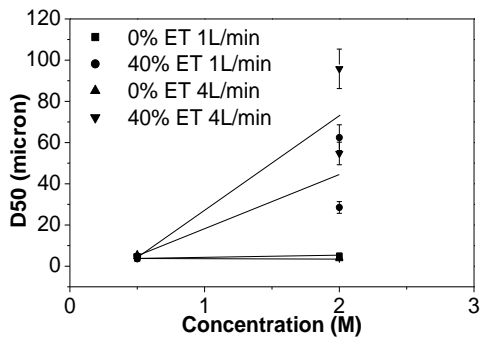
a
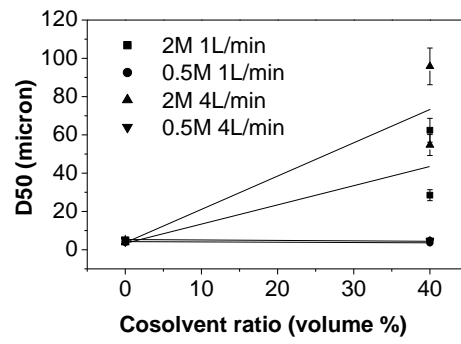
b
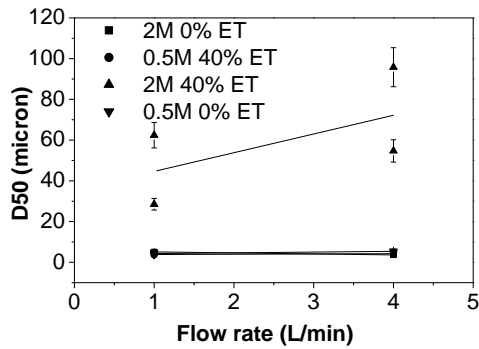
c
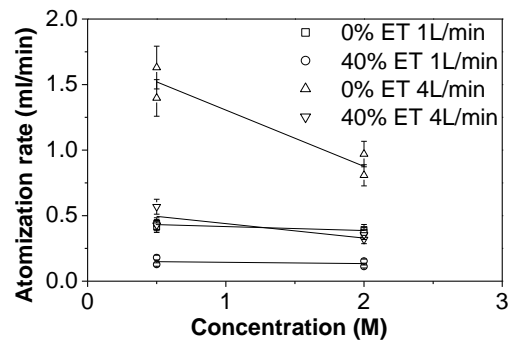
d
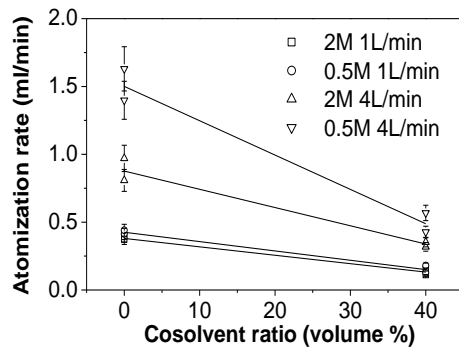
e
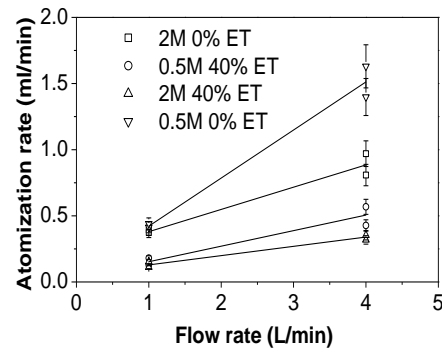
f

Figure 3.5. Interaction of concentration/ET volume ratio/carrier gas flow rate and droplet

diameter D50/atomization rate.

43

3.4.3. Bimodal droplet size distribution

From the discusion above, bimodal distributions and large droplet sizes appeared at high concentration and high cosovlent volume ratio conditions. Though a bimodal distribution of pure water was reported by Barreras (Barreras et al. 2002) with one range from 1 μm to 10 μm and the other from 50 μm to 100 μm emerged from a thin water layer (Barreras et al. 2002), experiments suggest that the bimodal distribution was more likely caused by a high viscosity. In order to test this hypothesis, three more copper nitrate/EG/water solutions were made. Surface tension, atomization rate, droplet diameter and compositon of each solution are listed in Table 3.7, and droplet size distributions are shown in Figure 6. The surface tension of solutions varied between 63.1 mN/m and 70.2 mN/m with a change of less than 10%. Viscosities increased from 2.21 mm^2/s to 6.14 mm^2/s. A nearly single modal distribution was observed with viscosity of 2.21 mm^2/s. A low intensity second peak appeared with a viscosity of 3.06 mm^2/s. Bimodal distributions were observed when viscosity was larger than 3 mm^2/s. For 2 M copper nitrate 40 vol% EG solution, the viscosity is 6.14 mm^2/s, and solution became hard to atomize with a low atomization rate of 0.01 ml/min. Measurements of the droplets with diameters larger than 200 μm may be not reliable because the number concentration of droplets with large diameter is very low.
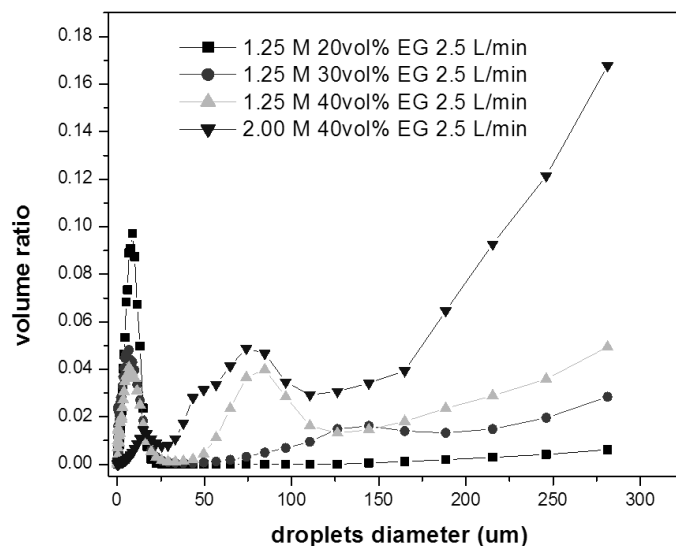
Figure 3.6. Copper nitrate/EG/water droplet size distributions.

Table 3.7. Copper nitrate/EG/water soltion properties, droplet diameter and atomizaiton

rate.

Concentration (M)	Co solvent volume	Carrier flow rate (L/min)	Surface tension (mN/m)	Viscosity (mm^2/s)	Atomization rate (ml/min)	D50 (μm)
1.25	20% EG	2.5	70.2	2.21	0.57	5.6
1.25	30% EG	2.5	65.9	3.06	0.12	5.3
1.25	40% EG	2.5	63.1	4.31	0.10	22.5
2	40% EG	2.5	66.8	6.14	0.01	160.0

3.4.4. Shadowgraphy investigation

Shadowgraphy was used for the investigation of droplet formation process. Pure water,

40 vol% EG aqueous solution and pure EG were atomized by the the ultrasonic generator,

and images of the process are shown in Figure 3.7. a-f. Surface tension and viscosity of

three liquids were listed in Table 3.8. Copper nitrate could not be used for image analysis,

because it would have reduced the transparency of the laser light and the quality of the images. During the atomization process, a liquid cone was activated in the center of the chamber. For the water, single modal droplet size distribution was observed and is shown in Figure 3.8 a. Because the droplets have diameters smaller than the camera resoluton, only a dense mist was observed around the center of the cone, indicating a high number concentration of the droplets. Neither capillary waves or cavitation were observed on the surface, probably because of the limit of the resolution. 40 vol% EG aqueous solution has a viscosity of 3.12 mm^2/s. Less dense droplets were observed around the cone, and it is in agreement with the conclusion that higher viscosity leads to lower atomization rate. A bimodal size distribution was shown in Figure 3.8 b. The droplets in the second mode with large diameters around 100 μm were observed in the amplified shadowgraphy image, and accompanied by lots of liquid filaments detected on the surface of the cone. From the images, the filaments had diameters between 50 μm and 100 μm, and have a length of more than 100 μm. Droplets with diameters greater than 30 μm could be easily formed from these filaments because of any small fluctuation of the environment. The same filaments were observed on the surface of pure EG, which has a high viscosity of 15.68 mm^2/s. A few droplets with large diameters were observed, but no small droplets were generated. The droplet size distribution was not available because the number of droplets generated from pure EG was not sufficient for the size distribution measurement.

a

b

c

d

e   f
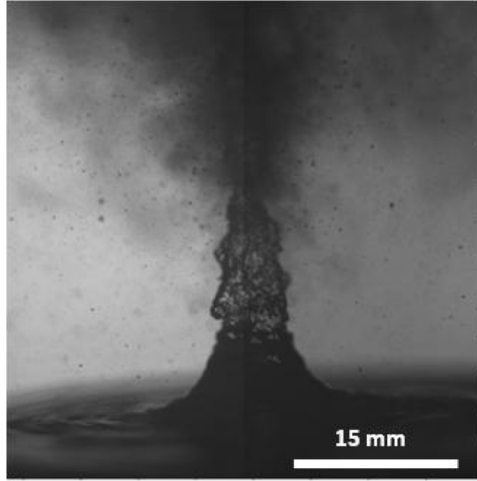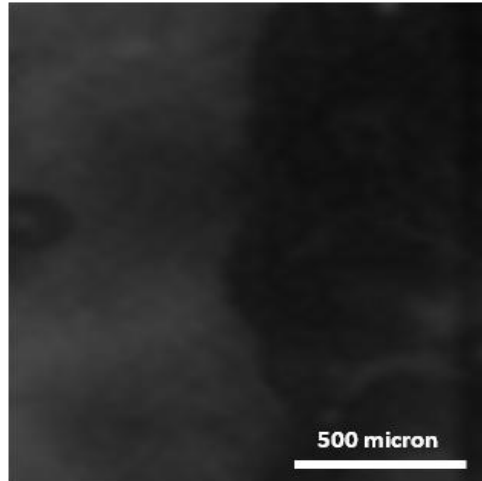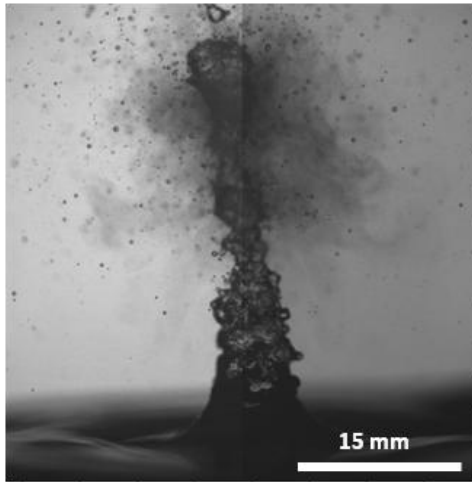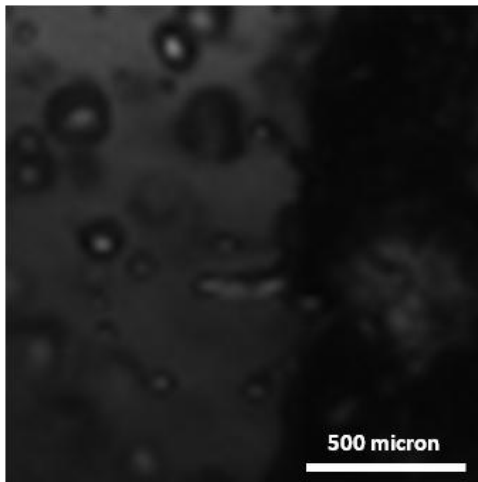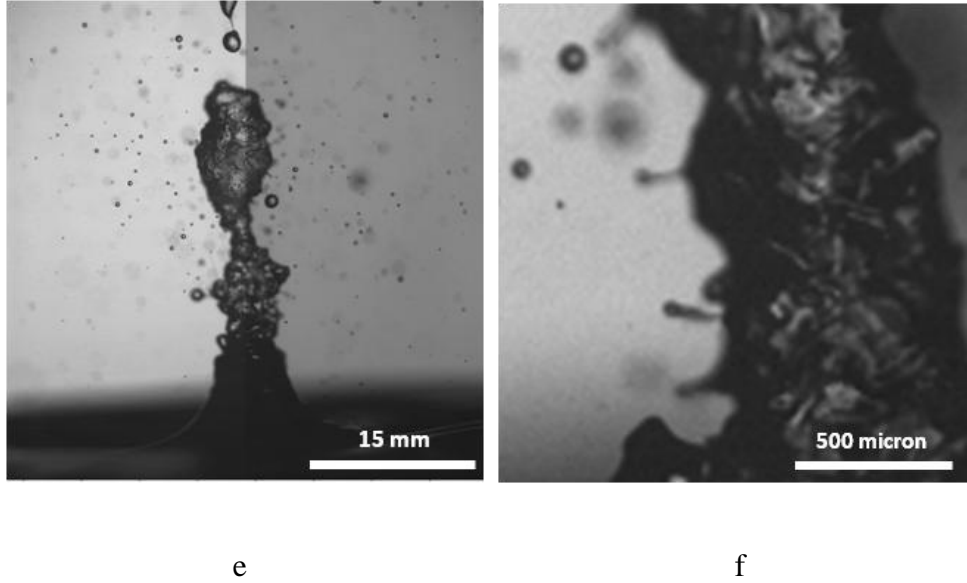
Figure 3.7. Shadowgraphy images of atomization process (a) pure water, (b) pure water (at high magnification), (c) 40% EG aqueous solution , (d) 40% EG aqueous solution (at high magnification), (e) pure EG and (f) pure EG (at high magnification).

a   b
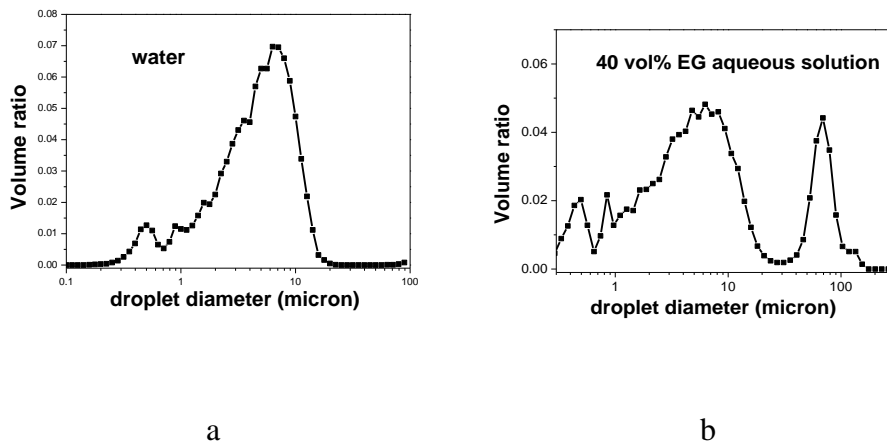
Figure 3.8. Droplet size distribution of (a) pure water and (b) 40% EG aqueous solution.

Table 3.8. Surface tension and viscosity of water, 40% EG aqueous solution and EG

measured at 25 $^{\circ}$C.

Solution	Surface tension (mN/m)	Viscosity (mm^2/s)
Pure water	72.0	0.90
40% EG solution	58.1	3.12
Pure EG	47.0	15.68

3.4.5. Relationship between droplet size and solution properties

Combining results from copper nitrate/EG/water and copper nitrate/ET/water experiments, I intended to figure out the relationship between droplet size and solution propertes. Lang's equation (Equation 3.1) gives an estimate of droplet diameters of 2.8 μm with a surface tension of 70 mN/m and a 1.7MHz frequency, and predicts the size will decrease with decreasing surface tension. However, 2.8 μm is much smaller than what I actually measured, and there is no simple relationship observed between droplet diameter D50 and surface tension, as shown in Figure 3.9. D50 versus viscosity is shown in Figure 3.9. With viscosities smaller than 4 mm^2/s, droplet diameters were around 5 μm, and did not change significantly with viscosity. Once viscosity is larger than 4 mm^2/s, the droplet diameter becomes large, which can be attributed to the bimodal distribution.

Dimesionless diameter and dimensionless frequency were calculated by equations 3.4,3.5,3.7 and 3.8, and are shown in Figure 3.10. A linear behavior of log(D) vs. log(Ω) was observed when $\Omega<0.1$. According to Donnelly's report (Donnelly et al. 2004), surface tension will dominate in this region, and D is proportional to $\Omega^{-2/3}$ theoretically. The fitting result indicated D=2.79$\Omega^{-0.602}$ with an index value of -0.60, which is very

close to the predicted number ($R^2 = 0.97$). When $\Omega > 0.1$, linear behavior of log(D) vs. log(Ω) is not observed. In this region, all solutions have a viscosity larger than 4 mm^2/s and produce bimodal droplet size distributions. The result that D does not follow the proportional relationship with $\Omega^{-2/3}$ could also be attributed to the bimodal distribution. Droplets not only come from capilary waves when $\Omega > 0.1$, and big droplets with diameters of tens of microns formed from the breakdown of the filament, which I observed in the shadowgraphy experiment. Results for $\Omega > 1$ are not available, because solutions with viscosity larger than 7 mm^2/s lead to small atomization rates, less than 0.01 ml/min, and the droplet szie distribution cannot be be measured.
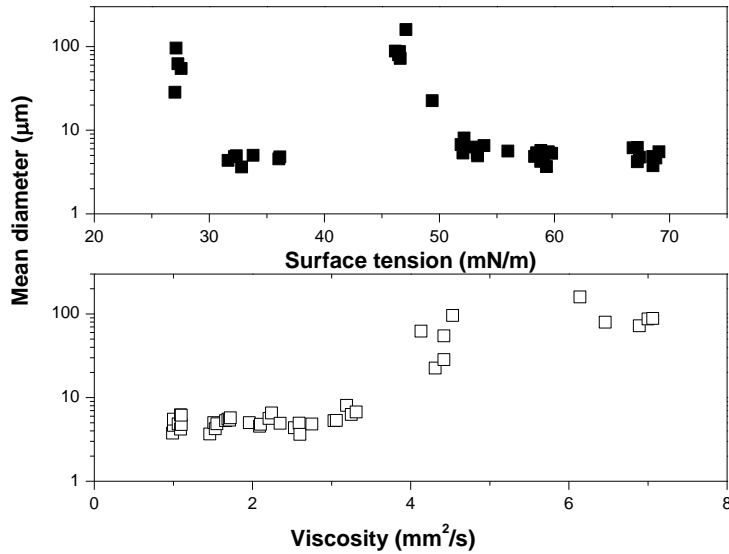
Figure 3.9. Droplet diameter D50 vs surface tension/viscosity.
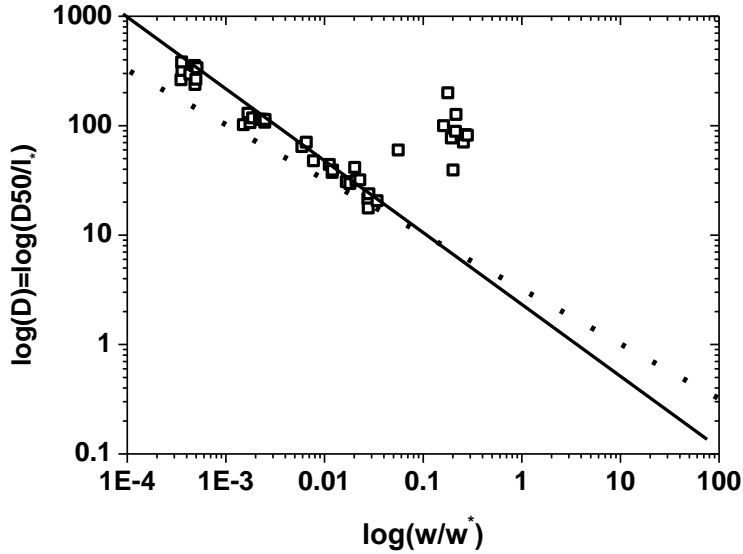
Figure 3.10. Correlation between dimensionless diameter and dimensionless frequency, solid line is $D=2.79\Omega^{-0.602}$. Solid dot line is $D \propto \Omega^{-0.5}$ as predicted in equation (3.9).

3.4.6. Relationship between atomization rate and solution properties

We discussed the positive effect of flow rate on atomization rate, and either increasing nitrate concentration or cosolvent volume ratio decreased the atomization rate in the previous statistical analysis. In Figure 3.11, a relationship between atomzation rate and viscosity is shown. As viscosity increased from 1 mm^2/s to 7 mm^2/s, atomization rate decreased significantly from 1.6 ml/min to 0.045 ml/min. A possible explaination is that the large viscosity resulted in a greater energy dissipation during the transport of the ultrasonic energy (Bhadra and Basu 1980), resulting in less energy available for the generation of wave fluctuations and thus droplets. Exponential functions AR=a+b*exp(-γ/c) could be used for the estimation of the atomization rate, where AR represents atomization rate. Parameters a, b and c were obtained by fitting experimental data in

different carrier gas flow rate conditions. Results are listed in Table 9. Increasing the carrier gas flow rate probably provided a stronger gas flow at the gas-liquid interface, which promoted the separation of droplets from the wave crest. Greater flow rate could also lead to a shorter residence time preventing droplets from falling back down to the generator. Therefore the atomization rate and the preexponential factor b increased from 0.73 to 3.28.
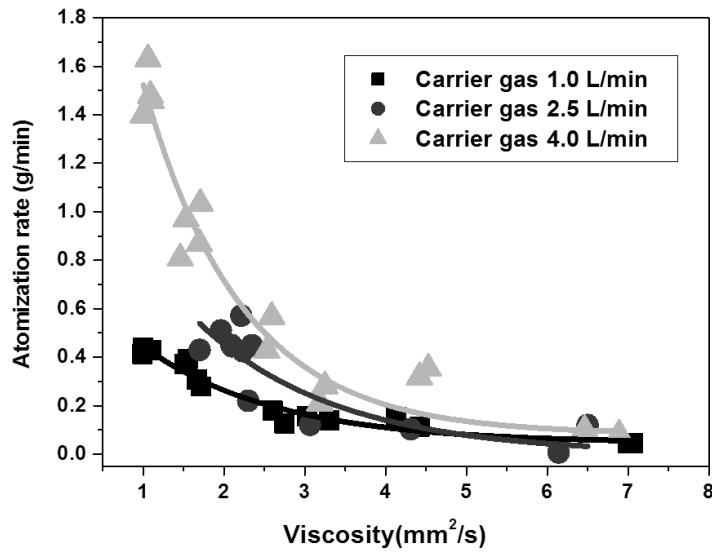
Figure 3.11. Correlation between atomization rate and viscosity for different carrier gas flow rates.

Table 3.9. Parameters of exponential fitting for atomization rate with different gas flow

rate

Carrier gas flow rate (L/min)	a	b	c	R^2
1	0.045	0.73(0.06)	1.65(0.16)	0.96
2.5	0	1.46(0.65)	1.71(0.60)	0.75
4	0.082	3.28(0.42)	1.21(0.14)	0.95

3.5. CONCLUSIONS

Droplet size distribution and atomization rate of copper nitrate/cosolvent/water solution were measured under different experimental conditions. Statistical analysis showed that either increasing nitrate concentration or cosolvent volume ratio increased the solution viscosity and the droplet diameter. At the same time, the atomization rate decreased. Detailed investigation indicated that the increasing droplet size was mainly attributed to the formation of bimodal droplet size distribution, the onset of which observed when the solution had a viscosity between 3 mm^2/s and 4 mm^2/s. Carrier gas flow rate had an effect on droplet size, but the change of the droplet diameter was not very significant. The atomization rate is promoted by increasing carrier gas flow.

In the test range of copper nitrate concentration and cosolvent volume ratio, the reported equations always gave a smaller estimate of droplet diameter than the measurements. Dimensionless droplet diameter and dimensionless frequency were calculated, and D was found to be proportional to $\Omega^{-0.6}$ when Ω is smaller than 0.1. In this region, droplets form from regular surface fluctuations, and surface tension is believed to be the dominant force during the process. Once Ω is bigger than 0.1, linear behavior does not describe

observations because larger droplets were formed from breakup of the liquid filaments. Both large droplets with diameters around 100 μm and filaments were observed by the tshadowgraphy experiment.

According to results, the properties of the droplets produced by ultrasonic atomization were dependent on the properties of the solution. For the spray pyrolysis process, a proper concentration and cosolvent ratio should be selected to achieve the right particle size, narrow size distribution and a high production rate.

Chapter 4: Particle generation by co-solvent spray pyrolysis: Effects of ethanol and ethylene glycol

4.1. ABSTRACT

A cosolvent spray pyrolysis process was used for the generation of micron sized pure copper particles. Ethylene glycol (EG) and ethanol (ET) were selected as cosolvents, and their effects on particle morphology and composition were systematically investigated. Experimental results showed that oxide-free copper particles could be generated at temperatures greater than 400 ^{o}C with either cosolvent. Hollow particles with cracks were generated with ET at temperatures from 400 ^{o}C to 1000 ^{o}C, while EG promoted the formation of porous particles at temperatures up to 600 ^{o}C and hollow shell particles with smooth surfaces at at 875 ^{o}C and 1000 ^{o}C. Results from short residence time experiments indicated that, during the generation process, lamellar and fragment-like $Cu_2(OH)_3NO_3$ precipitated when EG and ET were used respectively. $Cu_2(OH)_3NO_3$ then decomposed to CuO and Cu_2O. Finally the oxides were reduced to Cu in the reducing atmosphere created by EG and ET.

4.2. INTRODUCTION

Micron and submicron sized copper particles are used in electromagnetic interference packaging (Brusic et al. 1995), in electronically conductive pastes (Ohmi 2002; Songping and Shuyuan 2006) and in hybrid integrated circuits (Songping and Shuyuan 2006; Miki 1998; Tani and Naoaki Ogata 1998; Hosokura 2003). In addition to applications in the electronic industry, potential applications of copper particles in powder metallurgy are

also attracting more attention (Hao et al. 2009; Champion et al. 2005; Chung 2001). Porous bulk materials generated from copper particles by powder metallurgy techniques have adjustable damping capacity, thermal conductivity and mechanical strength, and can be used as impact energy absorbers, silencers, heat exchangers, and structural materials (Hao et al. 2009; Chung 2001).

Compared to particle generation methods reported in the literature, such as chemical reduction (Tsai and Dye 1991; Hirai et al. 1978), polyol method (Kurihara et al. 1995; Fievet et al. 1993) and vaporization techniques (Cardenas-Trivino et al. 1987; Satoh and Kimura 1989), spray pyrolysis has advantages of controllable particle size, simple experiment setup and large scale production ability (Jain, Skamser and Kodas 1997b; Majumdar et al. 1996; Nagashima et al. 1990). Spray pyrolysis devices are typically composed of a precursor reservoir, droplet generator, furnace reactor and particle collection equipment. Various metal salt precursors can be selected depending on the desired product particle composition. Particle diameter is tunable from tens of nanometers to micrometers by adjusting the salt concentration in the precursor. In addition, temperature and carrier gas flow rate are two important operating parameters for the control of particle morphology.

To achieve the desired conductivity and product reliability, copper particles free of copper oxide are required. To produce oxide-free particles using spray pyrolysis, a reducing environment is required to prevent the formation of a stable oxide (Stopic, Ilic and Uskokovic 1996; Xia, Lenggoro and Okuyama 2001; Gurmen et al. 2009; Biskos et al. 2008). Use of 10 vol% hydrogen was reported for copper nanoparticle generation, but hydrogen with a concentration from 4 vol% to 75 vol% (in air at 1 atm) leads to a risk of

56

explosion (Gurav et al. 1993a). In 2003, Kim *et.al.* reported the generation of copper nanoparticles using N_2 as a carrier gas and ethanol (ET) as a cosolvent (Kim et al. 2003). Under the reported conditions, the ET decomposes providing a reducing environment (Firmansyah et al. 2009b; Kim et al. 2003; Kim et al. 1997; Okuyama and Lenggoro 2003). The flash point of ET is 14 ^oC, however, which makes ET a National Fire Protection Association (NFPA) class 3 flammable material. For industrial applications, use of materials that have a flash point above 100 ^oC is preferred. Ethylene glycol (EG) has a flash point of 111 ^oC (Speight 2004), and is NFPA class 1 flammable material requiring preheating before ignition (NFPA 2007). In this work, I report generation of micron sized copper particles with either EG or ET at different temperatures. The effects of the cosolvent and temperature on particle morphology and composition were monitored, and the reaction process was investigated.

4.3. EXPERIMENT

4.3.1. Particle generation

A spray pyrolysis reactor system, illustrated in Figure 4.1, was developed which can produce several grams/hour of micron sized powder. The system is composed of a precursor solution reservoir, an ultrasonic droplet generator, tube furnaces, a quartz tube reactor and a filtration system for particle collection. 1.2 M copper nitrate solution with 40 vol% cosolvent, either ET or EG, was used as a precursor solution. Copper nitrate salt was selected because it is inexpensive, commercially available and highly soluble (145 g $Cu(NO_3)_2$ in 100 g water at room temperature) (Speight 2004). Precursor solutions were uniform and stable according to PH and FTIR test (Appendix A2). The ultrasonic generator operates at a frequency of 1.7 MHz, and atomizes the precursor solution to

droplets with volume average diameters of around 5 microns. Two tube furnaces, with a total length of 81 cm were combined in series. A quartz tube reactor with inner diameter of 2.5 cm was placed in the center of the furnaces. Temperatures in the furnaces ranged from 400 ^{o}C to 1000 ^{o}C. A polytetrafluoroethylene filter was used to collect the particles. Industrial grade nitrogen (N_2) with a minimum 95% purity was used as carrier gas. For regular copper particle generation, the carrier gas flow rate was 2.5 L/min leading to a residence time around 2 s with two furnaces used. A high flow rate of 10 L/min and a single furnace was used to decrease the residence time to less than 0.4 s for the investigation of the reaction process. Particles were quenched with additional 10 L/min nitrogen before collection.
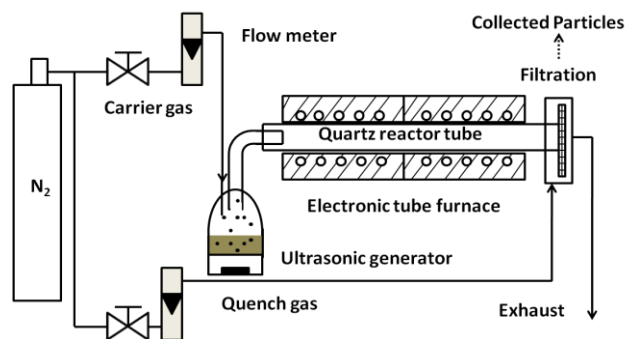
Figure 4.1. Illustration of the co-solvent spray pyrolysis process.

4.3.2. Particle characterization

Scanning electron microscopy (SEM, Hitachi SU-70) was used to image the particles. Particle diameter was manually measured from SEM images. For each particle, the diameter was determined by averaging the value of the vertical distance from the bottom to the top of the particle and the horizontal distance from the left to the right, and a minimum of 200 particle diameters were recorded for each sample. Cross section images

of the particles were achieved by ion beam milling pretreatment (Kratos Minibeam operated at 3.5 kv) and SEM. The particle sample was attached to the conductive paste, and an argon ion beam was directed to the paste with a contact angle of 60 ^{o} and an interaction area of around 1 cm^2. The intensity of the ion beam was approximately 26 μA cm^{-1}. This system was able to remove about a half micron of material in 2 hours. Transmission electron microscopy (TEM, JEOL JEM 2100 LaB6) was also used to examine the hollow structure of the particles. Particles were analyzed by an X-ray diffractometer (XRD, Bruker Smart 1000) with the diffraction angle ranging from 20 ^{o} to 90 ^{o}. Detailed information about crystal structure and phase abundance were obtained from Rietveld refinement. Particle density was measured by the pycnometry method (Micromeritics helium pycnometer). Particle composition was monitored by Fourier transform infrared (FTIR) spectroscopy. For FTIR, the sample and KBr were mixed in a 1:5 mass ratio and then pressed to form a pellet for the analysis. 24 scans were run for each sample with resolution of 4 cm^{-1}. The spectra were collected from 400 cm^{-1} to 4000 cm^{-1}.

4.4. DISCUSSION

4.4.1. Copper powder generated with ET

Particles were generated from 1.2 M copper nitrate solution at temperatures of 400 ^{o}C, 600 ^{o}C, 875 ^{o}C and 1000 ^{o}C. 40 vol% ET was added into the solution as the cosolvent, and a low carrier gas flow rate of 2.5 L/min was used, giving a residence time from 1.5 s to 3.3 s depending on the temperature. XRD of the particles generated at different temperatures (Figure 4.2) showed diffraction peaks located at 43.4 ^{o}, 50.5 ^{o}, 74.2 ^{o}, 90.0 ^{o} and 95.2 ^{o}. These diffraction peaks were attributed to a high symmetry FCC structure of

copper. No copper oxide peaks or any other impurity peaks were detected suggesting that oxide-free copper particles were successfully generated at temperatures ranging from 400 ^{o}C to 1000 ^{o}C. Increasing the temperature did not change the composition of the particles. However, different particle morphologies were detected as shown in Figure 4.3 a-d. At 400 ^{o}C, mainly hollow particles were generated (Figure 4.3 a). At higher temperatures, particles had smoother surfaces, and hollow particles were less prevalent but still always observed at 1000 ^{o}C. When increasing temperature from 400 ^{o}C to 1000 ^{o}C, the average diameter of the particles slightly decreased from 1.2 $\pm$ 0.4 microns to 0.9 $\pm$ 0.4 microns.
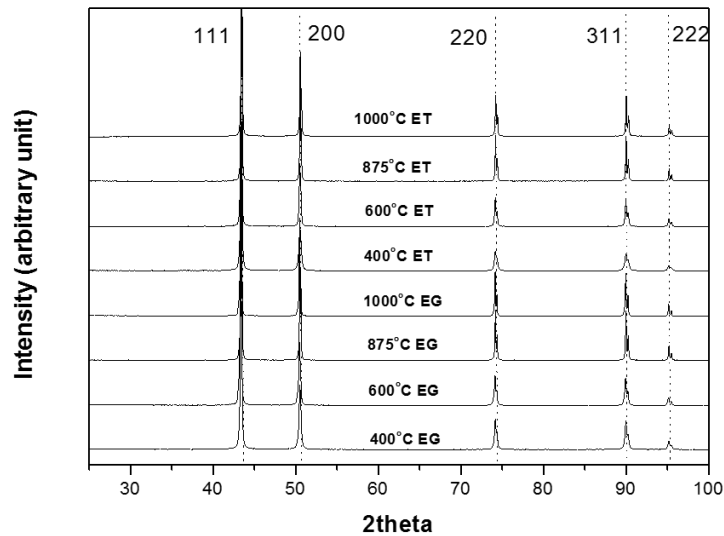
Figure 4.2. XRD of copper particles generated at different temperatures with ethanol (ET) or ethylene glycol (EG).
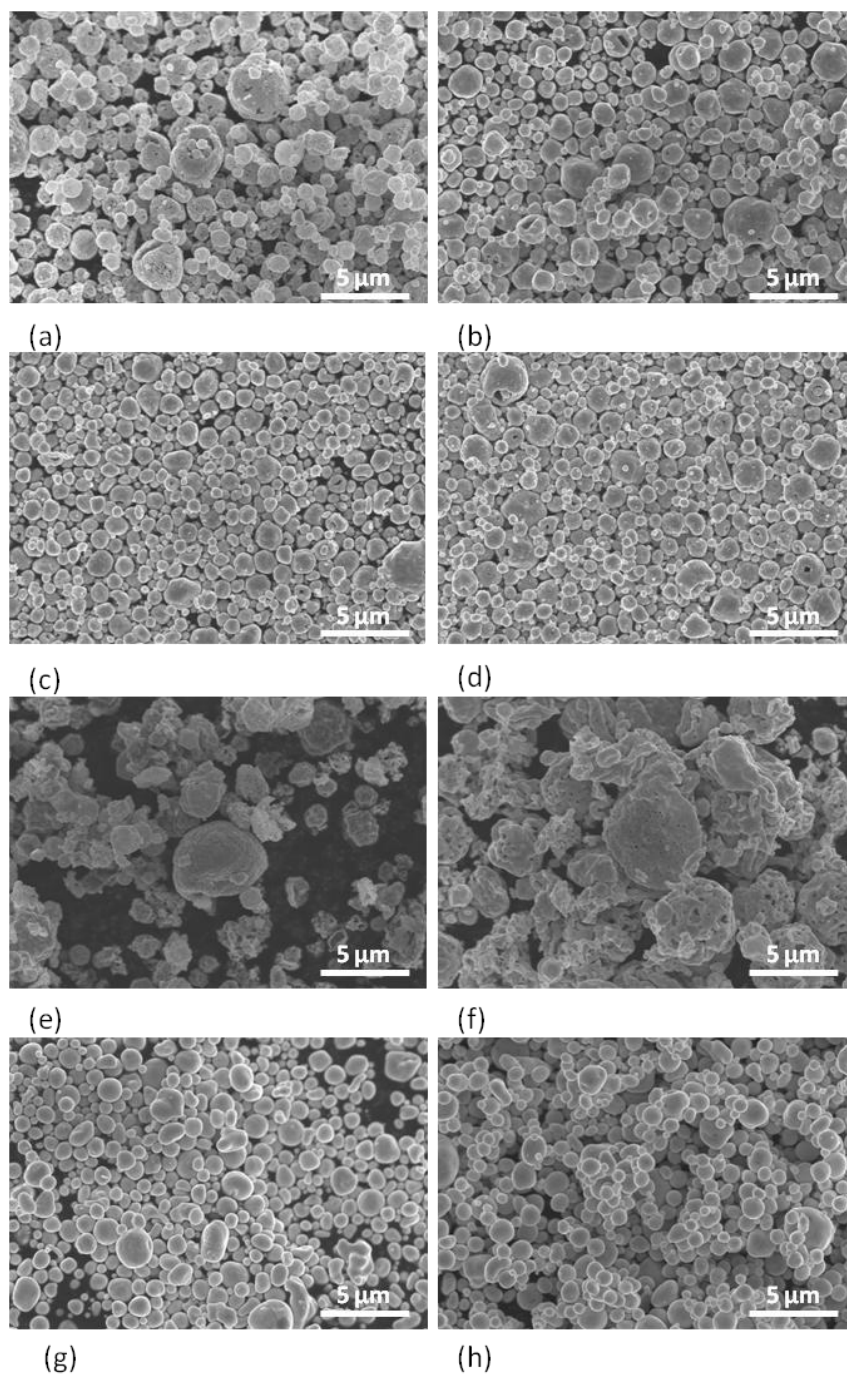
Figure 4.3. SEM images of copper particles generated at (a) 400 ^{o}C with ethanol (ET) (b) 600 ^{o}C with ET (c) 875 ^{o}C with ET (d) 1000 ^{o}C with ET (e) 400 ^{o}C with ethylene glycol (EG) (f) 600 ^{o}C with EG (g) 875 ^{o}C with EG (h) 1000 ^{o}C with EG.

Higher temperatures allow the metal atoms to have a greater mobility promoting densification. However, according to the helium pycnometry result, (Figure 4.4, red line and circle symbols) the particle apparent densities were significantly lower than the pure copper density of 8.9 g/cm^3 and the density decreased with increasing temperature. The greatest density was achieved at 400 ^{o}C rather than at 1000 ^{o}C, and this counterintuitive result may be explained by considering how the density measurement is made. The helium pycnometry test measures the volume of a known mass of particles enabling one to calculate density. At 400 ^{o}C, the particles were hollow with lots of cracks allowing for better permeation of the gas into the particles such that the particles have a smaller volume and therefore a larger density closer to the theoretical value. By increasing the furnace temperature to 1000 ^{o}C, a smoother shell was formed and the gas could not penetrate into the core of the particles causing the volume of the particles to be larger and the density smaller. This was confirmed by TEM images that show the existence of less electron dense regions inside the particles, indicated by the light area in the center of each particle (Figure 4.5 a). Cross section images of copper particles generated at 1000 ^{o}C were obtained by ion beam milling and shown in Figure 4.6 a. Hollow structured particles with solid shells were observed.
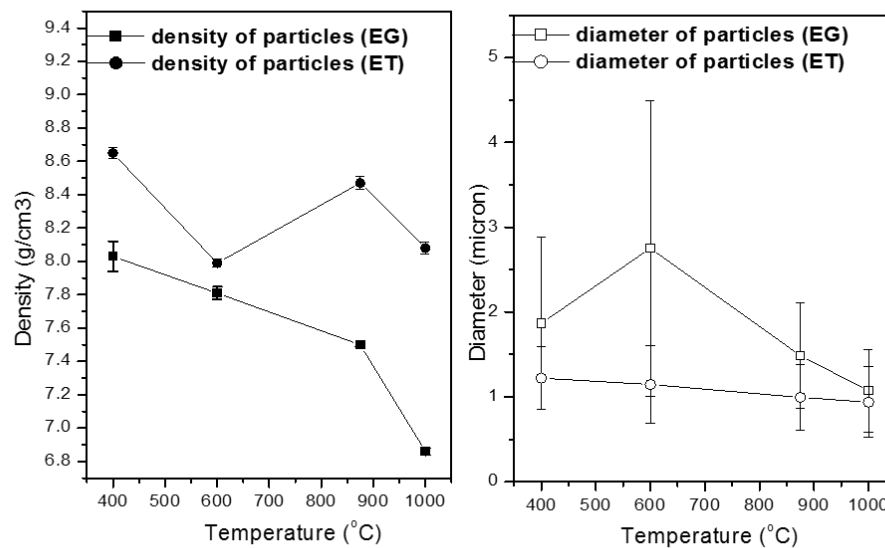
Figure 4.4. Density and number average diameter of copper particles as a function
of furnace operating temperature and cosolvent, ethanol (ET) or ethylene glycol (EG).
The error bars represent measurement uncertainty in the case of density and the standard
deviation of the particle size distribution in the case of diameter.
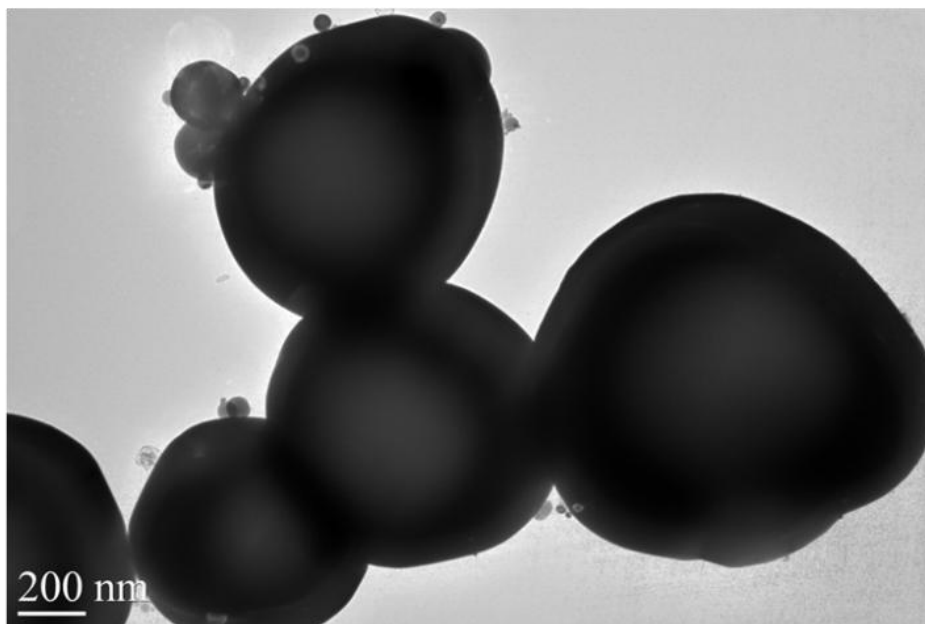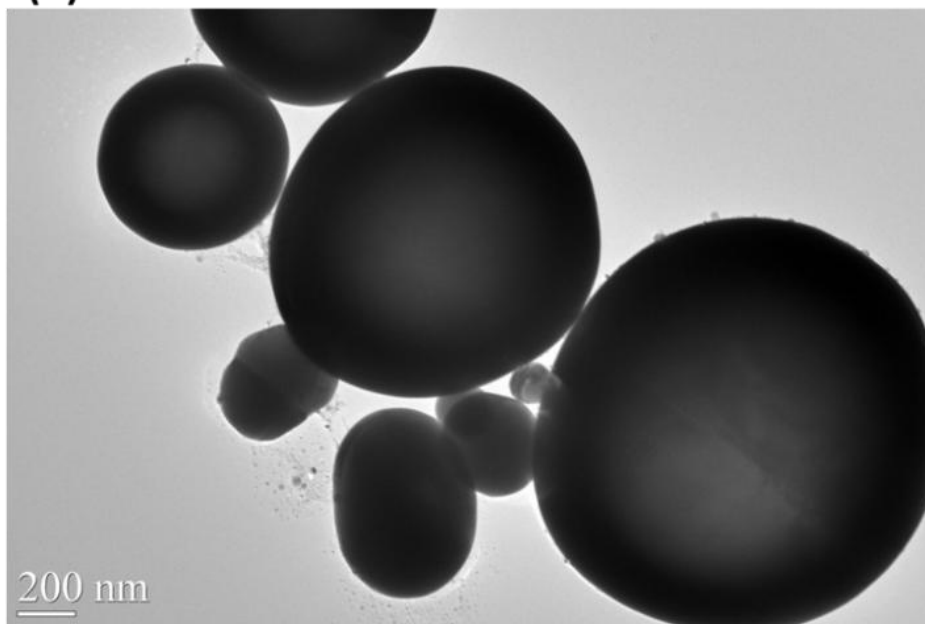
Figure 4.5. TEM pictures of copper particles generated at 1000 ^{o}C with (a) ethanol
and (b) ethylene glycol.
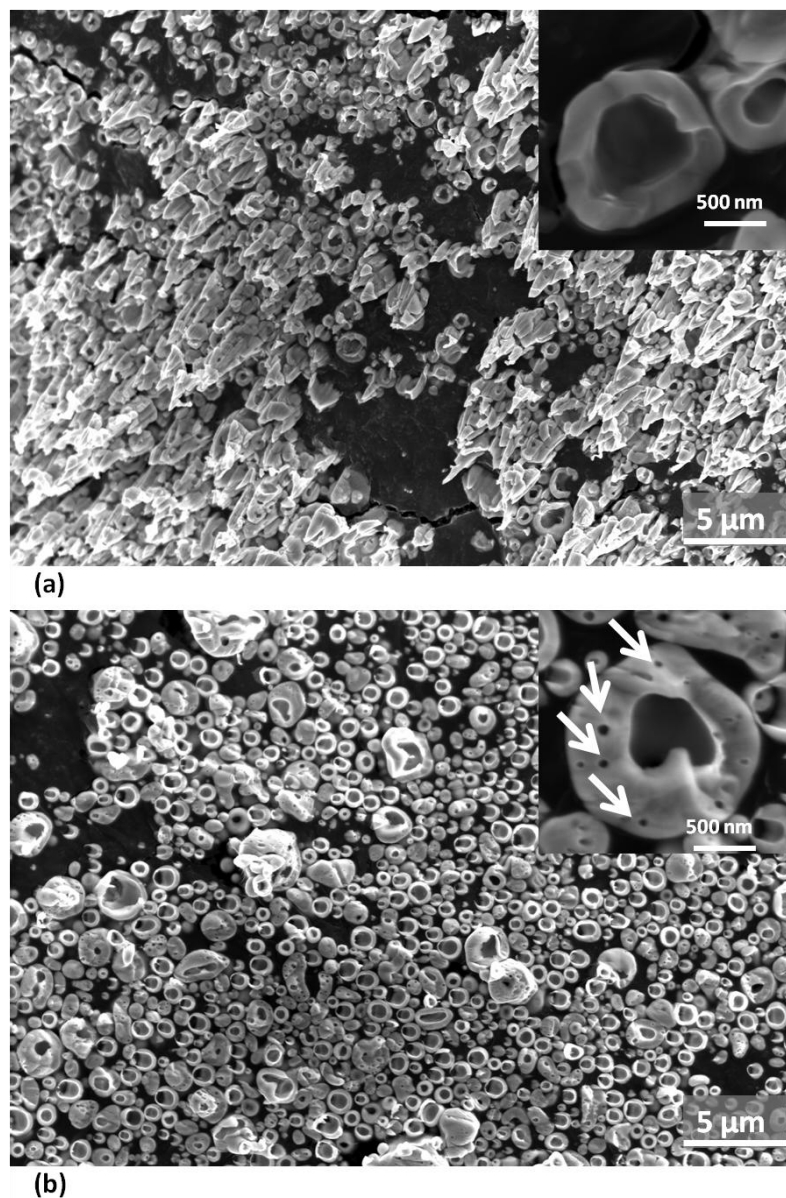
Figure 4.6. (a) SEM pictures of copper particles generated at 1000 $^{\circ}$C with cosolvent of 40 vol% ethanol. Hollow shell structures were observed. The inset image shows representative cross section morphology. (b) SEM pictures of copper particles generated at 1000 $^{\circ}$C with cosolvent of 40 vol% ethylene glycol. Particles have been pretreated by ion bombardment for two hours. When ethylene glycol was used as cosolvent, small pores in the shell wall formed, indicated by white arrows in the inset image.

4.4.2. Copper powder generated with EG

Copper particles were generated using conditions similar to the previous experiments, but with ethanol replaced by ethylene glycol. XRD, SEM images and the density of the particles generated at different temperatures are shown in Figure 4.2, Figure 4.3 e-h and Figure 4.4 (black line with square symbols) respectively. XRD indicates that all the particles were composed of pure copper regardless of the temperature used. SEM images in Figure 4.3 e show that, at 400 ^{o}C, porous particles were generated with pore diameters of less than one hundred nanometers. The average diameter of the generated particles was 1.9 ± 1.0 microns. In Figure 4.3 a, I show the images of particles generated with ET. Most of the particles were hollow, and big cracks could be observed on the surface of the particles. Based on the analysis of the images, I can find the particle morphology exhibited differences because of the change of the cosolvent. The effect of cosolvent on particle morphology became more obvious with a generation temperature of 600 ^{o}C. With ET, each particle had a primary hollow region (Figure 4.3 b), but multiple small pores could be detected on the surface of each particle generated with EG as shown in Figure 4.3 f. Further increasing temperature to 875 ^{o}C and 1000 ^{o}C, particle average diameter decreased to 1.5 ± 0.6 microns and 1.1 ± 0.5 microns respectively. At temperatures higher than 875 ^{o}C, the surface of the particles became smooth, and few hollow particles were observed (Figure 4.3 g and h). Increasing temperature from 400 ^{o}C to 600 ^{o}C, 875 ^{o}C and 1000 ^{o}C, as shown in Figure 4.4, resulted in a density decrease from 8.0 g/cm^3 to 7.8 g/cm^3, 7.5 g/cm^3 and 6.9 g/cm^3. The apparent densities of the particles generated with EG also decreased with increasing temperature. The low density of particles generated at high temperature may also be explained by the hollow shell structure of the particle and

poor permeability of helium. From TEM pictures of particles generated at 1000 ^{o}C (Figure 4.5 b), a significant light area in the center of each particle was observed, suggesting the existence of a shell structure. All particle samples made with EG have relatively lower apparent densities and greater particle size than those made with ET, suggesting that voids inside the particles were more easily formed when EG was used.

Cross section images of copper particles generated with EG at 1000 ^{o}C were obtained by ion beam milling and shown in Figure 4.6 b. Most of the particles show a shell structure with shell thickness of around 100 nm. Small pores were observed in the shell wall, indicated by white arrows. In prior literature (Jain et al. 1997b; Widiyastuti et al. 2007), formation of the shell structure was explained by the temperature and concentration gradient along the radial direction of the droplets that formed during the heating stage of the process. Higher temperatures on the surface of the droplets result in the evaporation of the solvent and the increasing of the precursor concentration within the droplet. Once the concentration is higher than the saturation concentration, the precursor precipitates at the droplet surface. It is believed that the small pores in the wall result from the initial lamellar structure of $Cu_2(OH)_3NO_3$ formed during the precipitation process, which will be discussed later.

4.4.3. Reaction process investigation

When the cosolvent was changed from ethanol to ethylene glycol, a change in particle morphology was observed. In order to better understand the processes occurring during particle formation, short residence time experiments were performed. In these experiments, incomplete reaction occurred and intermediate products and morphologies were observed allowing for a more detailed analysis of the particle formation process. A

larger carrier gas flow rate of 10 L/min was used with only one furnace. Residence time estimates are listed in Table 1. At 400 ^{o}C with 10 L/min carrier gas flow rate, it takes 0.4 s to pass through one furnace, and 3.3 s is needed if 2.5 L/min flow rate and two furnaces are used. All residence times were estimated based on the temperature measured along the furnace center line (J. H. Kim et al. 2003). SEM, XRD and FTIR were employed for the analysis of the particles.

The typical morphology of particles generated at 400 ^{o}C with ET and 0.4 s residence times is shown in Figure 4.7 a. Under these conditions, spherical solid particles with rough surfaces and hollow structures were observed. Similar hollow structures were observed when increasing the furnace temperature to 600 ^{o}C and 875 ^{o}C (Figure 4.7 b and c). The residence times were 0.3 s and 0.2 s correspondingly. According to previous work, a rapid increase in temperature, resulting from high furnace temperatures, will lead to rapid evaporation of solvent and the development of a salt concentration gradient in the droplet (A. Gurav et al. 1993a; Jain et al. 1997b). Once the salt concentration on the surface exceeds the saturation concentration, salt will precipitate out at the surface of the droplet and form a shell around the remaining liquid leading to the formation of hollow particles.
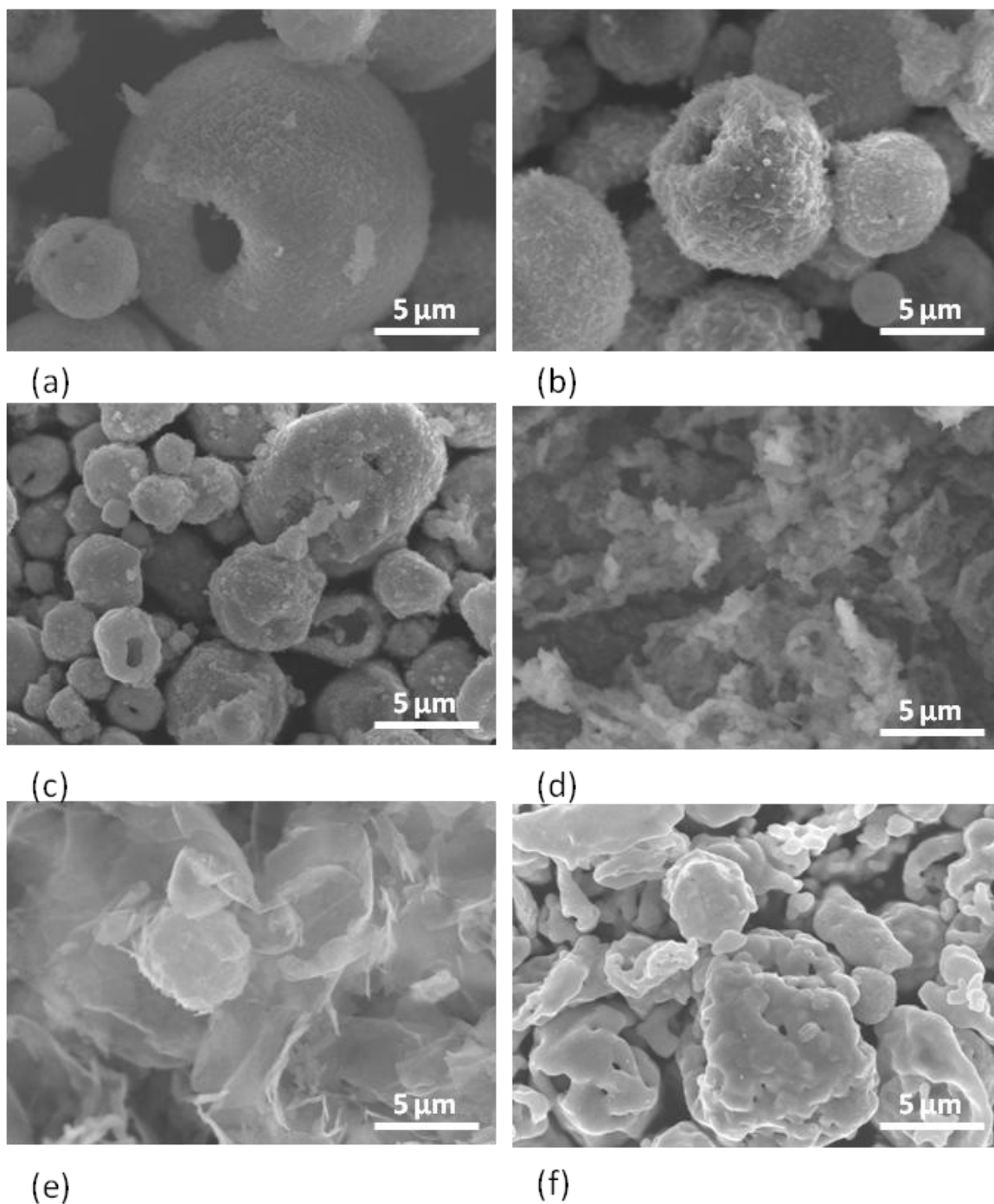
Figure 4.7. SEM images of particles generated under short residence time conditions at (a) 400 ^{o}C with ethanol (ET) (b) 600 ^{o}C with ET (c) 875 ^{o}C with ET (d) 400 ^{o}C with ethylene glycol (EG) (e) 600 ^{o}C with EG (f) 875 ^{o}C with EG.

In addition to the morphology changes, the chemical reaction process was also monitored. In the paper by Kim et. al., they proposed a reaction mechanism for the conversion of a solution of copper nitrate in water to copper particles (J. H. Kim et al. 2003). It was believed that $Cu(NO_3)_2$ decomposed to CuO, which further reduced to pure copper under the highly reducing atmosphere created from ET decomposition at temperatures above 600 ^{o}C. However, XRD results indicated that $Cu(NO_3)_2$ first reacts to give $Cu_2(OH)_3NO_3$. XRD of particles generated at 400 ^{o}C, 600 ^{o}C and 875 ^{o}C with 10 L/min N_2 are shown in Figure 4.8 a, and phase abundances of each composition in the particles were calculated based on Rietveld refinement (Table 4.1). For the 400 ^{o}C sample, the XRD was composed of primary peaks at 12.8, 25.7 and 33.5 ^{o} and a series of small peaks ranging from 20 to 70 ^{o}, belonging to $Cu_2(OH)_3NO_3$ with both monoclinic and orthorhombic crystal structures. Similar decomposition behavior for copper nitrate was also reported by Lvov (Lvov and Novichikhin 1995a) and Jackson (Jackson et al. 1995). Particles generated at 600 ^{o}C were composed of $Cu_2(OH)_3NO_3$, Cu, CuO, and Cu_2O. Signals from CuO and Cu_2O were relatively weak with primary peaks at 39 ^{o} and 36.5 ^{o} respectively, overlapping with the peaks from $Cu_2(OH)_3NO_3$. At 875 ^{o}C, particles were mainly Cu with 10% CuO and 3% Cu_2O.
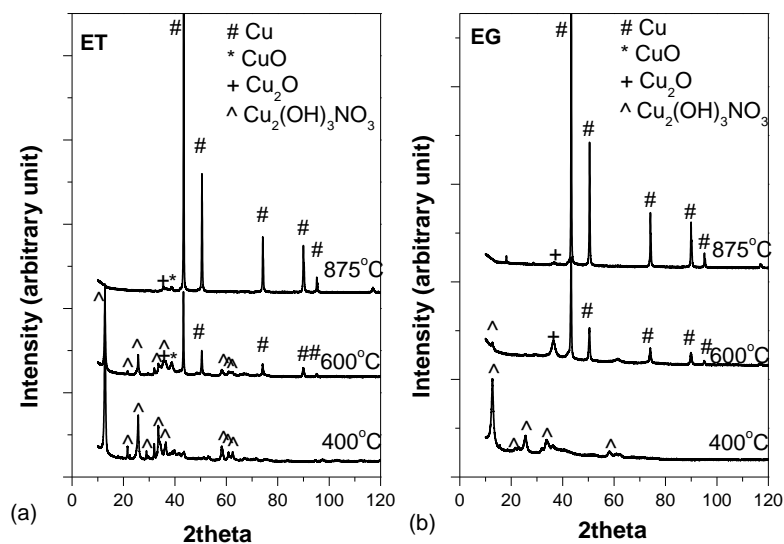
Figure 4.8. XRD of copper particles generated in short residence time at different

temperatures with cosolvent of ethanol (a) and ethylene glycol (b).

Table 4.1. Composition of samples generated under short residence time conditions at
various temperatures. Short residence times were achieved when a single furnace and 10
L/min carrier gas flow rate were used. The residence times listed in brackets were
estimated based on regular experimental conditions, where two furnaces and 2.5 L/min
carrier gas flow rate were used.

Solvent	Temperature (^{o}C)	residence time (s)	Phase abundance (%)			
			$Cu_2(OH)_3NO_3$	CuO	Cu_2O	Cu
ET	400	0.4 (3.3)	100	0	0	0
	600	0.3 (2.5)	26	37	14	23
	875	0.2 (1.7)	0	10	3	87
EG	400	0.4 (3.3)	91	5	4	0
	600	0.3 (2.5)	12	10	29	49
	875	0.2 (1.7)	0	3	1	96

FTIR results are shown in Figure 4.9-left. For the 400 $^{\circ}$C sample, the existence of Cu$_2$(OH)$_3$NO$_3$, was supported by FTIR, which had a strong absorption from 3500 cm^{-1} to 3200 cm^{-1}, attributed to the stretching of O-H bond in Cu$_2$(OH)$_3$NO$_3$. O-N bonds resulted in the absorption at 1420 cm^{-1}. The IR data is consistent with Park's report of Cu$_2$(OH)$_3$NO$_3$,(S.-H. Park and C. E. Lee 2005) except a sharp peak at 1380 cm^{-1}, which can be explained as the bending vibration of C-H in methyl from un-reacted ET. Particles at 600 $^{\circ}$C had similar IR absorption behavior as the 400 $^{\circ}$C sample, but with lower intensity because most of the Cu$_2$(OH)$_3$NO$_3$ has decomposed to CuO and Cu$_2$O. Samples at 875 $^{\circ}$C are mainly composed of Cu, and there was no IR absorption except background from KBr.

In order to see if use of EG results in a similar decomposition process, short residence time experiments were run using 40 vol% EG as the cosolvent. The typical morphology of particles at 400 $^{\circ}$C is shown in Figure 7 (d). Flake and fragment like structures were observed, indicating a different precipitation behavior during the evaporation of solvent when ET was replaced with EG. During the experiment at 400 $^{\circ}$C and 0.4 s residence time, most of the sample on the filter was visibly wet, suggesting that the solvent had not completely evaporated. This is likely because EG is less volatile (vapor pressure of 0.06 mmHg at 20 $^{\circ}$C) compared to water (18 mmHg at 20 $^{\circ}$C) and ET (43 mmHg at 20 $^{\circ}$C) (Speight 2004), and the evaporation rate is dominated by the vapor pressure if droplets are the same size and experience the same temperature history (Pruppacher and Klett 1996; Friedlander 1977). At 600 $^{\circ}$C, I can observe the outline of the particles, and lamellar structures were detected. Upon increasing temperature to 875 $^{\circ}$C, porous particles were generated as shown in Figure 4.7 f.
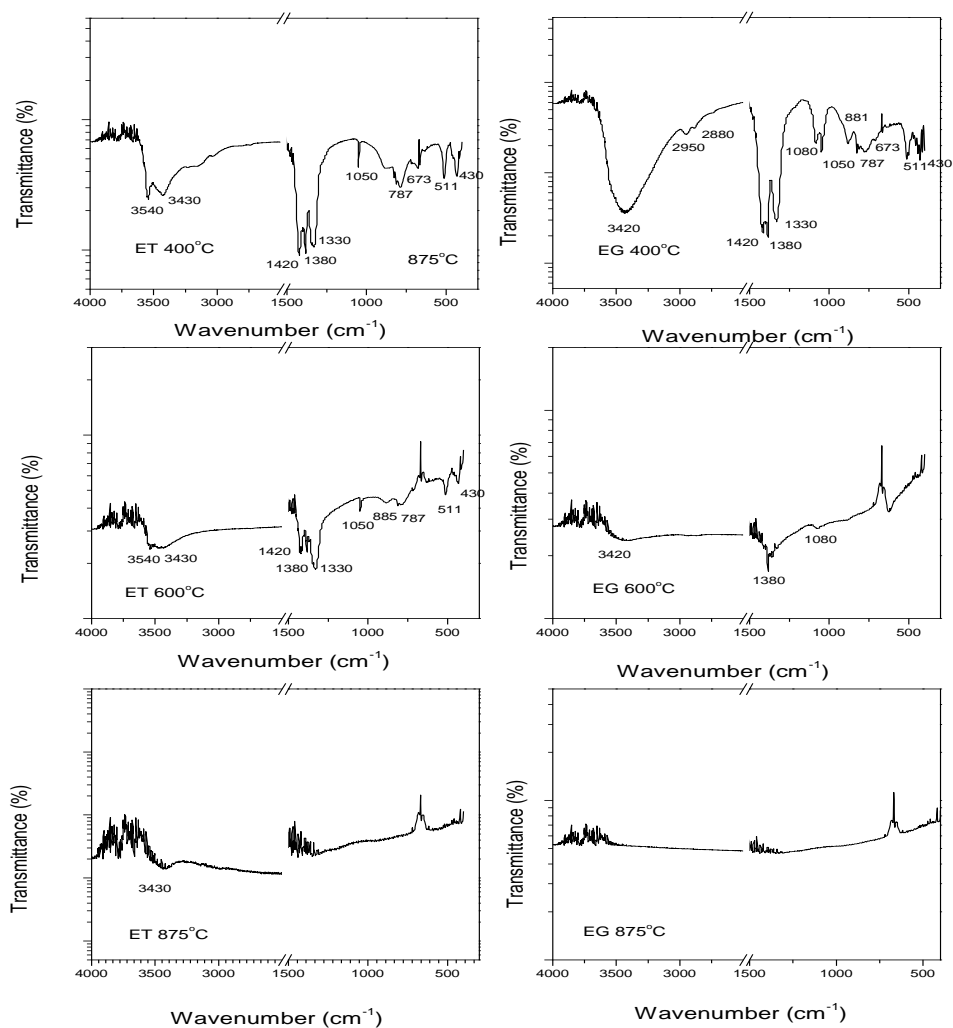
Figure 4.9. FTIR of particles generated in short residence times at different

temperatures with cosolvents of ET (left) and EG (right).

The composition of each sample was calculated based on Rietveld refinement of XRD patterns (Figure 4.8 b) and listed in Table 4.1. 400 ^{o}C samples were composed of 91 mol% $Cu_2(OH)_3NO_3$, with the remainder consisting of 5 mol% CuO and 4 mol% Cu_2O. The diffraction peaks were wider compared with the sample in ET, because EG was not totally evaporated and $Cu_2(OH)_3NO_3$ did not crystallize well. At 600 ^{o}C, strong and sharp

diffraction peaks at 43.4 ^{o}, 50.5 ^{o}, 74.2 ^{o}, 90.0 ^{o} and 95.2 ^{o} resulting from pure Cu were observed, with small diffraction peaks at 36.5 ^{o} and 12.8 ^{o} indicating the existence of Cu_2O and $Cu_2(OH)_3NO_3$. Refinement showed that particles consisted of 49 mol% Cu, 29 mol% Cu_2O, 10 mol% CuO and 12 mol% $Cu_2(OH)_3NO_3$. Particles generated at 875 ^{o}C contained 96 mol% copper, 1 mol% Cu_2O and 3 mol% CuO. The results indicated that EG promotes the formation of copper compared with ET at the same temperature. When ET was used as cosolvent, 23 mol% and 87 mol% Cu were detected in the particles generated at 600 ^{o}C and 875 ^{o}C separately.

FTIR results are shown in Figure 4.9-right. The IR of samples at 400 ^{o}C in EG is similar to the sample in ET, suggesting that both are composed of $Cu_2(OH)_3NO_3$, . The detection of the absorption of O-H from 3500 cm^{-1} to 3200 cm^{-1}, O-N bond around 1420 cm^{-1} and CuO bond vibration at 511 cm^{-1} and 430 cm^{-1} confirms this. However, it is important to note that the sample in EG showed a big broad peak at 3420 cm^{-1} rather than two separated ones which was observed in the ET sample from the $Cu_2(OH)_3NO_3$. This is because some EG was still in the sample as indicated by the stretching vibration of OH which has a broad absorption peak at 3370 cm^{-1}. Therefore the peak detected at 3420 cm^{-1} in the EG generated sample is a combination of three peaks at 3450 cm^{-1}, 3430 cm^{-1} and 3370 cm^{-1}. The existence of EG in the sample was also supported by the signals at 2950 cm^{-1} and 2280 cm^{-1} from C- C bond vibration and 1080 cm^{-1} from stretching vibration of C-O bond. Samples generated at 600 ^{o}C had weak FTIR signal with peaks at 3420 cm^{-1}, 1380 cm^{-1} and 1080 cm^{-1}. These peaks indicated that even at 600 ^{o}C, there was still some EG in the particles. The 875 ^{o}C sample was pure copper and led to no IR absorption except the background of KBr.

4.4.4. Proposed process mechanism

Considering all of the information from SEM, XRD and FTIR, I propose a copper particle formation process with ET as illustrated in Figure 4.10 a. After the evaporation of ET and water, copper nitrate hydrolyzes to $Cu_2(OH)_3NO_3$ which then decomposes to CuO and Cu_2O. Rapid evaporation of water and ET promote the formation of a concentration gradient in the droplet and the formation of hollow structures. The final step is the reduction of copper oxide in the reducing atmosphere created by ET decomposition. When particles are generated in EG, a different precipitation process takes place as shown in Figure 4.10 b. As droplet temperature increases, water evaporates, and $Cu(NO_3)_2$ hydrolyzes to $Cu_2(OH)_3NO_3$ with most of EG still in a liquid state resulting in the formation of a $Cu_2(OH)_3NO_3$ layer on the surface. Then these $Cu_2(OH)_3NO_3$ precipitates combine to make porous particles, which have a structure as observed in Figure 4.3 e and f. Higher temperatures and longer residence times allow the melting of the lamellar structure, resulting in the shell. It is hypothesized incomplete fusing leaves small pores in the wall as shown in Figure 4.6. Copper oxide could be reduced either by the CO and H_2 resulting from the decomposition of EG, or by reaction with EG when both were present.
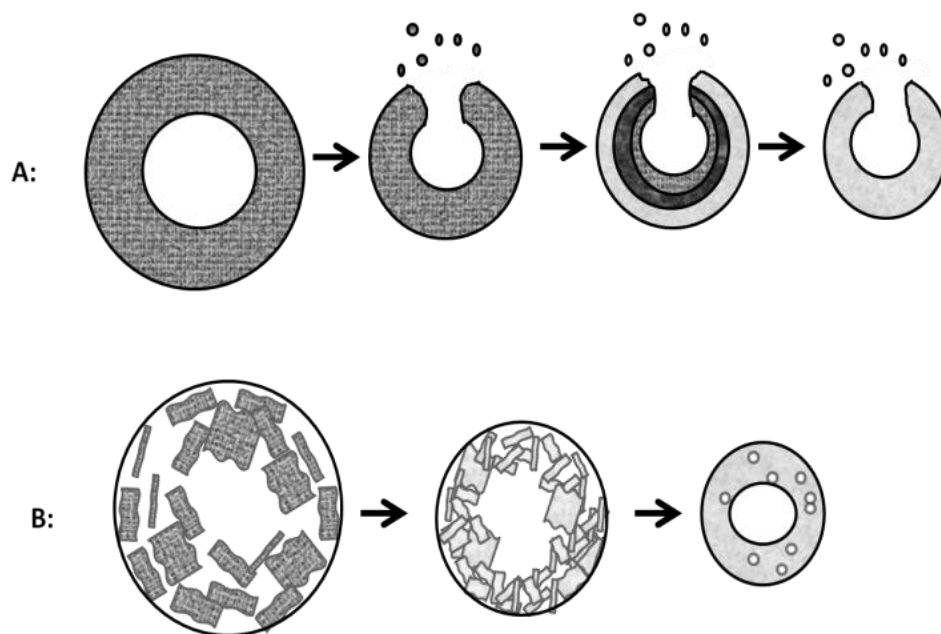
Figure 4.10. Illustration of possible copper particle formation process with cosolvents of (a) ethanol (b) ethylene glycol.

4.5. CONCLUSIONS

Copper particles were generated by a cosolvent spray pyrolysis process at furnace temperatures ranging from 400 ^{o}C to 1000 ^{o}C with 40% ethanol (ET) or ethylene glycol (EG) used as a cosolvent with nitrogen gas as the carrier gas. It is found that using ET as the cosolvent resulted in copper particles with a significant fraction of hollow structures, and big cracks were observed on the particle surface, while the use of EG resulted in porous structures at 400 ^{o}C and 600 ^{o}C, and hollow shell particles with smooth surfaces at 875 ^{o}C and 1000 ^{o}C. Because of the better gas permeation into hollow structure compared to porous and shell structures, particles generated with ET had an apparent density greater than those produced with EG. With either ET or EG, particle density was lower than the theoretical value, and decreased with increasing temperature. The decrease in density

76

with increasing temperature indicates that formation of hollow shell like particles is promoted by high furnace temperatures.

The reaction process was then investigated by short residence time experiments. Results indicated that copper nitrate first hydrolyzed to $Cu_2(OH)_3NO_3$, and then decomposed to CuO and Cu_2O, which was then reduced to pure copper. Differences in the evaporation rate of ET, EG and water resulted in the different precipitation behavior of $Cu_2(OH)_3NO_3$, which affected the morphology of the product particles.

Results from both standard and short residence time experiments indicated that the formation process and resulting particle morphology were strongly dependent on the cosolvent used. ET leads to denser particles, but hollow structured particles could not be completely eliminated even at 1000 ^{o}C. EG promotes the formation of copper at lower temperatures compared with ET. In experiments, micron sized spherical oxide free copper particles with smooth surfaces were generated with a cosolvent of EG at lowest temperature of 875 ^{o}C in 1.7 s, but void spaces inside the EG generated particles were observed.

Chapter 5: A spray pyrolysis approach for the generation of patchy particles

5.1. ABSTRACT

Bimetallic CuNi, AgNi and AgCu particles were generated by a spray pyrolysis process at 1000 ^{o}C using a cosolvent of ethylene glycol (EG). CuNi particles composed of 60 at% Cu and 40 at% Ni formed an uniform alloy. AgNi and AgCu particles consisting of 60 at% Ag/40 at% Ni and 60 at% Ag/40 at% Cu were generated, and different patchy structures were observed. AgNi particles were composed of a Ni core with most of the surface covered by Ag. AgCu particles had a two phase lamellar structure probably formed from a spinodal decomposition. The structure of AgCu particles could be varied by reducing the furnace temperatures and changing the composition of the precursor. These results indicate the potential of spray pyrolysis as a patchy particle generation method.

5.2. INTRODUCTION

A particle with precisely controlled dual or multiple patches of varying compositions is known as a "patchy particle". Patchy particles have been attracting attention in recent years because of the possibility of multiple surface functionalities and their use as building blocks in mesoscale particle assemblies (Glotzer and Solomon 2007; Zhang and Glotzer 2004; Pawar and Kretzschmar 2010). A Janus particle is the simplest example of a patchy particle with two hemispheres of different components (Casagrande et al. 1989; Degennes 1992; Paunov and Cayre 2004; Roh, Martin and Lahann 2005). Wide applications of Janus particles in photonic crystals (Liddell, Summers, and Gokhale 2003;

78

Cayre, Paunov and Velev 2003), drug delivery systems (Champion, Katare and Mitragotri 2007; Langer and Tirrell 2004), sensors (Takei and Shimizu 1997; Walther and Müller 2008; Ozin et al. 2005; Sundararajan et al. 2008; Nisisako et al. 2006; Anker et al. 2005) and electronics (Gratzel 2001) have been reported.

A variety of methods have been explored for the generation of patchy particles, such as the templating, vapor deposition, nanosphere lithography, and capillary fluid flow methods. The templating method (Cui and Kretzschmar 2006; Hong, Jiang and Granick 2006; Petit et al. 2001; Boker et al. 2007; Zhang et al. 2009) employs a template to cover part of the particle's surface, with the rest of the surface modified by reagents. Janus particles with a single patch could be generated after the template was removed. Vapor deposition requires a monolayer of particles to be closely packed (Takei and Shimizu 1997; Zhao et al. 2002). The relative angle of deposition respective to the particle layer is usually modified to control the patchy areas and shapes. Nanosphere lithography (Haynes and Duyne 2001; Himmelhaus and Takei 2000; Deckman and Dunsmuir 1982) uses nanospheres to mask the surface, and patches are generated by chemical vapor deposition. The resolution of the patch size and shape could be as small as the size of the nanospheres. The capillary fluid flow method employs microfluidic channels for the generation of multiphase polymer particles (Roh et al. 2005; Roh, Martin and Lahann 2006; Nisisako, Torii and Higuchi 2004). Advantages and disadvantages of these methods and other technologies, such as particle lithography, colloidal assembly, and polyamine-guided synthesis, are summarized in a recent review by Kretzschmar (Pawar and Kretzschmar 2010). Unfortunately, there is no simple scalable method that yields precise control of particle patchiness.

In this chapter, I tested ultrasonic spray pyrolysis as a potential patchy particle generation method. Spray pyrolysis is a simple one-step synthesis process and is widely studied for the generation of various metal and metal oxide particles (Gurav et al. 1993b; NAGASHIMA et al. 1987; Stopic et al. 1996; Pluym et al. 1993; Okuyama and Wuled Lenggoro 2003; Jian et al. 2007; Choa et al. 2003). Advantages of ultrasonic spray pyrolysis include the capability of scalable production and adjustable particle size from submicron to several microns. During the process, the precursor, typically a metal nitrate solution, is sprayed into droplets, which are then carried by a carrier gas into a tube furnace. In the tube furnace reactor, the metal nitrate decomposes to the oxide. The oxide then reduces to metal in a reductive atmosphere. A cosolvent was implemented in the precursor solution to create the reductive atmosphere and improve the safety of the technology (Kim et al. 2003). AgNi, CuNi and AgCu bimetallic particles were generated by this process in the lab. Various patchy structures of the particles were observed. The results indicated that the structure of particles mainly depended on the particle composition and could be controlled by the operating conditions.

5.3. EXPERIMENT

The bench scale spray pyrolysis system used here includes an ultrasonic droplet generator, a reactor consisting of a quartz tube heated by a reactor tube furnace and a filtration system as illustrated in privious chapter (Figure 4.1). During the process, the metal nitrate precursor solution was atomized and sent into the hot tube furnace reactor. In the reactor, the metal nitrate salt decomposed to oxide and then reduced to pure metal with the assistance of the cosolvent. In order to generate bimetallic particles, a mixture of metal

nitrates was used as the precursor. Particle size was determined by the total concentration of the precursor and could be roughly estimated by Equation 5.1.

$$D_p = D_d \sqrt[3]{\frac{M_1 C_1}{\rho_1} + \frac{M_2 C_2}{\rho_2}}$$ ……………………………………………………………..(5.1)

where D_p is the diameter of the particle, D_d is the diameter of the droplet, M is the molecular weight of the metal nitrate, C is the concentration of the nitrate and ρ is the density of the metal. The subscripts 1 and 2 represent the different metal and metal nitrate respectively.

In the experiments, AgNi, AgCu and CuNi bimetallic particles were generated. The ratio of metal nitrates in the precursor solution was selected according to the desired particle compositon. In every experiment, the total concentration (M_1+M_2) in the solution was 1.2 M, and 40 vol% cosolvent was used. For example, $Ag_{0.6}Ni_{0.4}$ particles were generated from an aqueous solution of $AgNO_3$ (99.5%, Strem) and $Ni(NO_3)_2$ (99.5%, Strem) composed of 0.72 M $AgNO_3$ and 0.48 M $Ni(NO_3)_2$. In order to make the precursor, 10.19 g $AgNO_3$ and 17.45 g $Ni(NO_3)_2$*$6H_2O$ were first disolved in a small mount of water. Then 40 ml ethylene glycol (EG) (99% Sigma Aldrich) was added into the solution as the cosolvent. Finanlly more water was added until the total volume of the solution was 100 ml.

The precursor solution was atomized by a custom built ultrasonic generator operated at a frequency of 1.7 MHz. The precursor droplet volume mean diameter was 5±2 μm, measured by the Malvern Ensemble Particle Condensation and Size (EPCS) system, which was based on the light scattering behavior of the droplets (Kim et al. 2003). The

tube reactor, of total length 81 cm, was placed in the furnace and operated at temperatures ranging from 750°C to 1000 °C. 2.5 L/min industrial nitrogen (95%, Airgas) was used to carry the droplets from generator to furnace. The residence time was defined as the time for the droplet to pass through the heated zone, from the beginning to the end of the furnace. It varied from 1.5 s to 2 s depending on the furnace operating temperature. Downstream of the furnace, industrial grade 10 L/min nitrogen (95%, Airgas) was used as a quench gas to cool down the generated particles. The final product was collected by filtration.

Scanning electron microscopy (SEM, Hitachi SU-70) was used to image the particles. For each particle, the diameter was determined by averaging the value of the vertical distance from the bottom to the top of the particle and the horizontal distance from the left to the right, and a minimum of 200 particle diameters were recorded for each sample. In order to observe the internal patchy structure of AgCu particles, Cu was removed by dipping AgCu particles into 2 M $FeCl_3$ solution. After 2 hours of ultrasonic treatment, the Cu phase was completely dissolved in the $FeCl_3$. Pretreated particles were separated by centrifuge, washed by distilled (DI) water and dried at room temperature. All the particles were examined with an X-ray diffractometer (XRD, Bruker Smart 1000) with the diffraction angle ranging from 20° to 90°. More detailed information about crystal structure and phase abundance was obtained from Rietveld refinement.

5.4. RESULTS AND DICUSSION

5.4.1. AgNi particle generation

AgNi bimetallic particles were generated by the cosolvent assisted spray pyrolysis process from a 60 at% $AgNO_3$ and 40 at% $Ni(NO_3)_2$ water solution. XRD results of the AgNi particles are shown in Figure 5.1 a. The result indicated that particles were composed of metallic phases of silver and nickel, both belonging to the space group of Fm3m. Primary diffraction peaks were located at 38 ^{o}, 44 ^{o} and 65 ^{o} from Ag, and peaks at 44 ^{o}, 52 ^{o} and 76° were attributed to the existence of Ni. Rietveld refinement indicated that particles were composed of 62 at% Ag and 38 at% Ni, close to the ratio in the precursor. The small deviation was possibly due to the calculation uncertainty of the refinement. Spherical particles with diameters of 0.6±0.3 micron were observed from backscatter SEM images as shown in Figure 5.1 b. The particle surfaces were mostly light with a small fraction appearing dark. EDS mapping (Figure 5.1 c) indicated that the light surface area contained a high concentration of silver, which was represented by red dots in the mapping images, and the dark area on the surface was enriched in Ni, represented by green in the mapping image. Quantitative analysis of EDS suggested a composition of 75±3 at % Ag and 24±3 at % Ni. Compared with the XRD result, a higher ratio of Ag was obtained from EDS. This is expected because EDS is a surface analysis technology, while XRD gives the phase abundance in the entire sample. EDS and XRD results indicated that the particles were most likely composed of a Ni core and a nearly continuous Ag layer on the surface.

The formation of the Ag layer on the surface could be attributed to two reasons. One is the immiscibility of Ag and Ni according to the phase diagram (Figure 5.1 d), and the

other is the small wetting angle between Ag and Ni; in helium silver was reported to form a 9 $^{\circ}$ contact angle on nickel(Nagesh and Pask 1983). During the particle formation process, $AgNO_3$ and $Ni(NO_3)_2$ hydrolyzed and decomposed to oxide, and then oxide was reduced to metallic Ag and Ni in the reducing atmosphere created by the cosolvent. Referring to the phase diagram of the Ag-Ni system, Ag and Ni have melting points at 961 $^{\circ}$C and 1455 $^{\circ}$C, and Ag and Ni are nearly immiscible below these melting points. Thus after particles reach 1000 $^{\circ}$C, solid Ni and liquid Ag may coexist, and the two phases should separate. The small wetting angle between Ag and Ni will allow the liquid silver to spread over and cover the Ni surface. At the end of the furnace, 10 L/min nitrogen was used as quench gas to cool down the particles. As particles were cooled down, liquid Ag solidified to a nearly continuous layer on the surface of the particle.

(a)

(b)

(c)

Atomic Percent Silver
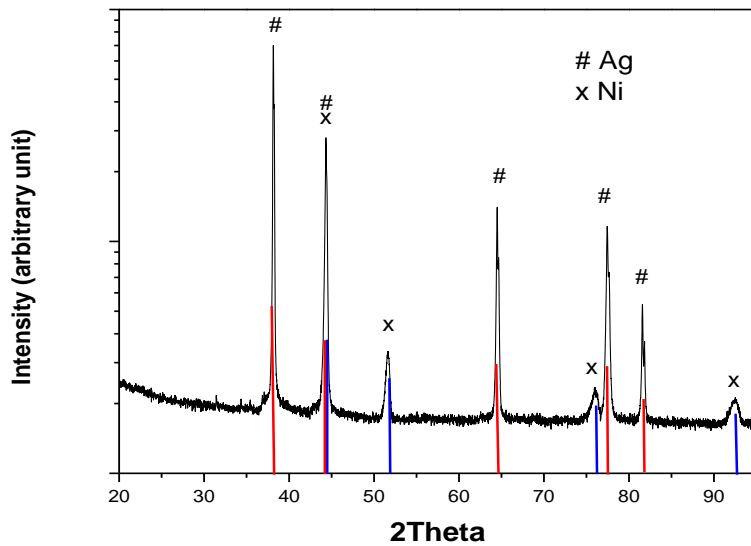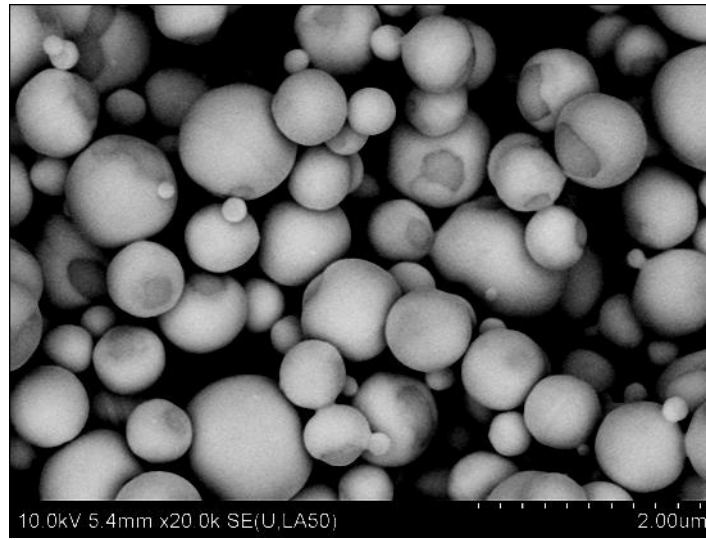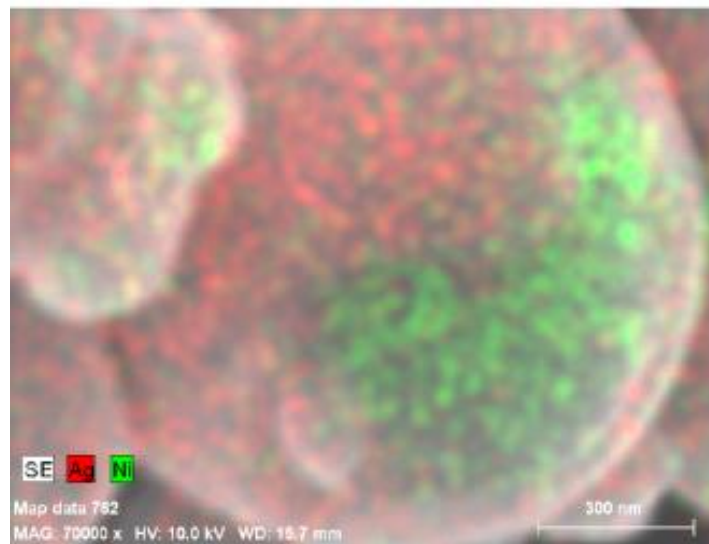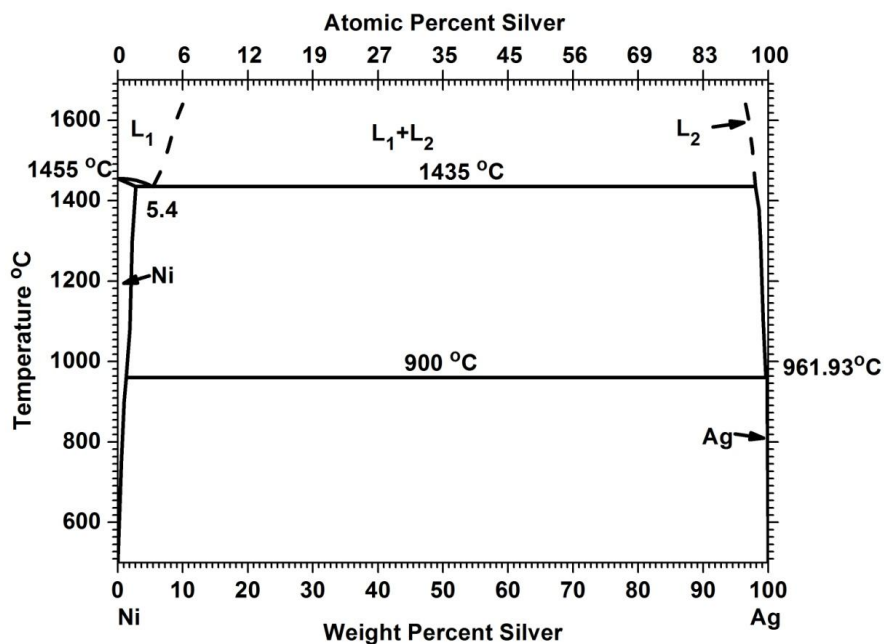
(d)

Figure 5.1. (a) XRD of AgNi particles, which were composed of 60 at% Ag and 40 at% Ni and generated at 1000 ^{o}C (b) Backscatter SEM images of AgNi particles (c) EDS mapping of AgNi particles and (d) phase diagram of Ag-Ni bimetallic system, adapted from the ASM Handbook (Asm 1992).

5.4.2. CuNi particle generation

In addition to AgNi particle generation, spray pyrolysis was applied to the generation of CuNi bimetallic particles with 60 at % Cu and 40 at % Ni. A $Cu(NO_3)_2$ /$Ni(NO_3)_2$ mixture solution with 40 volume % of EG was used as the precursor. Particle XRD results are shown in Figure 5.2 a, and three strong diffraction peaks at 44°, 51 ^{o} and 75° indicate that the particles were composed of a single alloy phase. In the SEM images (Figure 5.2 b), spherical particles were observed. EDS mapping (Figure 5.2 c) showed a uniform distribution of Cu and Ni on the surface, represented by red and green dots

86

respectively. Quantitative analysis of the EDS gave a surface composition of 63±3 at% Cu and 37±3 at% Ni. This composition is close to the initial ratio of Cu and Ni in the precursor, and also indicated that there were no differences in the composition between the surface and the center of the particles. According to the phase diagram (Figure 5.2 d), CuNi alloy is the thermodynamically favored state at temperatures between 354 ^{o}C and 1064 ^{o}C, which is the melting point of pure copper. At the operating temperature of 1000 ^{o}C, Cu and Ni were mixed at the atomic level, and a single alloy phase was generated to achieve a lower free energy of the system.
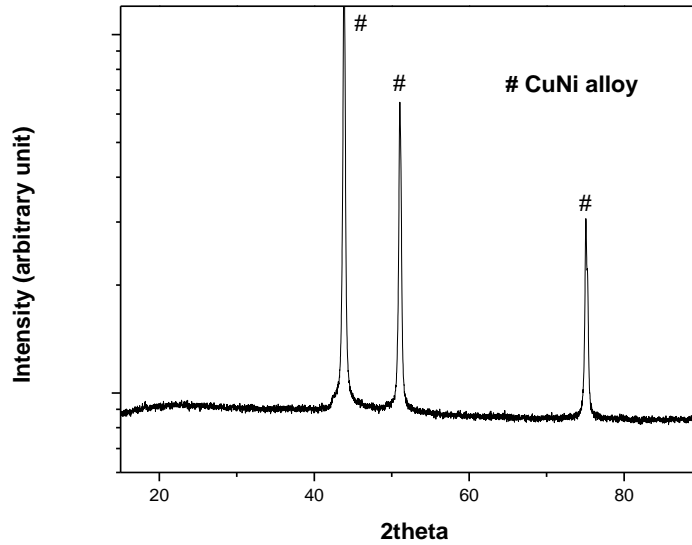
(a)
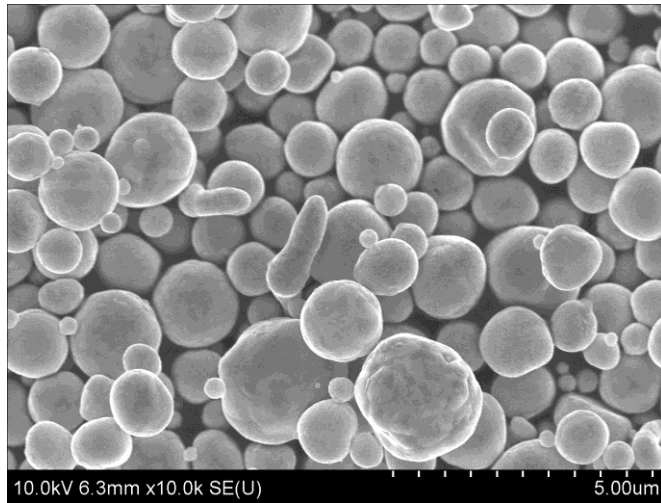
(b)
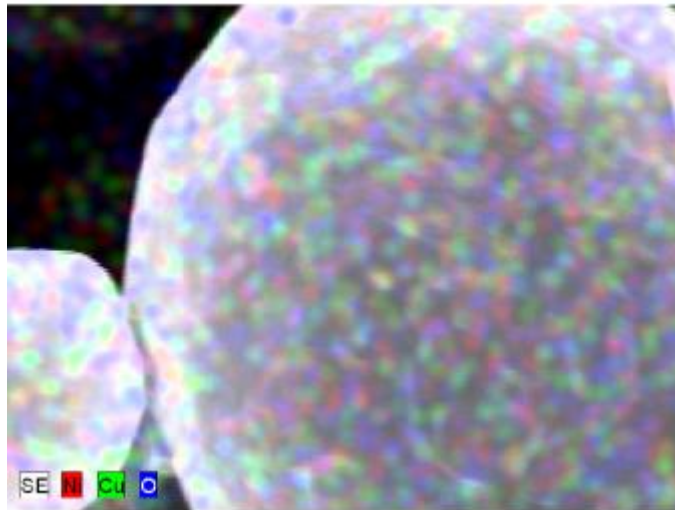
(c)
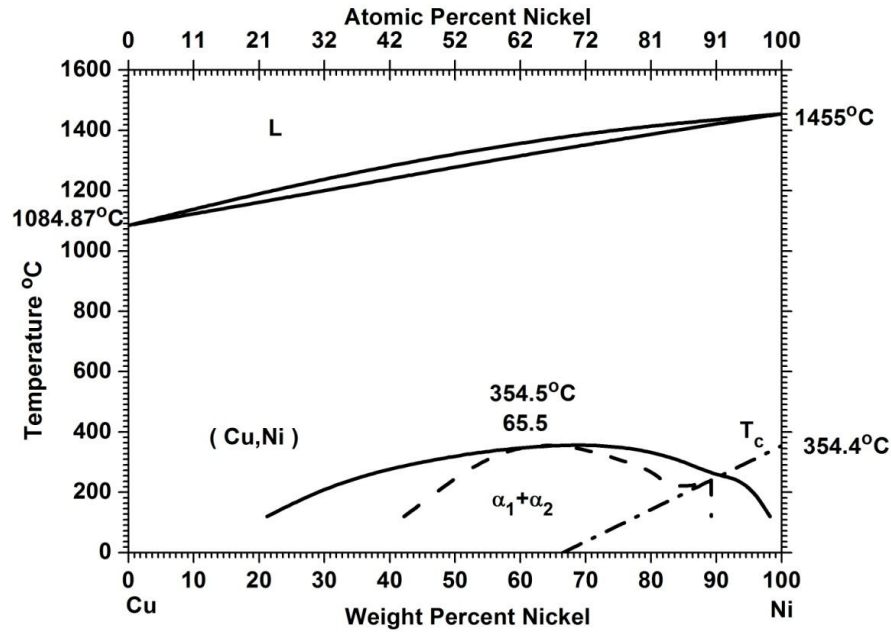
(d)

Figure 5.2. (a) XRD of CuNi particles, which were composed of 60 at% Cu and 40 at% Ni and generated at 1000 ^{o}C (b) SEM images of CuNi particles (c) EDS mapping of CuNi particles and (d) phase diagram of the Cu-Ni bimetallic system, adapted from the ASM Handbook (Asm 1992).

5.4.3. AgCu particle generation

More complicated particle structures were observed when spray pyrolysis was applied to the generation of AgCu particles. The concentration of $AgNO_3$ and $Cu(NO_3)_2$ in the precursor solution was controlled so that 60 at % Ag and 40 at % Cu were contained in the solution. XRD results of the particles are shown in Figure 5.3 a, and indicate that particles were composed of two phases. One is a Ag rich solid solution leading to the diffraction peaks at 38.8 ^{o}, 45 ^{o} and 65.4 ^{o} A right shift of the diffraction peaks of Ag solid solution was observed, compared with the diffraction peaks of pure Ag labeled by

89

the green line. This is because the impurity of Cu in the Ag solid solution will lead to a reduction in the cell dimensions, and then diffraction peaks will move to the larger angle according to the Bragg equation. Rietveld refinement indicated that the Ag solid solution was composed of 91 at% Ag and 9 at% Cu. Another phase detected in the particles is a Cu rich solid solution with a composition of $Cu_{91}Ag_9$. Diffraction peaks at 43.2 ^{o}, 50.2 ^{o} and 73.6 ^{o} were attributed to the Cu solid solution and shifted toward smaller angles compared with the diffraction peaks from pure Cu, which are labeled by the red line. The composition of the particles is 62at% Ag and 38 at% Cu, quite close to the initial ratio of 60 at % Ag and 40 at % Cu.

Backscatter SEM images are shown in Figure 5.3 b. Because of the different composition between Ag solid solution and Cu solid solution, a contrast was observed in the image of the particle surface. Areas with different gray shades represented Ag rich and Cu rich solid solutions. These two solid solutions are intermingled with a complicated nanoscale structure. EDS mapping (Figure 5.3 c) showed a mixture of green dots and red dots representing Ag and Cu respectively. There is no obvious nanostructure detected from EDS mapping because of the spatial resolution limit of the equipment. Quantitative analysis of EDS suggested a composition of 59±2 at% Ag and 41±5 at% Cu in agreement with the salt concentration in the precursor.

In order to further investigate the structure of the AgCu particles, the Cu rich solid solution phase in the particles was removed by etching using a $FeCl_3$ solution. A SEM image of an Ag rich solid solution skeleton with a spherical outline is displayed in Figure 4 d. Strips were mostly in a direction normal to the surface with a distance between adjacent strip layers of around 50 nm. The lamellar structure of particles indicates a

possibility of eutectic decomposition. As shown in the phase diagram (Figure 4 e), Ag-Cu alloy has an eutectic temperature of 779 ^{o}C, which is lower than the furnace operating temperature of 1000 ^{o}C, so in the furnace, the temperature is high enough for melting and complete mixing of Ag and Cu. During the quench process, the cooling of the particles led to a supercooled state possibly resulting in the spinodal decomposition and in the formation of the bimetallic layer as observed in Figure 5.3 d.
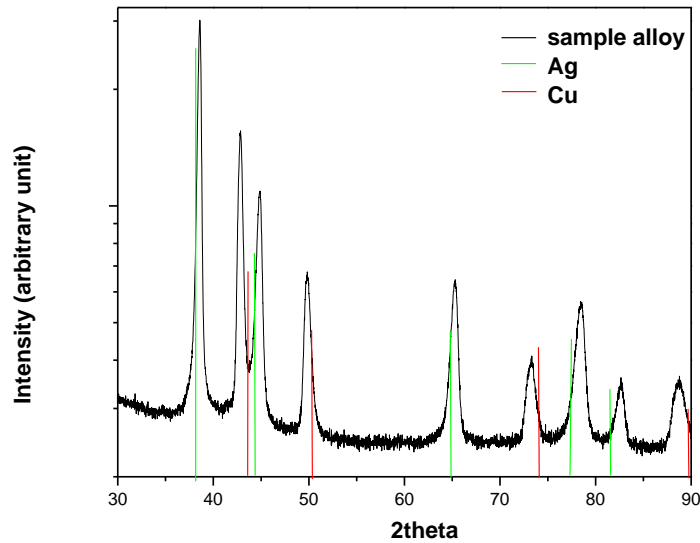
(a)
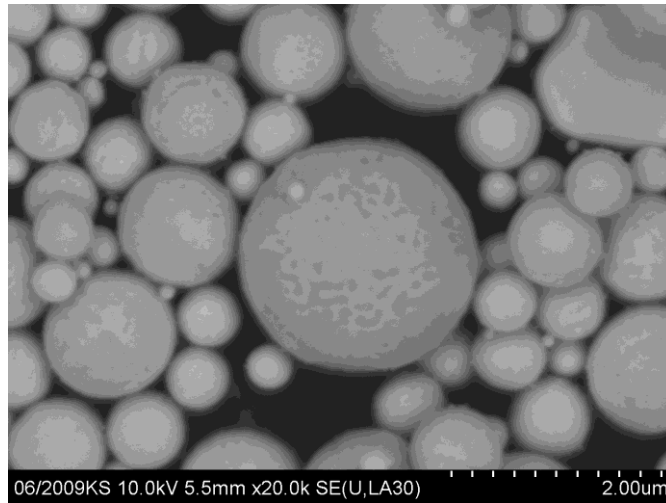
(b)
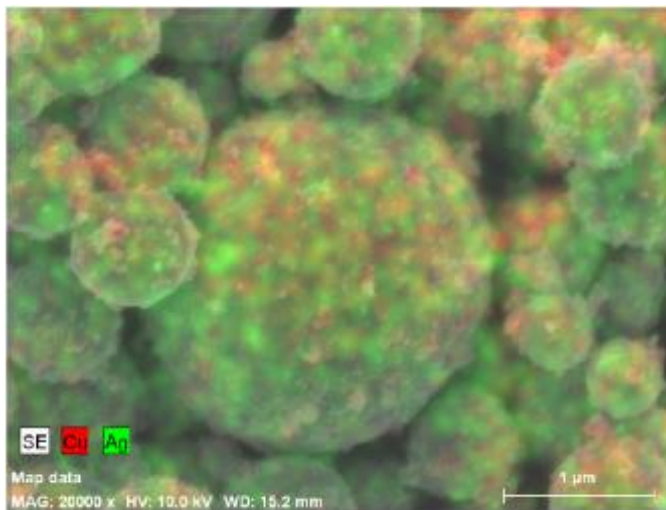
(c)
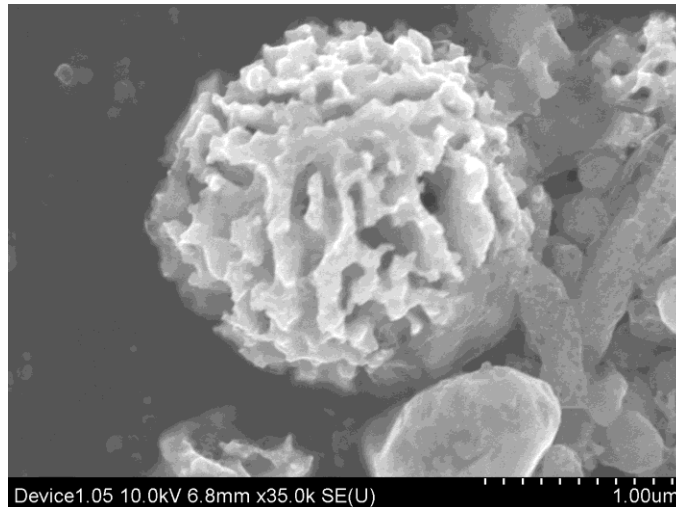
(d)
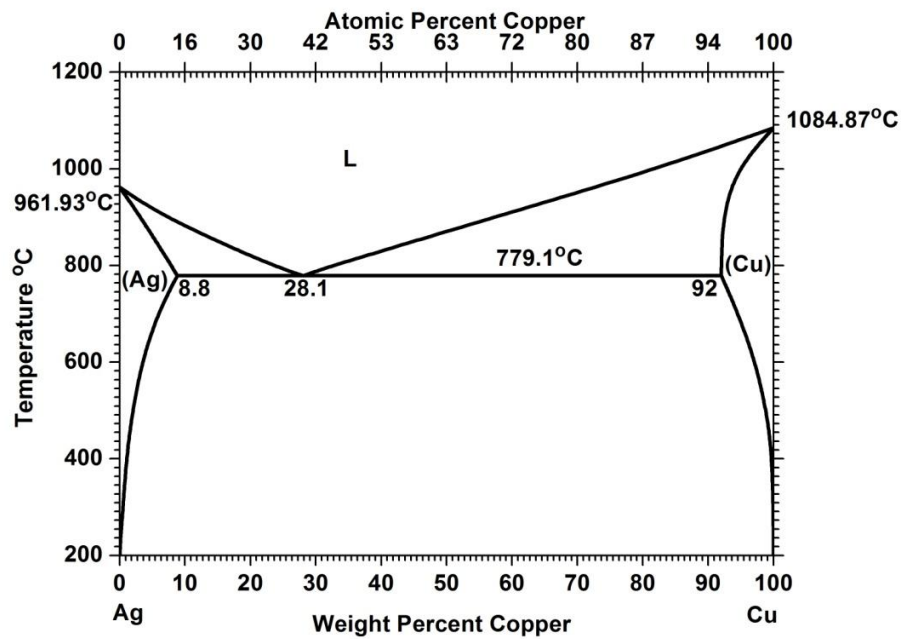
(e)

Figure 5.3. (a) XRD of AgCu particles, which were composed of 60 at % Ag and 40 at %

Cu and generated at 1000 ^{o}C (b) Backscatter SEM images of AgCu particles (c) EDS

mapping of AgCu particles (d) SEM images of AgCu bimetallic particles with Cu solid

solution removed and (e) Phase diagram of the AgCu bimetallic system, adapted from the

ASM Handbook(Asm 1992).

The bimetallic layers were composed of Ag rich and Cu rich solid solutions, which contained 9 at% Cu and 9 at% Ag respectively. The impurity concentrations in the solid solution phases deviated slightly from the equilibrium concentrations, which are 8.8 at% Cu and 8 at% Ag predicted by the phase diagram. The impurity concentrations in the solid solution were probably determined by the competition between the atom mobility and the cooling rate during the quench process. Thomas and Wolfgang investigated the spinodal decomposition process of AgCu alloy by one dimension numerical simulation (Boehme and Mueller 2007). An eutectic concentration (29 wt% of Cu) with one and two slight fluctuations was used as the initial concentration profile, and the diffusion equation was then solved with a time step of 0.00001 s. The results indicated that it takes take 0.56 s - 0.84 s for the formation of significant Ag/Cu concentration fluctuation at 727 ^{o}C. Here significant Ag/Cu concentration fluctuation means the lowest concentration of copper became smaller than 20 wt%. Complete diffusion between Ag and Cu to reach the thermodynamically equilibrium concentration (94.5 wt% of copper) requires even more than 10 s. In order to estimate the cooling rate during the quench process, the temperature of the collected particles was measured by attaching a surface thermocouple to the filter. With a carrier gas flow rate of 2.5 L/min, the particles were cooled down from 1000 ^{o}C, before mixing with the quench gas, to 200 ^{o}C after the quench. The distance from the quench gas inlet to the filter is 10 cm, so the quench process happened in less than 1 s with a cooling rate higher than 800 ^{o}C/s. The quick cooling process probably impeded the movement of atoms, and therefore led to the composition deviation from the equilibrium status.

A formation process for AgCu bimetallic particles is finally summarized. First, $AgNO_3$ and $Cu(NO_3)_2$ precipitate and decompose after water and EG evaporate. The separation of Ag and Cu nitrate probably happened during the evaporation because of their different solubility in the water/EG solvent (71.5 g $AgNO_3$/100 g saturated solution and 56.0 g $Cu(NO_3)_2 \cdot 6H_2O$/100g saturated solution at room temperature)(Speight 2004). Then at higher temperatures, pure Ag and Cu form from the oxide. At temperatures higher than 779 ^{o}C, Ag and Cu melt and mix together. In the final step, the particles composed of Ag rich and Cu rich solutions form, likely by spinodal decomposition during the quenching process, resulting in a nanoscale lamellar structure. During the formation process of the AgNi particle, Ag and Ni may separate as $AgNO_3$ and $Ni(NO_3)_2$ precipitate separately because of the different solubilities (77.0 g $Ni(NO_3)_2 \cdot 6H_2O$/100g saturated solution at room temperature)(Speight 2004).Because Ag and Ni has melting temperatures of 962 ^{o}C and 1455 ^{o}C, at a generation of 1000 ^{o}C, only Ag melts and surrounds the Ni which is still in the solid state. After particles cool down, particle surface is nearly covered by Ag as observed in Figure 5.1 b.

According to the results, the phase separation behavior appears to be mainly determined by the thermodynamic properties of the different metal components. However, further experiments indicated that the shape and size of the patchiness could be controlled by changing the operating conditions. In the generation of AgCu particles, reducing the temperature to below the eutectic point can lead to a more segregated mixture of the two components. Figure 5.4 a shows a SEM image of AgCu particles generated from 60% $AgNO_3$ and 40% $Cu(NO_3)_2$ at a temperature of 750 ^{o}C, and a carrier gas flow rate of 2.5 L/min. Silver and copper rich phases coexisted in the particles, indicated by green and red

in EDS mapping separately. Separation of Ag and Cu probably began during the evaporation process due to different solubilities of silver nitrate and copper nitrate, and because the generation temperature is lower than the eutectic point, a segregated structure was preserved through to the final product particles rather than the lamellar structure observed at 1000 ^{o}C.

Different ratios of patchiness can be obtained by changing the composition of precursor. Figure 5.4 b shows particles composed of 40 at % Ag and 60 at % Cu. The particles were generated at a temperature of 750 ^{o}C with a carrier gas flow rate of 2.5 L/min. A smaller portion of the surface was covered by Ag patches compared to particles composed of 60 at % Ag. More details of the bimetallic particle generation and properties are under investigation, but spray pyrolysis has displayed its potential for the generation of various patchy particles with controllable structures.

(a)

(b)

97
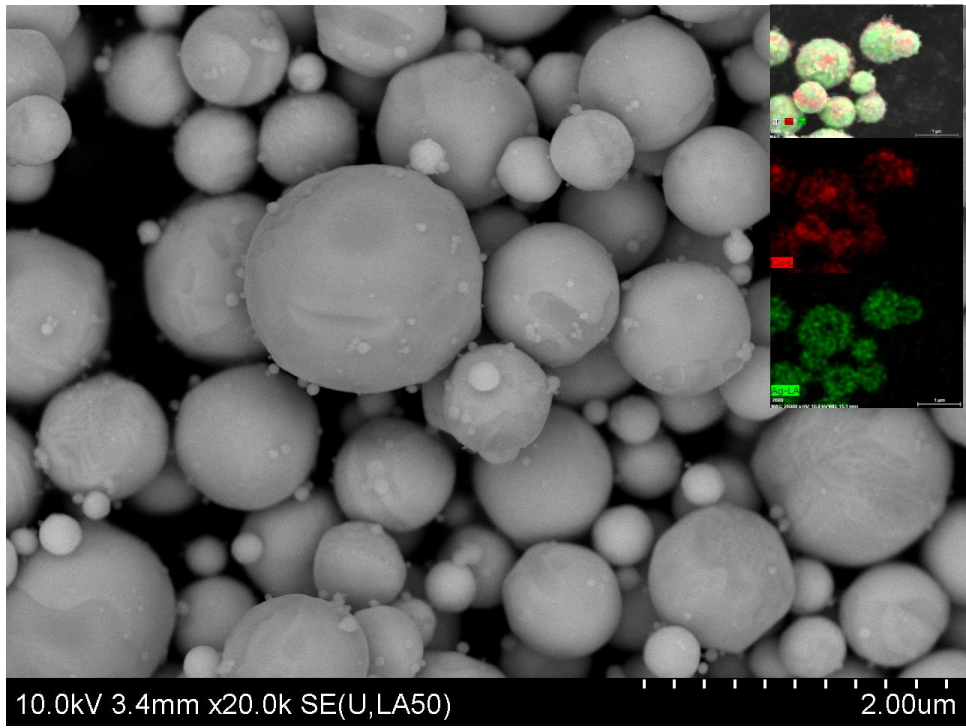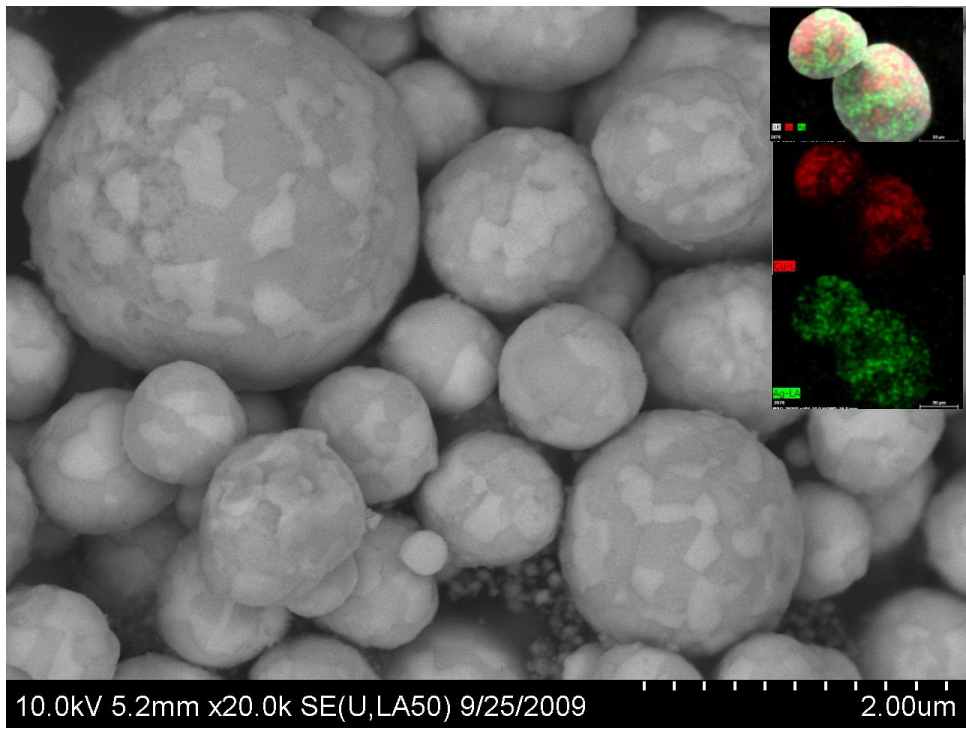
Figure 5.4. (a) SEM images of AgCu particles, which were composed of 60 at % Ag and 40 at % Cu and generated at 750 $^{\circ}$C. 2.5 L/min N_2 was used as carrier gas (b) Backscatter SEM images of AgCu. Particles were composed of 40 at % Ag and 60 at % cu and generated at 750 $^{\circ}$C. 2.5 L/min N_2 was used as carrier gas

5.5. CONCLUSIONS

Co-solvent spray pyrolysis was shown to be an effective way to make bimetallic particles. Patchy particles with various morphologies and structures were generated, and the particle structures were mainly determined by the thermodynamic properties of the particle components. Three kinds of particles were generated in the lab. The Ag-Ni system is an immiscible system, and AgNi particles with a surface nearly covered by a continuous Ag layer were observed, but for a fully miscible system, such as CuNi, uniform particles composed of an alloy phase were generated. AgCu particles were composed of two solid solution phases, and showed a substructure in the nanoscale. The lamellar substructure may be a result of spinodal decomposition.

Experimental results suggested that the change of the operating temperature and residence time will also lead to a change in particle morphology, indicating a possibility of generating particles with more functional structures. More research results on the detailed reaction steps and resulting particle properties will be reported in the next chapter.

Chapter 6: Generation of AgCu particles by the cosolvent spray pyrolysis process

6.1. ABSTRACT

AgCu particles are of interest as ingredients in metal pastes for electronic conductor applications and in isotropic conductive adhesives (ICA). Here, I report the generation of AgCu particles by the spray pyrolyisis process that has the advantages of simple experimental setup, large scale production ability and controllable particle size. A copper nitrate and silver nitrate were dissolved in DI water and used as the precursor. Either 40 vol% ethanol (ET) or 40 vol% ethylene glycol (EG) were used as the cosolvent. XRD and SEM were used for the characterization of AgCu particles. Phase separation was observed during the generation of AgCu particles, and particles mainly consisted of Ag rich and Cu rich solid solution phases. In order to understand the mechanism of this bi-component particle formation including the role of the co-solvent, short reactor residence time experiments were used. With a cosolvent of ET, Ag precipitated during the evaporation of the solvent, and agglomerated on the surface of the particles. $Cu(NO_3)_2$ decomposed to $Cu_2(OH)_3NO_3$ first, then to CuO and Cu_2O. CuO and Cu_2O were reduced to Cu in the reducing atmosphere resulting from ET decomposition. When EG was used, layered structures of $Cu_2(OH)_3NO_3$ and Cu_2O with embedded Ag particles were observed during the formation of the particles. The result indicated that both the cosolvent properties and operating conditions affect the structure of particles.

6.2. INTRODUCTION

Ag and Cu particles are of remarkable importance in catalytic, medical and electronic applications (Lewis 1993; Link and EI-Sayed 1999; Watari et al. 2004; Sheppard 1993; Kim et al. 2010; Yim et al. 2010). In the electronics industry, Ag and Cu particles are used for the fabrication of thick film conductive pastes or as filler particles in isotropic conductive adhesives (ICA) (Kim, Stach and Handwerker 2010; Yim et al. 2010; Tao et al. 2009; Lu and Wong 2008; Liu, Li and Zeng 2010). The diameter of the conductive filler particles range from 1 to 10 μm (Kang and Purushothaman 1999; Wu et al. 2007). Either in the thick film conductive pastes or in the ICA, metal particles contact each other forming the conductive network. Ag is more conductive than Cu, but is also more expensive. AgCu bicomponent particles are considered to be a wise selection because they combine the conductive benefits of Ag with the cost benefits of Cu.

Ultrasonic spray pyrolysis has been used for the generation of single and bi-component metal particles (Gurav et al. 1993a; Gurmen et al. 2009; Eroglu et al. 1996; Pluym al. 1995; Aoyagi et al. 2003; Jung et al. 2003; Yang, Kim and Kim 2008; Jang et al. 2009; Ju et al. 2009). Hydrogen, or a cosolvent, usually ethanol (ET) or ammonia is needed to generate oxide free particles (Kim et al. 2003; Zhong et al. 2012; Xia et al. 2000, 2001; Kim and Kim 2004). Compared with other particle generation methods such as chemical reduction (Tsai and Dye 1991; Hirai et al. 1978), polyol method (Kurihara et al. 1995; Fievet et al. 1993) and vaporization techniques (Cardenas-Trivino et al. 1987; Satoh and Kimura 1989), spray pyrolysis technology has the advantages of simple experimental setup, large scale production ability and controllable particle size (Jain et al. 1997b; Majumdar et al. 1996; Nagashima et al. 1990).

Recently bi-component AgCu particles were generated using the pyrolysis process with a cosolvent of ethylene glycol (EG). Particles composed of two solid solution phases with various patchy structures were detected, and the patchy structures were greatly affected by the operating conditions, such as the furnace temperature and the residence time. Cosolvent composition was another important factor for the change of the particle structure according to previous study of single component Cu particle generation (Zhong et al. 2012).

In order to make AgCu particles with controllable structures and electronic properties, it is important to understand the particle formation process and how it is affected by the operating conditions and the cosolvents. In this work, micron sized AgCu particles were generated by the ultrasonic spray pyrolysis process with a cosolvent of either ethanol (ET) or ethylene glycol (EG). Phase separation behavior between copper and silver and the reaction mechanism of the particle formation process was investigated by short residence time experiments.

6.3. EXPERIMENT

6.3.1. Particle generation

A detailed description of the cosolvent spray pyrolysis reaction system used in these experiments was reported in previous chapter (Chapter 4 and 5). The system is composed of a precursor solution reservoir, an ultrasonic droplet generator, tube furnaces, a quartz tube reactor and a filtration system for particle collection. For the generation of $Ag_{0.4}Cu_{0.6}$ particles, a mixture of silver nitrate ($AgNO_3$, purity of 99.5%, Strem) and copper nitrate hexahydrate ($Cu(NO_3)_2 6H_2O$, purity of 99.5%, Strem) mixture was used as the precursor

solution. AgNO$_3$ (8.15 g) and Cu(NO$_3$)$_2$6H$_2$O (17.40 g) were first dissolved in 20 ml water. Then 40 ml cosolvent of either ethanol (ET) or ethylene glycol (EG) and more water was added into the solution until the volume was 100 ml. The total concentration of Ag$^+$ and Cu^{2+} was 1.2 M. An ultrasonic generator, operating at a frequency of 1.7 MHz, atomizes the precursor solution to droplets with volume average diameters of around 5 microns. Two tube furnaces, with a total length of 81 cm were combined in series. A quartz tube reactor with inner diameter of 2.5 cm was placed in the center of the furnaces. A polytetrafluoroethylene filter was used to collect the particles. Industrial grade nitrogen (N$_2$) with a minimum 95% purity was used as carrier gas. A carrier gas flow rate of 2.5 L/min leads to a residence time around 2 s with two furnaces used at 875 ^{o}C. A high flow rate of 10 L/min and a single furnace at temperatures ranged from 400 ^{o}C to 875 ^{o}C was used to decrease the residence time to less than 0.4 s for the investigation of the reaction process. Particles were quenched with an additional 10 L/min of industrial grade nitrogen before collection.

6.3.2. Hydrogen concentration measurement

A Universal Gas Analyzer (UGA) 300 system was used to measure the hydrogen concentration in the outlet gas. 40 vol% ET or EG aqueous solution was sprayed into the tube furnace reactor, which was maintained at set points of 600 ^{o}C, 700 ^{o}C, 800 ^{o}C, 895 ^{o}C and 1000 ^{o}C. The mass of the solution in the reservoir was recorded every ten minutes so the atomization rates could be calculated. Two furnaces were used in series and the carrier gas flow rate was held constant 2.5 L/min for each test. After the furnace, the outlet flow was diluted by 10 L/min quench gas, and introduced into the UGA system via a capillary tube. An inbuilt mass spectrometer was used for the analysis of the gas

composition. The hydrogen concentration in the furnace is estimated as 5 times greater than the value measured by UGA system because the dilution of the quench gas.

In order to determine the possible maximum hydrogen concentration, Chemcad was used for the calculation of the equilibrium hydrogen concentration in the furnace by modeling the furnace as a Gibbs reactor, solving for the outlet gas composition such that the free energy of the system is minimized while mass is conserved. N_2, H_2O, ET/EG were set as input gas, and the ratio of each component was calculated based on the atomization rate and 2.5 L/min carrier flow, which was assumed to be pure N_2. Outlet gas included N_2, H_2O, ET/EG, H_2, CO and CO_2. At different temperatures, outlet gas composition with minimum system free energy was calculated. In order to simplify the calculation, metal nitrate species were not included in the calculation, but they can possibly change the equilibrium gas concentration as catalysts. The hydrogen concentrations I report here are the concentrations before the quench after correcting for the dilution introduced by the quench.

6.3.3. Particle characterization

Scanning electron microscopy (SEM, Hitachi SU-70) combined with energy dispersive spectroscopy (EDS) mapping and back scattered electron microscopy (BSEM) was used for the characterization of the particles. Particle composition was analyzed by an X-ray diffractometer (XRD, Bruker Smart 1000) with the diffraction angle ranging from 10° to 90°. Detailed information about crystal structure and phase abundance was obtained from Rietveld refinement. The calculated phase abundances usually have standard error of approximately 5%.

6.4. RESULTS AND DISCUSSION

6.4.1. Hydrogen concentration measurement

Hydrogen was generated from the decomposition of the cosolvents, and played an important role in the transition reaction from metal oxide to pure metal. Its concentration was experimental measured and theoretically calculated. The results are showed in Figure 6.1. When ET solution was used, the atomization rate is about 0.3 g/min. The equilibrium H_2 concentration was about 9 vol%, and decreased with increasing temperature. The concentration of CO was several orders smaller than H_2, so it was considered to make a negligible contribution to the metal salt reduction reactions. When thermodynamic equilibrium is achieved, more than 99.9% of the ET decomposes. However, the measured H_2 concentration was always lower than calculated value, and increased from 0.4% to 4.4% with increasing temperature from 600 ^{o}C to 1000 ^{o}C. This indicated that ET decomposition was limited by the kinetics of the reaction, and less than half of the ET decomposed in the furnace when two furnaces and 2.5 L/min carrier gas flow rate was used. About 0.15 g EG solution was atomized every minute, leading to a theoretical H_2 concentration of around 4 %. The calculated H_2 concentration from the EG solution was lower than the concentration from ET solution mainly because the EG solution had a lower atomization rate. The measured H_2 concentration resulting from the EG solution was between 0.1% and 0.8%, lower than the H_2 concentration from ET at the same temperature.
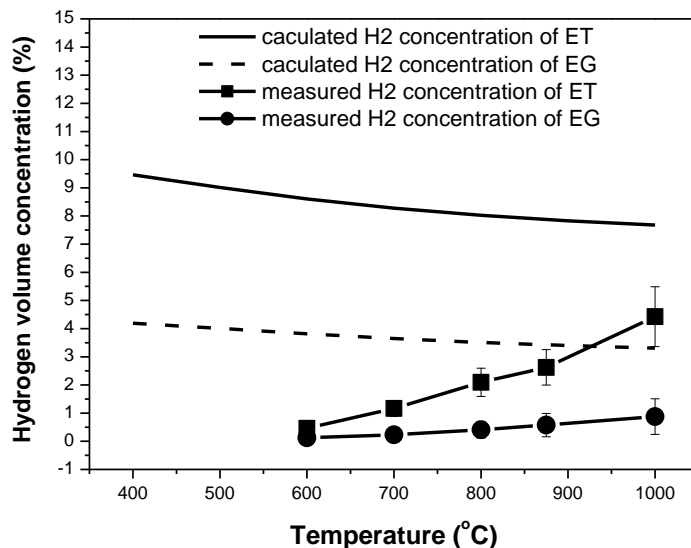
Figure 6.1. Calculated and measured hydrogen concentration in the outlet gas. 40 vol% EG or ET water solution was spray into the two furnaces. 2.5 L/min carrier gas flow rate was used. UGA 300 system was used to measure the hydrogen concentration in the outlet gas. Furnace temperatures were changed from 600 ^{o}C to 1000 ^{o}C.

6.4.2. AgCu particle generated by the spray pyrolysis process

Oxide free AgCu particles were generated at 875 ^{o}C with 40 vol% ET, 2.5 L/min carrier gas flow rate and two furnaces. The residence time was about 1.7 s. According to the XRD results (Figure 6.2), the particles were composed of two phases; one is a Ag rich solid solution phase leading to the diffraction peaks at 38.6 ^{o}, 44.9 ^{o} and 65.3 ^{o} and the other is a Cu rich solid solution phase with the diffraction peaks at 43.0 ^{o}, 50.0 ^{o} and 73.7^o. Compared to the diffraction peaks of pure Ag (38.1 ^{o}, 44.3 ^{o} and 64.5 ^{o}) and Cu (43.3 ^{o}, 50.4 ^{o} and 74.1^o) (ICDD PDF No. 01-071-3761 and 01-071-3762), there were slight shifts

105

in the diffraction peaks of Ag solid solution and Cu solid solution. According to the refinement result, the particles were composed of 40 at% Ag and 60 at% Cu.
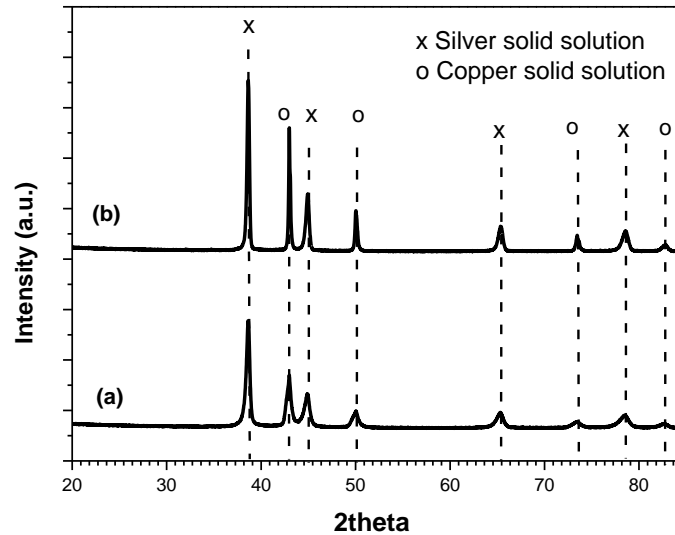
Figure 6.2. XRD of AgCu particles generated at 875 ^{o}C by spray pyrolysis process with the cosolvent of (a) ET and (b) EG.

SEM images of particles are shown in Figure 6.3 a. Particles were spherical with diameters ranging from 0.5 micron to 2 microns. The light and dark areas in the BSE images of the particles represent the two phases in the particles. The dark surface area was enriched in copper and the light area was enriched in silver because atoms with a higher atomic number are stronger scatterers than lighter atoms. EDS showed that particles contained 45 at% Ag and 55 at% Cu.
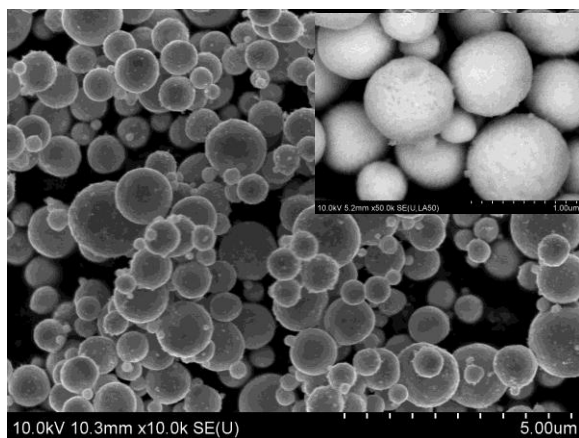
(a)
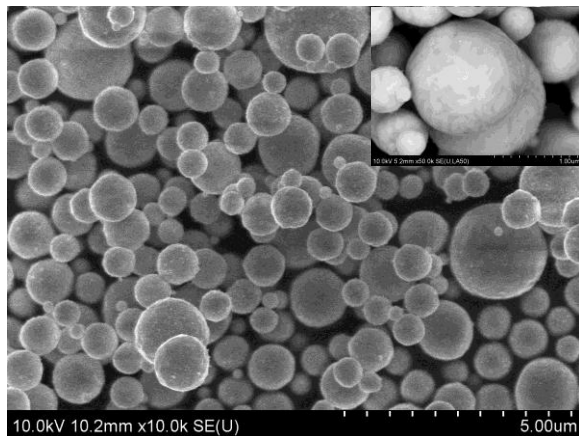
(b)

Figure 6.3. SEM images of AgCu particles generated at 875 ^{o}C by spray pyrolysis process with the cosolvent of (a) ethanol and (b) ethylene glycol, inserted images were taken in backscattered mode.

Oxide free particles also could be generated with the cosolvent of EG. SEM and BSE images of particles generated with the cosolvent of EG were shown in Figure 3 b. Ag rich solid solution and Cu rich solid solution phases with a total composition of 40% Ag and

60% Cu were detected by XRD (Figure 6.2). EDS gave a composition of 52 at% Ag and 48 at% Cu, possibly indicating a slight Ag enrichment on the surface.

6.4.3. Reaction process with the cosovlent of ET

The short residence time experimental method was used for the reaction mechanism investigation. In these experiments, a large carrier gas flow rate of 10 L/min was used with only one furnace. The residence time was less than a half second depending on the temperature. For example, it takes 0.4 s to pass through one furnace at 400 $^{\circ}$C with 10 L/min carrier gas flow rate, while 3.3 s are needed if 2.5 L/min flow rate and two furnaces are used. Because there is not enough residence time for complete reaction, the intermediate products could be collected allowing for the analysis of the detailed reaction process.

Short residence time experiments were carried out at temperatures from 400 $^{\circ}$C to 875 $^{\circ}$C. Experimental temperatures and corresponding residence times are listed in Table 1. Residence times were estimated based on the temperature measured along the furnace center line. Particles were collected and characterized by XRD and SEM.

XRD results of particles generated with ET at 400 $^{\circ}$C, 500 $^{\circ}$C, 600 $^{\circ}$C and 875 $^{\circ}$C are shown in Figure 6.4. At 400 $^{\circ}$C, the particles are mainly composed of $Cu_2(OH)_3NO_3$, CuO, $AgNO_3$ and Ag. CuO had primary peaks at 35.5 $^{\circ}$ and 39 $^{\circ}$. The observed peaks at 35.5 $^{\circ}$ and 39° indicate the existence of CuO, but the peak at 39 $^{\circ}$ partly overlaps with the signals from Ag. Peaks at 36.5 $^{\circ}$ could be attributed to Cu_2O or $Cu_2(OH)_3NO_3$, so the existence of Cu_2O is unclear. Rietveld refinement gave a particle composition of 66 at% $Cu_2(OH)_3NO_3$, 12 at% CuO, 1 at% Cu and 21 at% Ag. When the temperature was

increased to 500 ^{o}C and 600°C, residence times decreased to 0.36 s and 0.32 s respectively., Stronger peaks of Ag at 38 ^{o} and CuO at 35.5 ^{o} were observed and less signal from $Cu_2(OH)_3NO_3$ was detected because of the higher reaction rate at 500 ^{o}C and 600 ^{o}C. Particles generated at 875 ^{o}C were mainly composed of Ag rich and Cu rich solid solution phases. More XRD refinement results are listed in Figure 6.5 and in supporting information. $Cu_2(OH)_3NO_3$ decomposed to CuO (circle) and full decomposition was at 650°C. CuO achieved its maximum at 650°C, and further decomposed to Cu_2O in the reducing atmosphere. Cu was observed at 650 ^{o}C and became more prevalent as temperature increased.
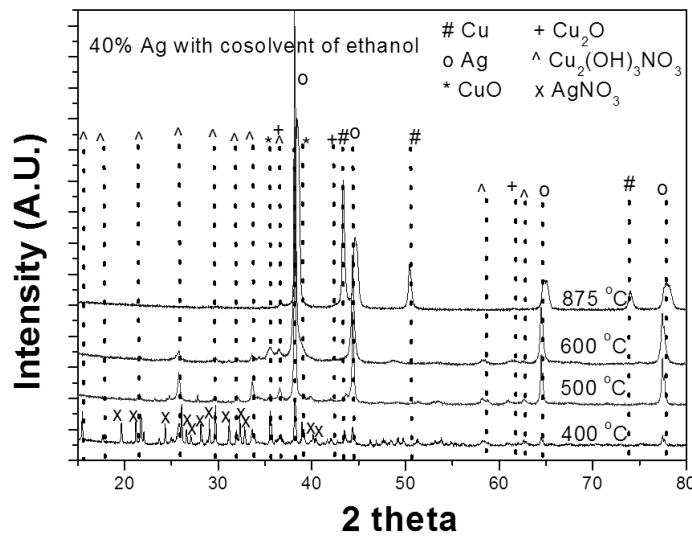
Figure 6.4. XRD of powders generated at 400 ^{o}C, 500 ^{o}C, 600 ^{o}C and 875 ^{o}C with a single furnace and 10 L/min carrier gas flow rate. Ethanol (ET) was used as the cosolvent.

Figure 6.5. XRD refinement results for powder generated at temperatures from 400 ^{o}C to 875 ^{o}C with a single furnace and 10 L/min carrier gas flow rate. Ethanol (ET) was used as the cosolvent.

SEM images of particles generated in the short residence time experiment are shown in Figure 6.6. At 400 ^{o}C, no distinct individual particles were observed from the images (Figure 6.6 a). A mixture composed of $Cu_2(OH)_3NO_3$ and Ag was observed with white patterns on the surface, which is probably indicative of the initial phase separation. At 500 ^{o}C, the outline of distinct particles, mainly composed of $Cu_2(OH)_3NO_3$ and Ag, started to appear (Figure 6.6 b), and the aggregation of Ag became observable according to the EDS mapping image, where the green dots represent Ag, and the red represent Cu. At 500 ^{o}C, individual particles were detected with more obvious separation between Ag, CuO and $Cu_2(OH)_3NO_3$. From the SEM and EDS image (Figure 6.6 c), it was found that each of the particles consists of two phases. One is the dark area enriched in Cu

110

according to the EDS mapping, and the other is the light area mainly composed of Ag. The Ag looks like it is forming a half shell, covering the surface of the mixture of CuO and $Cu_2(OH)_3NO_3$. Dark stripes in the primary particles were observed in the SEM images of the particles generated at 875 ^{o}C (Figure 6.6 d), indicating that AgCu particles contained two solid solution phases. Formation of the solid solution phases was probably due to the mutual diffusion between Ag and Cu, or possibly that $Ag_{0.4}Cu_{0.6}$ melted and mixed in liquid state, since $Ag_{0.4}Cu_{0.6}$ has a melting point between 850 ^{o}C and 900 ^{o}C according to the phase diagram (Okamoto 2000), or both.

(a)

(b)
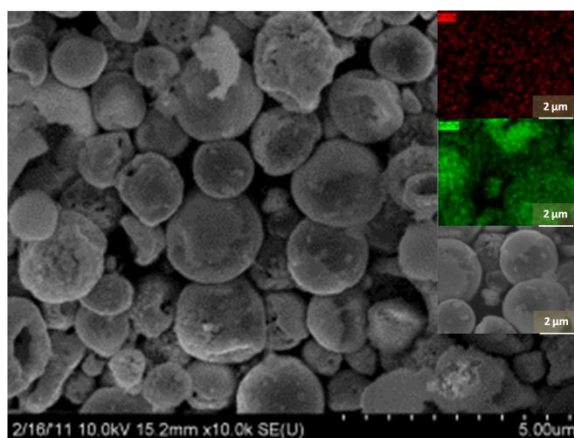
(c)

(d)

Figure 6.6. SEM images and EDS mapping of particles generated at different temperature with a single furnace and 10 L/min carrier gas flow rate. Ethanol (ET) was used as the cosolvent (a) 400 ^{o}C (b) 500 ^{o}C (c) 600 ^{o}c and (d) 875 ^{o}C.

According to the the XRD and SEM analysis of short residence time particles, a formation process for AgCu particles with the cosolvent of ET is proposed. When the precursor droplets are sent into the hot furnace, ethanol and water evaporates quickly, with $Cu(NO_3)_2$ decomposing to $Cu_2(OH)_3NO_3$. $Cu_2(OH)_3NO_3$ then decomposes to CuO

and Cu_2O. At the same time, $AgNO_3$ and Ag precipitate and agglomerate on the surface of the particles. As the particles are continually heated up to more than 600 ^{o}C, Cu is generated from oxide in the atmosphere created by the ethanol. Mutual diffusion probably happens between Ag and Cu, and lead to Ag rich and Cu rich solid solution phases. If the furnace temperature is higher than the melting point of the alloy, the particles could also melt, with spinodal decomposition occurring during the cooling process.

6.4.4. Reaction process with the cosovlent of ethylene glycol (EG)

The same short residence time experimental method was used to investigate the $Ag_{0.4}Cu_{0.6}$ formation process with the cosolvent of EG. XRD results of particles generated at temperatures from 400 ^{o}C to 875 ^{o}C were shown in Figure 6.7. At 400 ^{o}C, a wet sample was collected, and a significant portion of unevaporated solvent was observed on the filter. A similar phenomenon was reported during the generation of pure Cu particles with EG (Kai Zhong n.d.). According to the spectrum (Figure 6.8), samples collected at 400 ^{o}C mainly consisted of $Cu_2(OH)_3NO_3$ and Ag. At 500 ^{o}C, signals of $Cu_2(OH)_3NO_3$ were nearly undetectable, indicating a quick decomposition of $Cu_2(OH)_3NO_3$. The signals of CuO were not detected either. Besides $Cu_2(OH)_3NO_3$ and Ag, two other phases were detected: Cu_2O with primary peaks at 36.5 ^{o} and Cu with peaks at 43.4 ^{o}. This indicated that when EG was used as the cosolvent, $Cu_2(OH)_3NO_3$ experienced a quick decomposition reaction, leading to the formation of Cu_2O and Cu at a relatively low temperature of 500 ^{o}C. Diffraction signals of Cu_2O and Cu became more obvious at 600 ^{o}C. As temperature increased to 875 ^{o}C, Ag rich and Cu rich solid solution

phases were detected with slightly shifted diffraction peaks compared with pure Ag and

Cu.
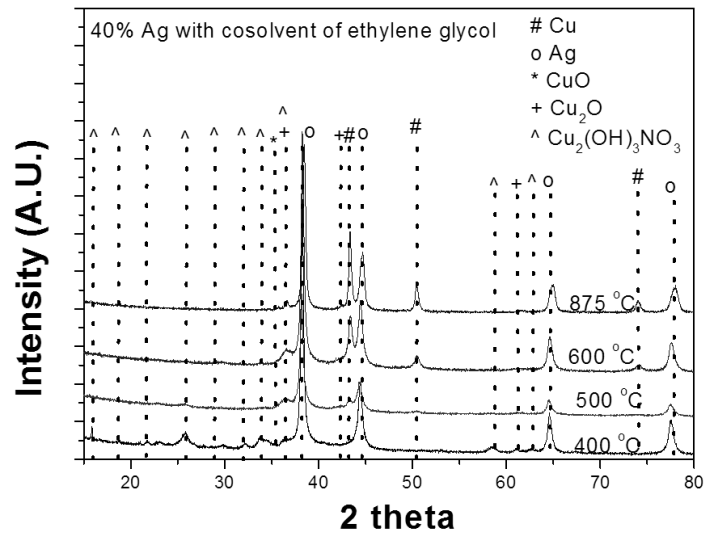
Figure 6.7. XRD of powders generated at 400 ^{o}C, 500 ^{o}C, 600 ^{o}c and 875 ^{o}C with a single

furnace and 10 L/min carrier gas flow rate. Ethylene glycol (EG) was used as the
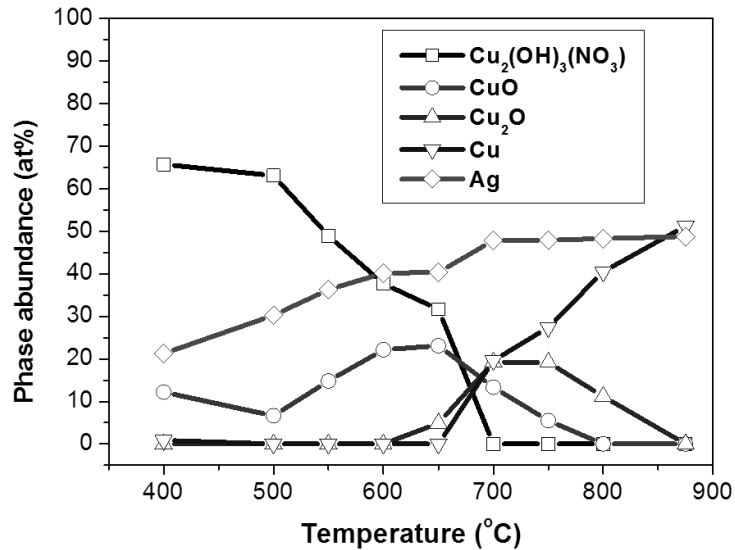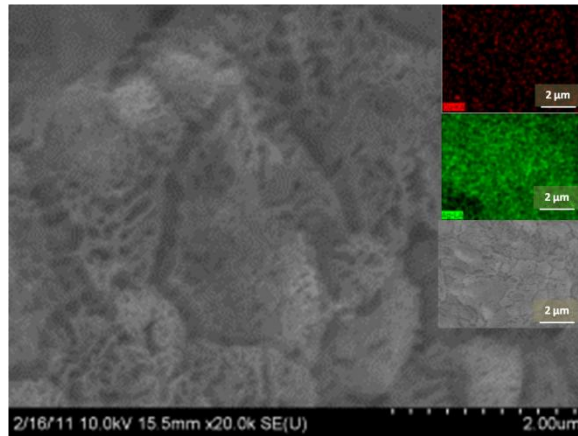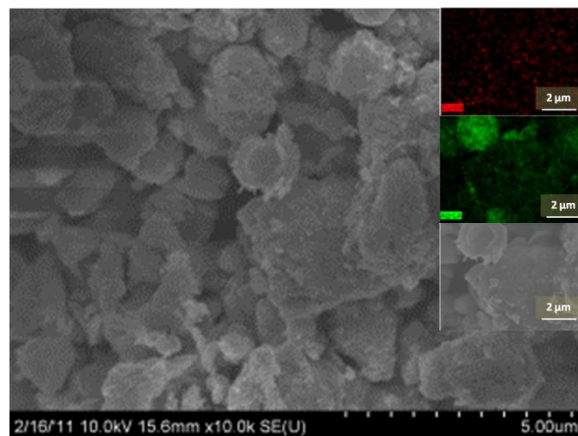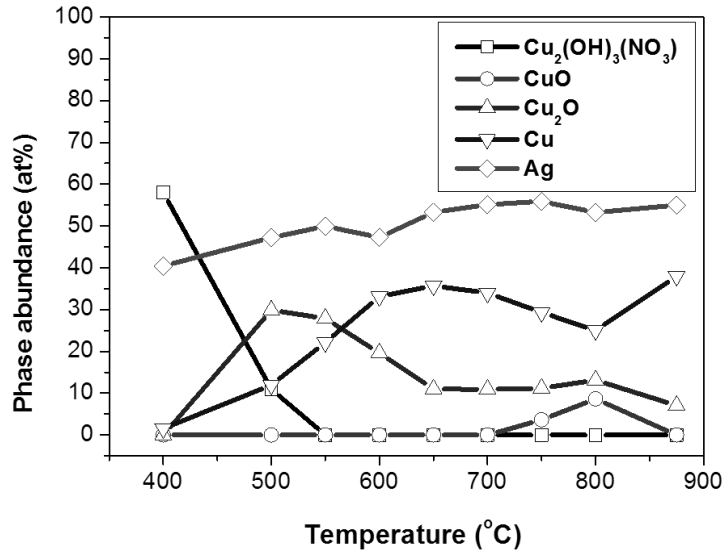
cosolvent.

Figure 6.8. XRD refinement results for powders generated at temperatures from 400 $^{\circ}$C to 875 $^{\circ}$C with a single furnace and 10 L/min carrier gas flow rate. Ethylene glycol (EG) was used as the cosolvent.

XRD refinement results are listed in Figure 6.8 and supporting information. At a low temperature of 400°C, $Cu_2(OH)_3NO_3$ and Ag precipitated as indicated by the square and the diamond in Figure 9. As temperature increased, $Cu_2(OH)_3NO_3$ decomposed to Cu_2O (triangle) with the existence of EG rather than CuO when using ET (circle). Full decomposition occurred at 550 $^{\circ}$C. Metallic Cu was observed at a very low temperature of 500 $^{\circ}$C and became more prevalent as temperature increased.

Differences in phase separation behavior also occurred when EG was used to replace ET. SEM images and EDS mapping of particles generated with EG are shown in Figure 6.9. At 400 $^{\circ}$C, Ag precipitated as individual spheres in the matrix of $Cu_2(OH)_3NO_3$ (Figure 6.9 a). At 500°C, small distinct spheres with diameters less than 100 nm were found in

some layered structures (Figure 6.9 b). EDS indicated that the layers contain Cu and Ag and the light dots contained mainly Ag. Also considering the XRD results discussed before, I believe the layer structures are a mixture of $Cu_2(OH)_3NO_3$, Cu_2O, metallic Cu and Ag, and the small dots in the layers are metal phase Ag. Increasing temperatures to 600 ^{o}C, porous particles could be observed with patterns on the surface (Figure 6.9 c). EDS showed that the pattern structures on the surface were enriched with Ag, and the primary particles contained both Cu and Ag. The porous particles consisted of Cu_2O, metallic Cu and some metallic Ag. At 875 ^{o}C, two solid solution phases were formed and mixed together. EDS cannot distinguish between two phases because of the limitation of the spatial resolution.

The formation process of AgCu particles with the cosolvent of EG was proposed. First is the evaporation of the solvents. The low evaporation rate of EG leads to the formation of nanosize Ag particles and layer structures which were mainly composed of $Cu_2(OH)_3NO_3$, Cu_2O, Cu. As temperature increased, $Cu_2(OH)_3NO_3$ decomposed to Cu_2O and then was reduced to Cu forming porous particles. Ag particles embedded in the matrix of Cu_2O and Cu. Finally particles composed of Ag and Cu solid solution phases were generated.

116

(a)

(b)

(c)

117

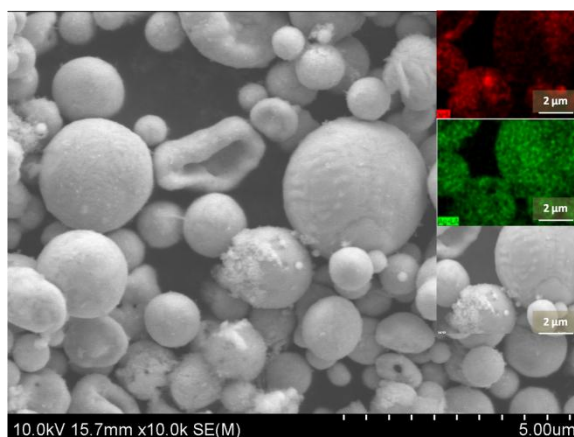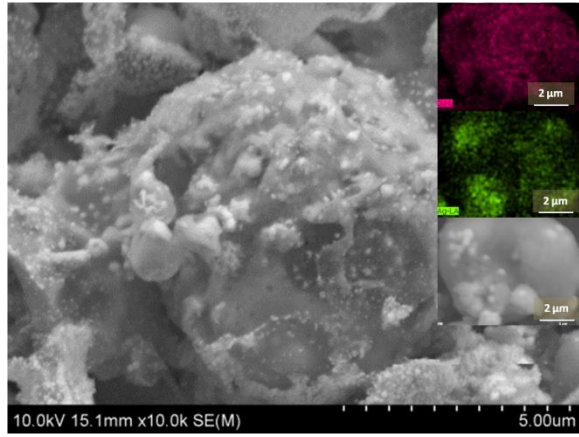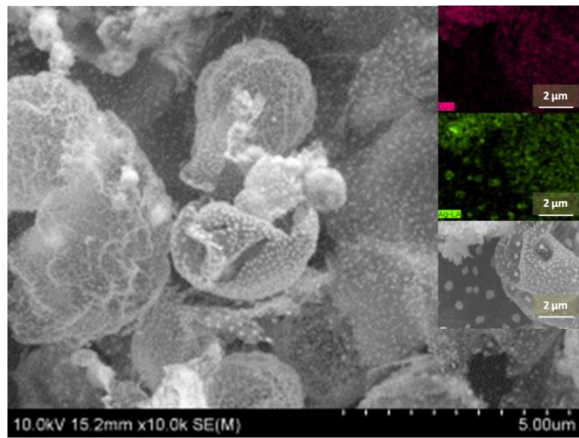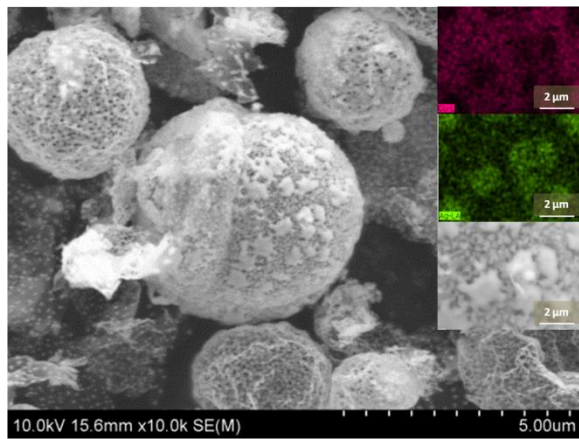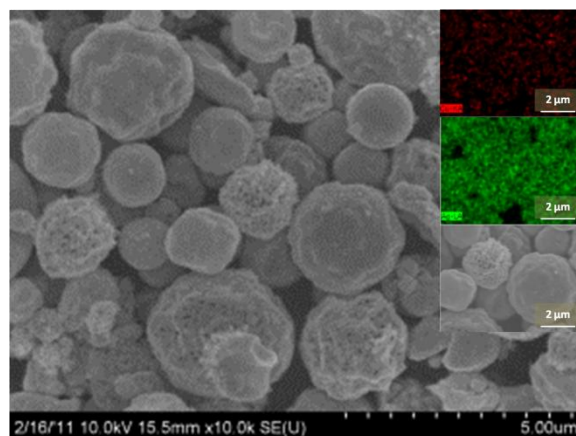**(d)**

Figure 6.9. SEM images and EDS mapping of particles generated at different temperature with a single furnace and 10 L/min carrier gas flow rate. Ethylene glycol (EG) was used as the cosolvent (a) 400 ^{o}C (b) 500 ^{o}C (c) 600 ^{o}c and (d) 875 ^{o}C.

When comparing the generation process using ET and EG, two significant differences were noticed. One is the morphology of precipitated Ag. The other difference is the reaction path between Cu $(NO_3)_2$ and Cu. When ET was used, agglomerated Ag was observed on the surface, while Ag precipitated as nanoparticles with EG. This could be explained by the difference in the evaporation rate of ET versus EG. ET has a higher vapor pressure (43 mmHg at 20 ^{o}C) than water (18 mmHg at 20 ^{o}C) (Speight 2004), and evaporated in a shorter time before complete decomposition of $AgNO_3$ according to the XRD result (Figure 4). Precipitation behavior was determined by the solubility (71.5 g $AgNO_3$/100 g saturated solution and 56.0 g $Cu(NO_3)_2 \cdot 6H_2O$/100g saturated solution at room temperature)(Speight 2004). In our case (8.15 g $AgNO_3$ and 17.4 $Cu(NO_3)_2 \cdot 6H_2O$ in 100 ml solution), $Cu(NO_3)_2 \cdot 6H_2O$ will precipitate, followed by $AgNO_3$.   The precipitation in that order will lead to the separation as described in Figure 6.6 a-c. While

118

EG has vapor pressure of 0.06 mmHg at 20 ^{o}C, nearly 1000 times less than ET, it will take 1000 times longer for the evaporation of EG than ET if they are at the same temperature (Pruppacher and Klett 1996; Friedlander 1977). As I discussed above, more than 0.4 s is required for the full evaporation of EG at 400 ^{o}C. During such a long evaporation process, EG and $AgNO_3$ are coexistent and heated. Ag^+ is probably reduced to Ag^0 by EG, leading to the formation of nanoparticles of silver that were observed in Figure 6.9 (Kurihara et al. 1995; Fievet et al. 1989, 1993).

The other difference between using ET and EG was the decomposition of $Cu(NO_3)_2$. With ET, $Cu(NO_3)_2$ first decomposed to CuO, then Cu_2O and Cu. This process was reported previously by other groups (Lvov and Novichikhin 1995b; Jackson et al. 1995). However, when using EG as the cosolvent, a direct transition from $Cu(NO_3)_2$ to Cu_2O was observed. Two possible reasons could be used for the explanation of the CuO disappearing. One is that EG created a greater reducing atmosphere and a higher H_2 concentration than ET. A large H_2 concentration allows a quick transition from CuO to Cu_2O, so no CuO can be detected. However, H_2 concentration measurement results showed that less H_2 were actually generated from EG than from ET. Another possible reason is that EG reacted with $Cu(NO_3)_2$, reducing Cu^{2+} to Cu_2O, and the EG was oxidized to an aldehyde or acid.

6.4.5. Activation energy calculation

The reaction rate (V) of the transition from $Cu(NO_3)_2$ to Cu with different cosolvent was estimated by the moles of Cu generated per unit time:

$$V = \frac{C_{Cu} \times P_{Cu}}{2P_{Cu2(OH)3NO3} + 2P_{Cu2O} + P_{Cu}} \bullet \frac{1}{t_r} \quad \dots\dots\dots\dots\dots\dots\dots\dots\dots\dots\dots\dots\dots\dots\dots\dots(6.1)$$

where C_{cu} is the Cu^{2+} concentration in the precursor, equal to 0.72 M. $P_{Cu2(OH)3NO3}$, P_{Cu2O}, P_{CuO} and P_{Cu} are the phase abundance of $Cu_2(OH)_3NO_3$, Cu_2O, CuO and Cu, which are showed in supporting materials. t_r is the residence time under various experimental conditions. For a comprehensive comparison, previous results for pure copper particles generation are shown together. For the generation of pure copper, 1.2 M $Cu(NO_3)_2$ with either ET or EG was used as the precursor, leading to a C_{Cu} of 1.2 M. Rietveld refinement results have been discussed in Chapter 3. Natural logarithm of copper formation rates (Ln(V)) from different precursors are shown versus reciprocal of the temperature (1/T) in Figure 6.10. A linear equation was used for the fitting of the data, and results are summarized in Table 6.2.

Squares show the copper formation rate from $Cu(NO_3)_2$ precursor with ET. Circles show the formation rate with $Cu(NO_3)_2$ precursor and a cosolvent of ethylene glycol (EG). Triangles represent formation rate of Cu when $Cu(NO_3)_2/Ag(NO_3)_2$ mixture was used as the precursor and ethanol (ET) was used as the cosolvent. Diamonds indicate the formation rate from mixture precursor and EG cosolvent. Lines represent the fit to the Arrhenius equation, and apparent activation energies were estimated from the slopes of the lines.
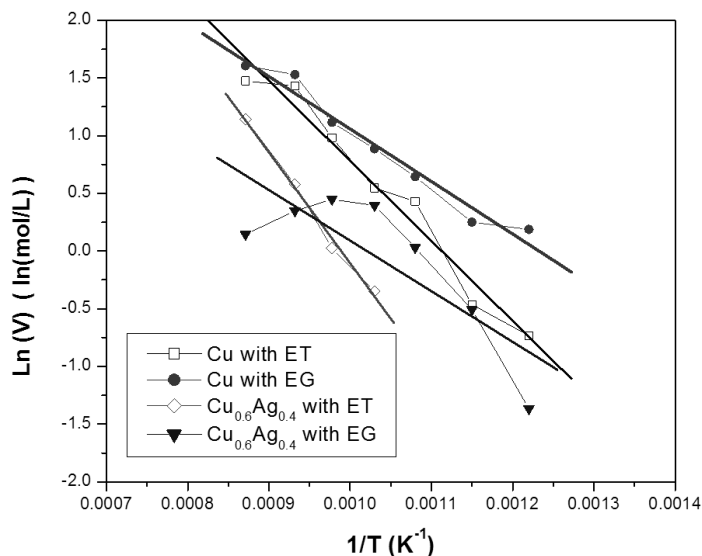
Figure 6.10. Natural logarithm of copper formation rate versus reciprocal of temperature.

Table 6.1. Linear fitting results and activation energy (E_a).

Precursor composition	Intercept (I)	Slope (S $\times 10^3$)	R^2	Activation energy (Ea/ kJ·mol^{-1})
$Cu(NO_3)_2$/ET	7.7($\pm$0.62)	-6.9 ($\pm$0.6)	0.98	58($\pm$5)
$Cu(NO_3)_2$/EG	5.6($\pm$0.40)	-4.6($\pm$0.4)	0.98	38($\pm$3)
$Cu(NO_3)_2$/$AgNO_3$/ET	9.5($\pm$0.59)	-9.6 ($\pm$0.6)	0.99	80($\pm$5)
$Cu(NO_3)_2$/$AgNO_3$/EG	4.5($\pm$1.43)	-4.4($\pm$1.4)	0.82	36($\pm$11)

Apparent activation energy (E_a) could be calculated by the multiplying slope (S) with constant R=8.31$\times10^{-3}$ kJ/mol if the reaction obeyed the Arrhenius law. According to the Ea listed in Table 1, ET always resulted in a larger E_a than with EG, indicating the reaction rate will be more sensitive to the temperature when ET was used as the cosolvent. This is because probably higher temperatures are required for the decomposition of ET, but EG could reduce the oxide even without decomposition.

When ET was used as the cosolvent, $Cu(NO_3)_2/AgNO_3$ mixture precursor lead to lower reaction rate, which could be attributed to two possible reasons. One is the dilute effect of Ag resulting in a lower C_{Cu}, and the other reason is that Ag probably played the role of reaction inhibitor, leading to a E_a of 80($\pm$5) kJ/mol, greater than 58($\pm$5) kJ/mol when pure $Cu(NO_3)_2$ precursor used. When EG was used as the cosolvent, $Cu(NO_3)_2/AgNO_3$ mixture precursor and pure $Cu(NO_3)_2$ precursor have E_a of 36($\pm$11) kJ/mol and 38($\pm$3) kJ/mol separately, which are quite close. This indicated that adding Ag did not change the reaction mechanism with a cosolvent of EG, and the decrease in the Cu formation rate was mainly because of the dilution effect caused by addition of Ag.

6.5. CONCLUSIONS

$Ag_{0.4}Cu_{0.6}$ particles were generated by the spray pyrolysis process from $Cu(NO_3)_2$ and $AgNO_3$ precursor solution with the cosolvent of either ET or EG. The hydrogen concentration in the outlet gas was measured. ET resulted in concentration between 0.4 vol% and 4.4 vol%, and EG had H_2 concentration between 0.1 vol% and 0.8 vol%. Decomposition of both ET and EG was limited by the reaction kinetics. Particles were oxide free and composed of Ag rich and Cu rich solid solution phases. Short residence time experiments were used for the investigation of the details of the particle formation process.

With a cosolvent of ET, Ag precipitated during the evaporation of the solvent, and agglomerated on the surface of the particles. $Cu(NO_3)_2$ decomposed to $Cu_2(OH)_3NO_3$, then CuO and Cu_2O. CuO and Cu_2O were reduced to Cu in the reducing atmosphere resulting from ET, and finally Ag and Cu diffused into each other, leading to the

formation of solid solution phase. With a cosolvent of EG, nanosized Ag particles were generated during the evaporation process. Layer structures of $Cu_2(OH)_3NO_3$ and Cu_2O with Ag particles embedded were observed during the formation of the particles. EG probably interacted with $Cu_2(OH)_3NO_3$, resulting in the formation of Cu_2O and Cu at a lower temperature than ET.

Kinetic calculations indicated that formation rate of Cu was slowed down during the generation of AgCu particles compared with the generation of pure Cu particles with a cosolvent of either ET or EG. When ET was used, adding Ag led to a decreased C_{Cu} and an increased Ea, both played negative effects on the formation rate of Cu. When EG was used, there were no significant change of Ea, and decreasing reaction rate was mainly attributed to the dilution effect caused by addition of Ag.

The results indicated the phase separation between Ag and Cu strongly depends on the properties of the cosolvent. A cosolvent with high evaporation rate leads to the separation during the evaporation process, while a cosolvent like EG, which evaporates more slowly than ET and has strong reduction, probably results in the reaction in the liquid phase, and the separation behavior is then be determined by the thermodynamically properties of the component. Choice of the cosolvent and experiment conditions probably lead to controllable AgCu particle structures. Understanding the role of the cosolvent during the generation of AgCu particles also could also be helpful for the other bicomponents particles generation.

Chapter 7: Conclusions and Future Work

7.1. CONCLUSIONS

Cosolvent assisted ultrasonic spray pyrolysis process was successfully used for the generation of various oxide free micron sized metal particles. In this study, experimental results on the precursor solution atomization behavior, single component particle generation, bi-component patchy particle generation and reaction mechanisms during the formation of AgCu particles were discussed. The final results indicated that spray pyrolysis process is a promising technology for the generation of various micron sized metal particles. Particle size, composition and structure could be adjusted by changing the precursor solution, temperature and residence time. The work we showed in this dissertation has increased understanding of the metal particle generation process, which may enable greater usage of the ultrasonic cosolvent assisted spray pyrolysis technique in real industry applications.

At first, atomization behavior of copper nitrate/cosolvent/water solution was investigated via a 1.7 MHz ultrasonic droplet generator. Solutions with viscosity lower than 3 mm^2/s led to droplets with a relative mono disperse size distribution. D50 was around 5 μm. Increasing nitrate concentration or cosolvent volume ratio increased the solution viscosity and the droplet diameter. At the same time, the atomization rate decreased. Bimodal droplet size distribution was observed when the viscosity were greater than 3 mm^2/s. Dimensionless droplet diameter D and dimensionless frequency Ω were calculated, and D was found to be proportional to $\Omega^{-0.6}$ when Ω is smaller than 0.1 (viscosity smaller than 3 mm^2/s) . In this region, droplets form from periodic surface fluctuations, and surface

tension is believed to be the dominant force during the process. Once Ω is bigger than 0.1, the relationship does not hold because larger droplets are formed from breakup of the liquid filaments. Both large droplets with diameters around 100 μm and filaments were observed by the shadowgraphy experiment. Understanding the formation process of the droplets via the ultrasonic allow us to the select a right precursor concentration and control the product particle size.

Then, copper particles were generated by a cosolvent spray pyrolysis process at furnace temperatures ranging from 400 ^{o}C to 1000 ^{o}C with either 40% ethanol (ET) or ethylene glycol (EG) used as a cosolvent with nitrogen gas as the carrier gas. I found that using ET as the cosolvent resulted in copper particles with a significant fraction of hollow structures, and big cracks were observed on the particle surface, while the use of EG resulted in porous structures at 400 ^{o}C and 600 ^{o}C, and hollow shell particles with smooth surfaces at 875 ^{o}C and 1000 ^{o}C. Particle density was lower than the theoretical value, and decreased with increasing temperature. The decrease in density with increasing temperature indicates that formation of hollow shell-like particles is promoted by high furnace temperatures. The reaction process was then investigated by short residence time experiments. Results indicated that copper nitrate first hydrolyzed to $Cu_2(OH)_3NO_3$, and then decomposed to CuO and Cu_2O, which was then reduced to pure copper. Differences in the evaporation rate of ET, EG and water resulted in the changes to the precipitation behavior of $Cu_2(OH)_3NO_3$, which affected the morphology of the product particles.

Multicomponent patchy particles with various morphologies and structures were generated, and the particle structures were mainly determined by the thermodynamic properties of the particle components. Three kinds of particles were generated in the lab.

125

The Ag-Ni system is an immiscible system, and AgNi particles with a surface nearly covered by a continuous Ag layer were observed, but for a fully miscible system, such as CuNi, uniform particles composed of an alloy phase were generated. AgCu particles were composed of two solid solution phases, and showed a substructure in the nanoscale. The lamellar substructure may be a result of spinodal decomposition. With change the generation temperature and stoichiometry ratio between Ag and Cu, the morphology of AgCu particles was changed successfully.

At last, the formation process of AgCu particles was investigated using a short residence time method. Either ET or EG was used as the cosovlent. The hydrogen concentration in the outlet gas was measured. ET resulted in concentration between 0.4 vol% and 4.4 vol%, and EG had H_2 concentration between 0.1 vol% and 0.8 vol%. Decomposition of both ET and EG was limited by the reaction kinetics. With a cosolvent of ET, Ag precipitated during the evaporation of the solvent, and agglomerated on the surface of the particles. $Cu(NO_3)_2$ decomposed to $Cu_2(OH)_3NO_3$, then CuO and Cu_2O. CuO and Cu_2O were reduced to Cu in the reducing atmosphere resulting from ET, and finally Ag and Cu diffused into each other, leading to the formation of solid solution phase. With a cosolvent of EG, nanosized Ag particles were generated during the evaporation process. Layer structures of $Cu_2(OH)_3NO_3$ and Cu_2O with Ag particles embedded were observed during the formation of the particles. EG probably interacted with $Cu_2(OH)_3NO_3$, resulting in the formation of Cu_2O and Cu at a lower temperature than ET. Kinetics calculations indicated that the formation rate of Cu was slowed down during the generation of AgCu particles compared with the generation of pure Cu particles with a cosolvent of either ET or EG. When ET was used, adding Ag led to a decreased C_{Cu} and

an increased Ea, both played negative effects on the formation rate of Cu. When EG was used, there were no significant change of Ea, and decreasing reaction rate was mainly attributed to the dilution effect caused by addition of Ag.

7.2. FUTURE WORK

7.2.1. Carbon black and sucrose used as reducing agents

In this dissertation, I used ET and EG as cosolvents to improve the safety of the pyrolysis process. An ideal cosolvent should be reductive and safe. However, the flash point of ET is 14 ^{o}C, which makes ET a National Fire Protection Association (NFPA) class 3 flammable material. For industrial applications, use of materials that have a flash point above 100 ^{o}C is preferred. Ethylene glycol (EG) has a flash point of 111 ^{o}C (Speight 2004), but it increases the viscosity of the precursor and decreases the atomization rate of the system. So I am still looking for other potential reducing agents. Carbon black and sucrose seem to be good choices, because they are safe for use and have relative low price. In the preliminary experiment, 0.02 M $Cu(NO_3)_2$/0.01 M $C_{12}H_{22}O_{11}$ mixture solution was used as the precursor, and particles were generated at 450 ^{o}C, 600 ^{o}C and 900 ^{o}C. XRD results indicate that particles were mainly composed of Cu even at the lowest temperature of 450 ^{o}C. The effects of carbon and sucrose on the reaction can be further investigated.

7.2.2. Structure fabrication using colloid precursor

AgCu particles are widely used in thick film conductive pastes and isotropic conductive adhesives (ICA) (S. J. Kim et al. 2010; Yim et al. 2010; Yu Tao et al. 2009; D. D. Lu and Wong 2008; J. Liu et al. 2010), where particles contact with each other forming the

conductive network. In order to combine the conductive benefits of Ag with the cost benefits of Cu, particles are required to have core shell structure with surface covered by Ag layer. However, according to the conclusion in Chapter 6 and Chapter 7, generation of AgCu particles form $AgNO_3/Cu(NO_3)_2$ precursor leads to multiple layer structures because of the thermodynamics of AgCu mixtures. I proposed to fabricate core shell AgCu particles using colloid precursors. CuO particles will be first be covered by polyvinyl alcohol (PVA) by mixing with PVA/ethanol solution and spray dying. Then particles will be suspended in the $AgNO_3$ aqueous solution. PVA layer is designed to protect the CuO from the corrosion of acid solution. The suspension solution will be used as the precursor, and the furnace temperature will be controlled in a low level, so that $AgNO_3$ will decompose to Ag. PVA will also decompose quickly when temperature higher than 200 ^{o}C, and react with CuO. The process is showed in Figure 7.1.
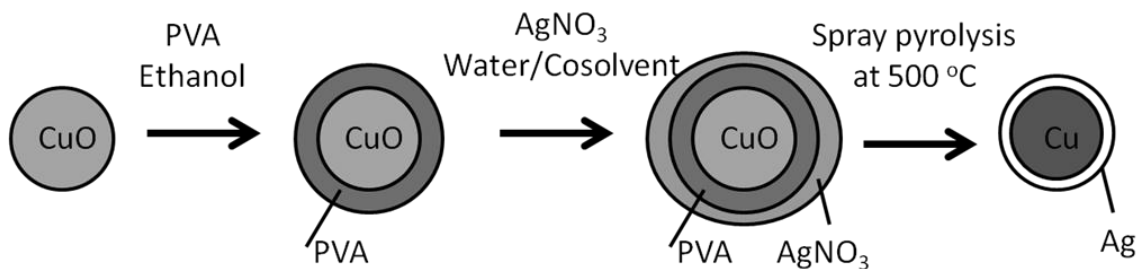
Figure 7.1. Fabrication of AgCu core shell particles by spray pyrolysis process.

Three challenges I can expect for this experiment: (1) the spray drying process of PVA/CuO suspended solution, (2) appropriate ratio of PVA vs CuO and (3) choice of the operation temperature. During the spray dying, PVA will increase the viscosity of the precursor and make it hard to be atomized as we discussed in Chapter 3. In order to get over this problem, we could decrease the viscosity of the PVA solution by slightly

heating it up to around 50 ^{o}C, and at the same time increase the carrier gas flow rate to promote the formation of the droplets. The mole ratio of polymer vs CuO is also very important. If there is not enough PVA, CuO cannot be protected from the corrosion of AgNO$_3$ solution, but too much PVA will lead to the residual carbon in the final particle. A correct reaction temperature should be selected, and I believe it is between 400 ^{o}C and 900 ^{o}C. Because furnace temperature higher than 900 ^{o}C will lead to the melt of AgCu mixture, and 400 ^{o}C is the temperature I found Cu could be made (Chapter 4). A series experiments are needed to finally figure all these problems out.

Appendices

A1. 2^3 design of experiment

The statistical software package Minitab 15 was used for the 2^3 full factorial experiment design and result analysis.(Montgomery and Runger 2006) The covariance Y, which could be the droplet mean diameter or atomization efficiency, was determined by the linear combination of the main factors X_1, X_2 and X_3. We can express it in an equation

$$Y_{ijk}=\beta_0+\beta_1*X_{1i}+\beta_2*X_{2j}+\beta_3*X_{3k}+\beta_4*X_{1i}*X_{2j}+\beta_5*X_{3k}*X_{2j}+\beta_6*X_{1i}*X_{3k}+\varepsilon_{ijk} \ldots\ldots\ldots(A1.1)$$

where β_0, β_1, β_2 and β_3 are the coefficients; X_1 is the change of the concentration at two different levels of 0.5 M and 2 M respectively; X_2 is co-solvent volume ration at 0% and 40% respectively; X_3 is carrier gas flow rate at 1 L/min and 4 L/min respectively. High and low levels were selected based on experimental conditions required for metal particle preparation. $\beta_4X_1*X_2$, $\beta_5X_3*X_2$ and $\beta_6X_1*X_3$ are the change of Y that resulted from the interaction between two factors. ε is random error corresponding to a normal distribution. i,j and k represent the ith, jth and kth sample of X_1, X_2, and X_3. A full factorial design required 2^3 experiments to include all the possible situations, and each experiment was repeated to ensure the test was reliable. Another three center points were used to check the linearity of the model. For both copper nitrate/water/ET and copper nitrate/water/EG system, copper nitrate concentration, cosolvent (ET/EG) volume ratio and flow rate was designed as three factors. High/low level was 0.5 M/2 M, 0 vol%/40 vol% and 1 L/min/4 L/min separately. These are the most common conditions for the copper particles generation. Each test was repeated, and three center points were added. There are a total of 19 samples for each system.

A2. PH and FTIR properties of precursor solutions

Our precursor solution contained metal nitrate, water and cosolvent, so one question is whether ethanol (ET) or ethylene glycol (EG) could be oxidized by the metal nitrate. If there are interactions between cosolvent and metal nitrate at room temperature, the composition of the precursor will change, potentially leading to formation of more reactive compounds and posing a safety risk. In order to prove that our precursor solution is stable before being sent into the furnace, pH and FTIR spectra of precursor solutions were measured.

1.2 M copper nitrate solutions were used for the ph test. 40 vol% cosolvent was added in the solutions. pH values of the precursor solutions were measured every half hour. Results are shown in Figure A2.1. With the cosolvent of EG, precursor solution had pH around 2.5, and did not change significantly after 1 hour. With the cosolvent of ET, pH was between 2.6 and 2.7. Considering the error from the test, we believe the change of the pH was not significant either. The results indicated pH of solutions with cosolvent of either ET or EG remained stable during our test.

FTIR of the solutions are shown in Figure A2.2. Before the FTIR test, solutions were kept in 20 oC for 12 hours. With either ET or EG, FTIR of precursor solutions had similar shape. A strong absorption from 3000 cm-1 to 4000 cm-1 could be attributed to the stretching of O-H from water and the cosovlent. Peaks from 2800 cm-1 to 3000 cm-1 were from C-H bond. O-N bonds resulted in the absorption from 1200 cm-1 to 1800 cm-1. From 1000 cm-1 to 1200 cm-1, there are two sharp peaks from C-O vibration. FTIR of pure ET, pure EG and copper nitrate aqueous solution are also shown in Figure A2.2.

Results indicated that, when mixed the nitrate and the cosolvent together, there was no peak eliminated or new peak generated. The precursor solutions were still composed of copper nitrate, water and the cosolvent.

According to the pH and FTIR of the solution, it can be concluded that there is no significant reaction between copper nitrate and the cosolvent in 12 hours if the solutions are at room temperature.
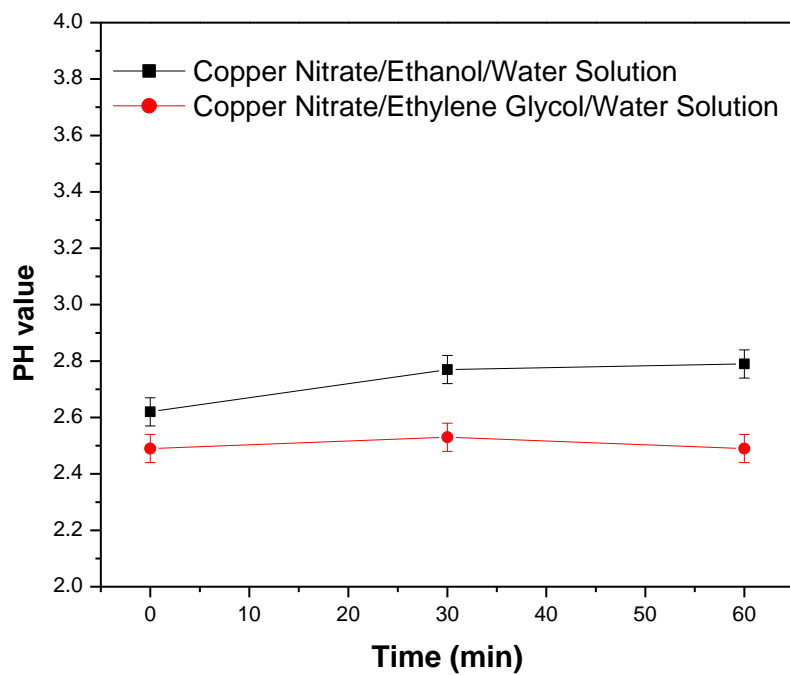
Figure A2.1 pH value of copper nitrate/ethanol/water solution
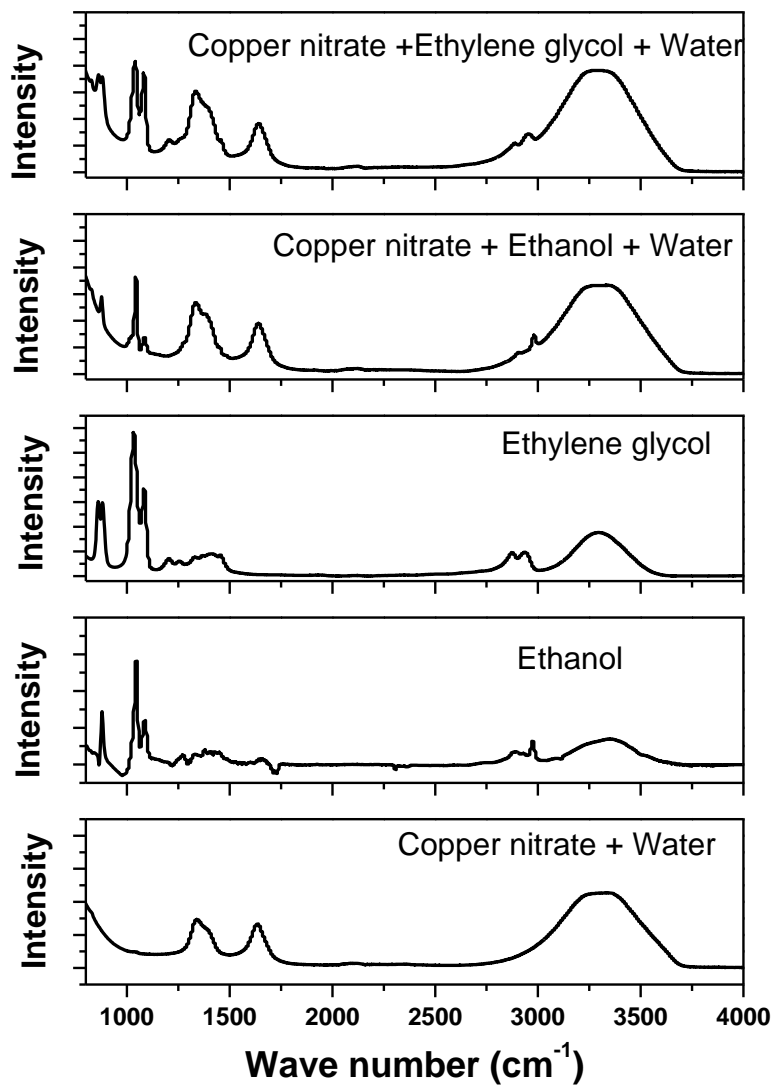
Figure A2.2 FTIR spectra of copper nitrate /water solution, pure ethanol, pure ethylene glycol, nitrate/ethanol /water solution and nitrate/ethylene glycol /water solution

A3. Composition of AgCu particles generated in short residence times

Table A3.1. Composition of samples generated under short residence time conditions at various temperatures. Short residence times were achieved when a single furnace and 10 L/min carrier gas flow rate were used.

Cosolvent	Temperature (°C)	Residence time (s)	Phase abundance (%)					Reaction rate** (mole L^{-1} min^{-1})
			$Cu_2(OH)_3NO_3$	CuO	Cu_2O	Cu	Ag	
ET	400	0.41	66	12	0	1	11*	0.01
ET	500	0.36	63	7	0	0	30	0
ET	550	0.34	49	15	0	0	36	0
ET	600	0.32	38	22	0	0	40	0
ET	650	0.3	32	23	5	0	40	0
ET	700	0.28	0	13	19	20	48	0.71
ET	750	0.27	0	6	19	27	48	1.02
ET	800	0.26	0	0	11	41	48	1.78
ET	875	0.23	0	0	0	51	49	3.13
EG	400	0.41	58	0	0	2	40	0.02
EG	500	0.36	11	0	30	12	47	0.26
EG	550	0.34	0	0	28	22	50	0.60

EG	600	0.32	0	0	20	33	47	1.03
EG	650	0.3	0	0	11	36	53	1.48
EG	700	0.28	0	0	11	34	55	1.57
EG	750	0.27	0	4	11	29	56	1.42
EG	800	0.26	0	9	13	25	53	1.16
EG	875	0.23	0	0	7	38	55	2.28

*At 400 ^{o}C with the cosolvent of ET, samples contained 10 % AgNO$_3$.

** Reaction rate was estimated by the moles of copper generated in unit time from 1 L precursor solution.

References

(NFPA), National Fire Protection Association. 2007. *NFPA 704*: Standard system for the identification of the hazards of materials for emergency response. NFPA.

Ahn KW, Hyun JY, and Kim SG. "Nickel-impregnated mesoporous silica prepared in an aerosol reactor." *Aerosol Science and Technology* 2012; 46(4):419–427.

Anker JN, Behrend CJ, Huang H, and Kopelman R. "Magnetically-modulated optical nanoprobes and systems." *Journal of Magnetism and Magnetic Materials* 2005; 293(1):655–662.

Aoyagi N, Ookawa T, Ueyama R, Ogata N, and Ogihara T. "Preparation of Ag-Pd alloy particles by ultrasonic spray pyrolysis and application to electrode for LTCC." *Electroceramics in Japan VI* 2003; 248:187–190.

Asm. 1992. *ASM* Handbook: Volume 3: Alloy phase diagrams (Asm Handbook). 10th ed. ASM International.

Avvaru B, Patil MN, Gogate PR, and Pandit AB. "Ultrasonic atomization: Effect of liquid phase properties." *Ultrasonics* 2006; 44(2):146–158.

Aymard L, Beaudoin B, Dumont B, and DelahayeVidal A. "Formation mechanism of a crystalline $Ag_{50}Pd_{50}$ solid solution by impact ball-materials interaction." *Journal of Materials Chemistry* 1996; 6(9):1537–1541.

Barreras F, Amaveda H, and Lozano A. "Transient high-frequency ultrasonic water atomization." *Experiments in Fluids* 2002; 33(3):405–413.

Benjamin JS. "Dispersion strengthened super alloys by mechanical alloying." *Metallurgical Transactions* 1970; 1(10):2943–&.

Bhadra TC, and Basu M. "The attenuation of ultrasound in water-alcohol mixtures by the method of streaming." *Ultrasonics* 1980; 18(1):18–22.

Biskos G, Vons V, Yurteri CU, and Schmidt-Ott A. "Generation and sizing of particles for aerosol-based nanotechnology." *Powder and Particle Journal* 2008; 26:13-33.

Boehme T, and Mueller WH. "On the simulation of the spinodal decomposition process and phase growth in a leadfree brazing material." *Computational Materials Science* 2007; 39(1):166–171.

Böker A, He J, Emrick T, and Thomas PR. "Self-assembly of nanoparticles at interfaces." *Soft Matter* 2007; 3(10):1231.

Brusic V, Frankel GS, Roldan J, and Saraf R.. "Corrosion and protection of a conductive silver paste." *Journal of the Electrochemical Society* 1995; 142(8):2591–2594.

Cardenas-Trivino G,]Klabunde KJ, and Dale EB. "Living colloidal palladium in nonaqueous solvents. Formation, stability, and film-forming properties. Clustering of metal atoms in organic media." *Langmuir* 1987; 3(6):986–992.

Casagrande C, Fabre P, Raphael E, and Veyssie M. "Janus beads - Realization and behavior at water oil interfaces." *Europhysics Letters* 1989; 9(3):251–255.

Cayre O, Paunov VN, and Velev OD. "Fabrication of asymmetrically coated colloid particles by microcontact printing techniques." *Journal of Materials Chemistry* 2003; 13(10):2445.

Champion JA, Katare YK, and Mitragotri S. "Making polymeric micro-and nanoparticles of complex shapes." *Proceedings of the National Academy of Sciences* 2007; 104(29):11901.

Champion Y, Langlois C, Guerin S, Lartigue-Korinek S, Langlois P, Hytch MJ. "Plasticity of copper with small grain size." *Materials structure & Micromechanics of fracture IV* 2005; 482:71–76.

Che SL, Takada K, Takashima K, Sakurai O, Shinozaki K, Mizutani N. "Preparation of dense spherical Ni particles and hollow NiO particles by spray pyrolysis." *Journal of Materials Science* 1999; 34(6):1313–1318.

Choa YH, Yang JK, Kim BH, Jeong YK, Lee JS, Nakayama T, Sekino T, Niihara K. "Preparation and characterization of metal/ceramic nanoporous nanocomposite powders." *Journal of Magnetism and Magnetic Materials* 2003; 266(1-2):12–19. Retrieved July 26, 2010.

Chung DDL. "Materials for thermal conduction." *Applied Thermal Engineering* 2001; 21(16):1593–1605.

Cui JQ, and Kretzschmar I. "Surface-anisotropic polystyrene spheres by electroless deposition." *Langmuir* 2006; 22(20):8281–8284.

Deckman HW, and Dunsmuir JH. "Natural lithography." *Applied Physics Letters* 1982; 41(4):377–379.

Degennes PG. "Soft matter." *Reviews of Modern Physics* 1992; 64(3):645–648.

Dobre M., and Bolle L. "Practical design of ultrasonic spray devices: experimental testing of several atomizer geometries." *Experimental Thermal and Fluid Science* 2002; 26(2-4):205–211.

Donnelly TD, Hogan J, Mugler A, Schommer N, Schubmehl M, Bernoff AJ, Forrest B. "An experimental study of micron-scale droplet aerosols produced via ultrasonic atomization." *Physics of Fluids* 2004; 16(8):2843.

Donnelly TD, Hogan J, Mugler A, Schubmehl M, and Schommer N. "Using ultrasonic atomization to produce an aerosol of micron-scale particles." *Review of Scientific Instruments* 2005; 76(11):113301.

Eroglu S, Zhang SC, and Messing GL. "Synthesis of nanocrystalline Ni-Fe alloy powders by spray pyrolysis." *Journal of Materials Research* 1996; 11(9):2131.

Esumi K, Suzuki A, Aihara N, Usui K, and Torigoe K. "Preparation of gold colloids with UV irradiation using dendrimers as stabilizer." *Langmuir* 1998; 14(12):3157–3159.

Field BO, and Hardy CJ. "Inorganic nitrates and nitrato-compounds." *Quarterly Reviews* 1964; 18(4):361–388.

Fievet F, Fievetcincent F, Lagier JP, Dumont B, and Figlarz. "Controlled nucleation and growth of micrometer-size copper particles prepared by the polyol process." *Journal of Materials Chemistry* 1993; 3(6):627–632.

Fievet F, Lagier JP, Blin B, Beaudoin B, and Figlarz M. "Homogeneous and heterogeneous nucleations in the polyol process for the preparation of micron and submicron size metal particles." *Solid State Ionics* 1989; 32-3:198–205.

Firmansyah DA, Kim T, Kim S, Sullivan K, Zachariah MR and Lee D. "Crystalline phase reduction of cuprous oxide (Cu_2O) nanoparticles accompanied by a morphology change during ethanol-assisted spray pyrolysis" *Langmuir* 2009; 25(12):7063–7071.

Fordham S. "On the calculation of surface tension from measurements of pendant drops." *Proceedings of the Royal Society of London Series a-Mathematical and Physical Sciences* 1948; 194(1036):1–16.

Forsman J, Tapper U, Auvinen A, and Jokiniemi J. "Production of cobalt and nickel particles by hydrogen reduction." *Journal of Nanoparticle Research* 2008; 10(5):745–759.

Friedlander SK. 1977. Smoke, dust, and haze: fundamentals of aerosol behavior. Wiley.

Gaceur M, Giraud M, Hemadi M, Nowa S, Menguy N, Quisefit JP, David K, Jahanbin T, Benderbous S, Boissiere M, Ammar S. "Polyol-synthesized $Zn_{0.9}Mn_{0.1}S$ nanoparticles as potential luminescent and magnetic bimodal imaging probes: synthesis, characterization, and toxicity study." *Journal of Nanoparticle Research* 2012 14(7).

Glotzer SC, and Solomon MJ. "Anisotropy of building blocks and their assembly into complex structures." *Nature Materials* 2007; 6(8):557–562.

Goodridge CL, Shi WT, Hentschel HGE, and Lathrop DP. "Viscous effects in droplet-ejecting capillary waves." *Physical Review E* 1997; 56(1):472.

Gratzel M. "Photoelectrochemical cells." *Nature* 2001; 414(6861):338–344.

Gurav A, Kodas T, Pluym T, and Xiong Y. "Aerosol processing of materials." *Aerosol Science and Technology* 1993; 19(4):411–452.

Gurmen S, Ebin B, Stopic S, and Friedrich B. "Nanocrystalline spherical iron-nickel (Fe-Ni) alloy particles prepared by ultrasonic spray pyrolysis and hydrogen reduction (USP-HR)." *Journal of Alloys and Compounds* 2009; 480(2):529–533.

Gurmen S, Guven S, Ebin B, Stopic S, and Friedrich B. "Synthesis of nano-crystalline spherical cobalt-iron (Co-Fe) alloy particles by ultrasonic spray pyrolysis and hydrogen reduction." *Journal of Alloys and Compounds* 2009; 481(1-2):600–604.

Hamai K, Takenaka N, Nanzai B, Okitsu K, Bandow H, Maeda Y. "Influence of adding salt on ultrasonic atomization in an ethanol-water solution." *Ultrasonics Sonochemistry* 2009; 16(1):150–154.

Hao GL, Xu QP, Han FS, Li WD, and Bai SM. "Processing and damping behaviour of porous copper." *Powder Metallurgy* 2009; 52(2):145–150.

Haynes CL, and Duyne RPV. "Nanosphere lithography: A versatile nanofabrication tool for studies of size-dependent vanoparticle optics." *The Journal of Physical Chemistry B* 2001; 105(24):5599–5611.

Himmelhaus M, and Takei H. "Cap-shaped gold nanoparticles for an optical biosensor." *Sensors and Actuators B-Chemical* 2000; 63(1-2):24–30.

Hirai H, Nakao Y, and Toshima N. "Colloidal rhodium in poly(vinylpyrrolidone) as hydrogenation catalyst for internal olefins." *Chemistry Letters* 1978; (5):545–548.

Hong L, Jiang S, and Granick S. "Simple method to produce Janus colloidal particles in large quantity." *Langmuir* 2006; 22(23):9495–9499.

Hosokura T, and Omihachiman JP. "Metal powder, method for producing the same, and conductive paste." 2003. Patent No. 6620219B1

Jackson JG, Fonseca RW, and Holcombe JA. "Mass spectral studies of thermal decomposition of metal nitrates." *Spectrochimica Acta Part B-Atomic Spectroscopy* 1995; 50(12):1449–1457.

Jain S, Skamser DJ, and Kodas TT. "Morphology of single-component particles produced by spray pyrolysis." *Aerosol Science and Technology* 1997; 27(5):575. Retrieved June 3, 2010.

Jang HC, Ju SH, and Kang KC. "Spherical shape Ni-Co alloy powders directly prepared by spray pyrolysis." *Journal of Alloys and Compounds* 2009; 478(1-2):206–209.

Jian NW, Li Z, Fan Y, and Zhao MS. "Synthesis of carbon encapsulated magnetic nanoparticles with giant coercivity by a spray pyrolysis approach." *Journal of Physical Chemistry B* 2007; 111(8):2119–2124.

Ju J, Yamagata Y, Ohmori H, and Higuchi T. "High-frequency surface acoustic wave atomizer." *Sensors and Actuators A: Physical* 2008; 145:437–441.

Ju SH, Jang HC, Kang YC, and Kim DW. "Characteristics of Sn-Ni alloy powders directly prepared by spray pyrolysis." *Journal of Alloys and Compounds* 2009; 478(1-2):177–180.

Jung CH, Lee HG, Kim CJ, and Bhaduri SB. "Synthesis of Cu-Ni alloy powder directly from metal salts solution." *Journal of Nanoparticle Research* 2003; 5(3-4):383–388.

Jung DS, Koo HY, and Kang YC. "Electrical and morphological properties of conducting layers formed from the silver-glass composite conducting powders prepared by spray pyrolysis." *Journal of Colloid and Interface Science* 2010; 343(1):1–6.

Jung KY, Lee JH, Koo HY, Kang YC, and Bark SB. "Preparation of solid nickel nanoparticles by large-scale spray pyrolysis of Ni $(NO_3)_2 \cdot 6H_2O$ precursor: Effect of temperature and nickel acetate on the particle morphology." *Materials Science and Engineering: B* 2007; 137(1-3):10–19.

Kang DJ, Kim SG, and Kim HS. "Morphologies and properties of nickel particles prepared by spray pyrolysis." *Journal of Materials Science* 2004; 39(18):5719–5726.

Kalidindi SB, Sanyal U, and Jagirdar BR. "Chemical synthesis of metal nanoparticles using amine-boranes." *Chemsuschem* 2011; 4(3):317–324.

Kang SK, and Purushothaman S. "Development of conducting adhesive materials for microelectronic applications." *Journal of Electronic Materials* 1999; 28(11):1314–1318.

Kang YC, and Park SB. "Preparation of zinc oxide-dispersed silver particles by spray pyrolysis of colloidal solution." *Materials Letters* 1999; 40(3):129–133. Retrieved June 3, 2010.

Kao ST, and Duh JG. "Effect of Cu concentration on morphology of Sn-Ag-Cu solders by mechanical alloying." *Journal of Electronic Materials* 2004; 33(12):1445–1451.

Kato A, Takayama A, and Morimitsu Y. "Preparation of silver particles by spray pyrolysis technique." *Nippon Kagaku Kaishi* 1985; (12):2342–2344.

Kieda N, and Messing GL. "Preparation of silver particles by spray pyrolysis of silver-diammine complex solutions." *Journal of Materials Research* 1998; 13(6):1660–1665.

Kim CS, Park EK, and Kim SG. "Silica-silver nanostructured spheres prepared by spray pyrolysis of sol containing silver precursor." *Journal of Sol-Gel Science and Technology* 2008; 47(1):7–15.

Kim JH, Babushok VI, Germer TA, Mulholland GW, and Ehrman SH. "Cosolvent-assisted spray pyrolysis for the generation of metal particles." *Journal of Materials Research* 2003; 18(7):1614–1622.

Kim JH, Germer TA, Mulholland GW, Ehrman, SH. "Size-monodisperse metal nanoparticles via hydrogen-free spray pyrolysis." *J. Appl. Phys* 1997; 36:L714.

Kim JY, Rodriguez JA, Hanson JC, Frenkel AI, and Lee PL. "Reduction of CuO and Cu_2O with H-2 : H embedding and kinetic effects in the formation of suboxides." *Journal of The American Chemical Society* 2003; 125(35):10684–10692.

Kim KN, and Kim SG. "Nickel particles prepared from nickel nitrate with and without urea by spray pyrolysis." *Powder Technology* 2004; 145(3):155–162.

Kim SJ, Stach EA, and Handwerker CA. "Fabrication of conductive interconnects by Ag migration in Cu-Ag core-shell nanoparticles." *Applied Physics Letters* 2010; 96(14).

Kimura K, and Bandow S . "The study of metal colloids produced by means of gas evaporation technique. 1. Preparation method and optical properties in ethanol." *Bulletin of The Chemical Society of Japan* 1983; 56(12):3578–3584.

Koch CC, Cavin OB, Mckamey CG, and Scarbrough JO. "Preparation of amorphous Ni60NB40 by mechanical alloying." *Applied Physics Letters* 1983; 43(11):1017–1019.

Koudelka M, Sanchez J, and Augustynski J. "Electrochemical and surface characteristics of the photocatalytic platinum deposits on titania." *The Journal of Physical Chemistry* 1982; 86(22):4277–4280.

Kraeutler B, and Bard AJ. "Heterogeneous photocatalytic preparation of supported catalysts. Photodeposition of platinum on titanium dioxide powder and other substrates." *Journal of the American Chemical Society* 1978; 100(13):4317–4318.

Kurihara LK, Chow GM, and SCHOEN PE. "Nanocrystalline metallic powders and films produced by the polyol method." *Nanostructured Materials* 1995; 5(6):607–613.

Lang RJ. "Ultrasonic atomization of liquids." *The Journal of the Acoustical Society of America* 1962, 34(1):6–8.

Langer R, and Tirrell DA. "Designing materials for biology and medicine." *Nature* 2004; 428(6982):487–492.

Laurell T, Petersson F, and Nilsson A. "Chip integrated strategies for acoustic separation and manipulation of cells and particles." *Chemical Society Reviews* 2007; 36(3):492.

LaVan DA, McGuire T, and Langer R. "Small-scale systems for in vivo drug delivery." *Nature Biotechnology* 2003; 21(10):1184–1191.

Lee JH, Jung KY, and Park SB. "Modification of titania particles by ultrasonic spray pyrolysis of colloid." *Journal of Materials Science* 1999; 34(16):4089–4093.

Lewis LN. "Chemical catalysis by colloids and clusters." *Chemical Reviews* 1993; 93(8):2693–2730.

Liddell CM, Summers CJ, and Gokhale AM. "Stereological estimation of the morphology distribution of ZnS clusters for photonic crystal applications." *Materials characterization* 2003; 50(1):69–79.

Lierke EG. "Techniques and applications of ultrasonic atomisation - 35 years of research and development in retrospect." *Chemie Ingenieur Technik* 1998; 70(7):815–826.

Link S, and El-Sayed MA. "Spectral properties and relaxation dynamics of surface plasmon electronic oscillations in gold and silver nanodots and nanorods." *Journal of Physical Chemistry B* 1999; 103(40):8410–8426.

Liu J, Li X, and Zeng X. "Silver nanoparticles prepared by chemical reduction-protection method, and their application in electrically conductive silver nanopaste." *Journal of Alloys and Compounds* 2010; 494(1-2):84–87.

Lu DD, and Wong CP. "Recent advances in developing high performance isotropic conductive adhesives." *Journal of Adhesion Science and Technology* 2008; 22(8-9):835–851.

Lvov BV, and Novichikhin AV. "Mechanism of thermal decomposition of hydrated copper nitrate in vacuo." *Spectrochimica Acta Part B-Atomic Spectroscopy* 1995; 50(12):1459–1468.

M. Faraday. "On the forms and states assumed by fluids in contact with vibrating elastic surfaces." *Philos. Trans. R. Soc. London* 1831; 121(52):319–340.

Majumdar D, Glicksman HD, and Kodas TT. "Generation and sintering characteristics of silver-copper (II) oxide composite powders made by spray pyrolysis." *Powder Technology* 2000; 110(1-2):76–81.

Majumdar D, Shefelbine TA, Kodas TT, and Glicksman HD. "Copper (I) oxide powder generation by spray pyrolysis." *Journal of Materials Research* 1996; 11(11):2861–2868.

Mancic L, Marinkovic B, Vulic P, and Milosevic O. "Aerosol processing of fine Ag:(Bi,Pb)2223 composite particles." *Physica C: Superconductivity* 2004; 408-410:42–43.

Messing Gl, Zhang Sc, and Jayanthi Gv. "Ceramic powder synthesis by spray-pyrolysis." *Journal of the American Ceramic Society* 1993; 76(11):2707–2726.

Miki H. 1998. "Method for producing copper powder." Patent No. 5741347.

Montgomery DC, and Runger GC. 2006. Applied Statistics and Probability for Engineers, 4th ed. John Wiley & Sons.

Morozov IV, Znamenkov KO, Korenev YM, and Shlyakhtin OA. "Thermal decomposition of $Cu(NO_3)*3H_2O$ at reduced pressures." *Thermochimica Acta* 2003; 403(2):173–179.

Mu J, and Perlmutter DD. "Thermal decomposition of carbonates, carboxylates, and hydroxides." *Thermochimica Acta* 1981; 49(2-3):207–218.

Murty BS. "Mechanical alloying—a novel synthesis route for amorphous phases." *Bulletin of Materials Science* 1993; 16(1):1–17.

Murty BS, and Ranganathan S. "Novel materials synthesis by mechanical alloying/milling." *International materials reviews* 1998; 43(3):101–141.

Nagashima K, Iwaida T, Sasaki H, Katatae Y, and Kato A. "Preparation of fine, spherical copper particles by spray pyrolysis technique." *Nippon Kagaku Kaishi* 1990; (1):17–24.

Nagashima K, Morimitsu Y, and Kato A. "Preparation of fine metal particles from aqueous solutions of metal nitrate by chemical flame method." *Nippon Kagaku Kaishi 1*987; (12):2293–2300.

Nagashima K, Wada M, and Kato A. "Preparation of fine Ni particles by the spray pyrolysis technique and their film forming properties in the thick film method." *Journal of Materials Research* 1990; 5(12):2828–2834.

Nagata Y, Mizukoshi Y, Okitsu K, and Maeda Y. "Sonochemical formation of gold particles in aqueous solution." *Radiation Research* 1996, 146(3):333–338.

Nagesh VK., and Pask JA. "Wetting of nickel by silver." *Journal of Materials Science* 1983; 18(9):2665–2670.

Nisisako T, Torii T, and Higuchi T. "Novel microreactors for functional polymer beads." *Chemical Engineering Journal* 2004; 101(1-3):23–29.

Nisisako T, Torii T, Takahashi T, and Takizawa Y. "Synthesis of monodisperse bicolored Janus particles with electrical anisotropy using a microfluidic co-flow system." *Advanced Materials* 2006; 18(9):1152–1156.

Ohmi T. "ULSI reliability through ultraclean processing." *Proceedings of the IEEE* 2002; 81(5):716–729.

Okamoto H. 2000. Desk handbook: phase diagrams for binary alloys. ASM International.

Okitsu K, Mizukoshi Y, Bandow H, Maeda Y, Yamamoto T, Nagata Y. "Formation of noble metal particles by ultrasonic irradiation." *Ultrasonics Sonochemistry* 1996; 3(3):S249–S251.

Okitsu K, Bandow H, Maeda Y, and Nagata Y. "Sonochemical preparation of ultrafine palladium particles." *Chemistry of Materials* 1996; 8(2):315–317.

Okuyama K, and Lenggoro IW. "Preparation of nanoparticles via spray route." *Chemical Engineering Science* 2003, 58(3-6):537–547.

Ozin GA, Manners I, Fournier-Bidoz S, and Arsenault A. "Dream nanomachines." *Advanced Materials* 2005; 17(24):3011–3018.

Pabi SK, Joardar J, and Murty BS. "Formation of nanocrystalline phases in the Cu-Zn system during mechanical alloying." *Journal of Materials Science* 1996, 31(12):3207–3211.

Pabi SK, and Murty BS. "Mechanism of mechanical alloying in Ni-Al and Cu-Zn systems." *Materials Science and Engineering A- Structural Materials properties* 1996a; 214(1-2):146–152.

Pabi SK, Joardar J, and Murty BS. "Synthesis of nanocrystalline alloys and intermetallics by mechanical alloying." *Bulletin of Materials Science* 1996b; 19(6):939–956.

Park, SH, Kim CH, Kang YC, and Kim YH. "Control of size and morphology in Ni particles prepared by spray pyrolysis." *Journal of Materials Science Letters* 2003; 22(21):1537–1541.

Park SH, and Lee CH. "Layered copper hydroxide *n*-alkylsulfonate salts: synthesis, characterization, and magnetic behaviors in relation to the basal spacing." *The Journal of Physical Chemistry B* 2005; 109(3):1118–1124.

Paunov VN, and Cayre OJ. "Supraparticles and 'Janus' particles fabricated by replication of particle monolayers at liquid surfaces using a gel trapping technique." *Advanced Materials* 2004; 16(9-10):788–791.

Pawar AB, and Kretzschmar I. "Fabrication, assembly, and application of patchy particles." *Macromolecular Rapid Communications* 2010; 31(2):150–168.

Peskin RL, and Raco RJ. "Ultrasonic atomization of liquids." *The Journal of the Acoustical Society of America* 1963; 35(9):1378–1381.

Petit L, Manaud JP, Mingotaud C, Ravaine S, and Duguet E. "Sub-micrometer silica spheres dissym-metrically decorated with gold nanoclusters." *Materials Letters* 2001; 51(6):478–484.

Pluym TC, Powell QH, Gurav AS, Ward TL, Kodas TT, Wang LM, Glicksman HD. "Solid silver particle production by spray pyrolysis." *Journal of Aerosol Science* 1993; 24(3):383–392.

Pluym TC, Lyons SW, Powell QH, Gurav AS, Ward TL, Kodas TT, Wang LM, Glicksman HD. "Palladium and palladium oxide particle production by spray pyrolysis." *Materials Research Bulletin* 1993; 28(4):369–376.

Pluym TC, Kodas TT, Wang LM, Glicksman HD. "Silver-Palladium alloy particle production by spray-pyrolysis." *Journal of Materials Research* 1995; 10(7):1661–1673.

Priego CF, and Castro MDL. "Ultrasound in analytical chemistry." *Analytical and Bioanalytical Chemistry* 2006; 387(1):249–257.

Pruppacher HR, and Klett JD. 1996. Microphysics of Clouds and Precipitation. Springer.

Rajan R, and Pandit AB. "Correlations to predict droplet size in ultrasonic atomisation." *Ultrasonics* 2001; 39(4):235–255.

Roh KH, Martin DC, and Lahann J. "Triphasic nanocolloids." *Journal of the American Chemical Society* 2006; 128(21):6796–6797.

Roh KH, Martin DC, and Lahann J. "Biphasic Janus particles with nanoscale anisotropy." *Nature Materials* 2005; 4(10):759–763.

Rudin T, Wegner K, and Pratsinis SE. 2011. "Uniform nanoparticles by flame-assisted spray pyrolysis (FASP) of low cost precursors." *Journal of Nanoparticle Research* 2011; 13(7):2715–2725.

Ryu SK, Lee WK, and Park SJ. "Thermal decomposition of hydrated copper nitrate [$Cu(NO_3)_2$ $3H_2O$] on activated carbon fibers." *Carbon Science 2004;* 5(4):180–185.

Satoh N, and Kimura K. "Metal colloids produced by means of gas evaporation technique. 5. Colloidal dispersion of Au fine particles to hexane, poor dispersion medium for metal sol." *Bulletin of the Chemical Society of Japn* 1989; 62(6):1758–1763.

Sheppard L. "Progress continues in capacitor technology." *American Ceramic Society Bulletin* 1993; 72(3):44–&.

Shi X, Wang S, Duan X, and Zhang Q. "Synthesis of nano Ag powder by template and spray pyrolysis technology." *Materials Chemistry and Physics* 2008; 112(3):1110–1113.

Silvert PY, Vijayakrishnan V, Vibert P, HerreraUrbina R, and Elhsissen KT. "Synthesis and characterization of nanoscale Ag-Pd alloy particles." *Nanostructured Materials* 1996; 7(6):611–618.

Songping W, and Shuyuan M. "Preparation of micron size copper powder with chemical reduction method." *Materials Letters* 2006; 60(20):2438–2442.

Sonvico F, Dubernet C, Colombo P, and Couvreur P. "Metallic colloid nanotechnology, applications in diagnosis and therapeutics." *Current Pharmaceutical design* 2005; 11(16):2091–2105.

Speight J. 2004. Lange's Handbook of Chemistry, 70th Anniversary Edition. 16th ed. McGraw-Hill Professional.

Stopic S, Ilic I, and Uskokovic DP. "Preparation of nickel submicron powder by ultrasonic spray pyrolysis." *International Journal of Powder Metallurgy* 1996; 32(1):59–65.

Stopic S, Nedeljkovic J, Rakocevic Z, and Uskokovic D. "Influence of additives on the properties of spherical nickel particules prepared by ultrasonic spray pyrolysis." *Journal of Materials Research(USA)* 1999; 14(7):3059–3065.

Strutt JW. 2009. "On the pressure developed in a liquid during the collapse of a spherical cavity." *Scientific Papers, Cambridge Library Collection - Mathematics* 2009; 6:1911–1919.

Suh WH, and Suslick KS. "Magnetic and porous nanospheres from ultrasonic spray pyrolysis." *Journal of the American Chemical Society* 2005; 127(34):12007–12010.

Sundararajan S, Lammert PE, Zudans AW, Crespi VH, and Sen A. "Catalytic motors for transport of colloidal cargo." *Nano Letters* 2008; 8(5):1271–1276.

Takei H., and Shimizu N. "Gradient sensitive microscopic probes prepared by gold evaporation and chemisorption on latex spheres." *Langmuir* 1997; 13(7):1865–1868.

Tani H, and Ogata N. 1998. "Production of copper powder." Patent No. 5850047.

Taniguchi I. "Physical and electrochemical pProperties of spherical nanostructured LiCr$_x$Mn$_{2-x}$O$_4$ particles synthesized by ultrasonic spray pyrolysis." *Industrial & Engineering Chemistry Research* 2005; 44(17):6560–6565.

Taylor TJ, Dollimore D, and Gamlen GA. "Deaquation and denitration studies on copper nitrate." *Thermochimica Acta* 1986; 103(2):333–340.

Tao Y, Xia YP, Wang H, Gong FH, Wu HP, Tao GL. "Novel isotropical conductive adhesives for electronic packaging application." *IEEE Transactions on Advanced Packaging* 2009; 32(3):589–592.

Torigoe K, and Esumi K. "Preparation of bimetallic silver-palladium colloids from silver (I) bis (oxalato) palladate (II)." *Langmuir* 1993; 9(7):1664–1667.

Tsai KL, and Dye JL. "Nanoscale metal particles by homogeneous reduction with alkalides or electrides." *Journal of the American Chemical Society* 1991; 113(5):1650–1652.

Tsai SC, Cheng CH, Wang N, Song YL, Lee CT, Tsai CS. "Silicon-based megahertz ultrasonic nozzles for production of monodisperse micrometer-sized droplets." *IEEE Transactions on Ultrasonics, Ferroelectrics and Frequency Control* 2009; 56(9):1968–1979.

Usmani OS, "Regional lung deposition and bronchodilator response as a function of 2-agonist particle size." *American Journal of Respiratory and Critical Care Medicine* 2005; 172(12):1497–1504.

Walther A, and Müller AHE. "Janus particles." *Soft Matter* 2008; 4(4):663.

Wang WN, Purwanto A, Lenggoro IW, Okuyama K, Chang H, Jang HD. "Investigation on the correlations between droplet and particle size distribution in ultrasonic spray pyrolysis." *Industrial & Engineering Chemistry Research* 2008, 47(5):1650–1659.

Watari F, Yokoyama A, Omori M, Hirai T , Kondo H, Uo M, Kawasaki T. "Biocompatibility of materials and development to functionally graded implant for bio-medical application." *Composites Science and Technology* 2004; 64(6):893–908.

Widiyastuti W, Wang WN, Lenggoro IW, Iskandar F, and Okuyama K. "Simulation and experimental study of spray pyrolysis of polydispersed droplets." *Journal of Materials Research* 2007; 22(7):1888–1898.

Wu HP, Wu XJ, Ge MY, Zhang GQ. "Properties investigation on isotropical conductive adhesives filled with silver coated carbon nanotubes." *Composites Science and Technology* 2007; 67(6):1182–1186.

Wu HP, Wu XJ, Ge MY, Zhang GQ. "Effect analysis of filler sizes on percolation threshold of isotropical conductive adhesives." *Composites science and technology* 2007; 67(6):1116–1120.

Xia B, Lenggoro IW, and Okuyama K. "The roles of ammonia and ammonium bicarbonate in the preparation of nickel particles from nickel chloride." *J. Mater. Res* 2000; 15(10):2158.

Xia B, Lenggoro IW, and Okuyama K. "Preparation of Ni particles by ultrasonic spray pyrolysis of $NiCl_2 \cdot 6H_2O$ precursor containing ammonia." *Journal of materials science* 2001; 36(7):1701–1705.

Yang SY, Kim K, and Kim SG. "Reductive crystallization of each metal in composite particles spray-pyrolyzed from silver/nickel mixed nitrates." *Korean Journal of Chemical Engineering* 2008; 25(2):359–363.

Yim MJ, Li Y, Moon KS, and Wong CP. "High performance anisotropic conductive adhesives using copper particles with an anti-oxidant coating layer." *Journal of Electronic Packaging* 2010; 132(1):011007.

Yonezawa Y, Sato T, Kuroda S, and Kuge K. "Photochemical formation of colloidal silver peptizing action of acetone ketyl radical." *Journal of the Chemical Society-Faraday Transactions* 1991; 87(12):1905–1910.

Yu Y, Boguslavskii, and Eknadiosyants, "Physical mechanism of the acoustic atomization of a liquid." *Soviet Physics-Acoustics* 1969; 15(1):14–21.

Yule AJ, and Suleimani YA. "On droplet formation from capillary waves on a vibrating surface." *Proceedings of the Royal Society A: Mathematical, Physical and Engineering Sciences* 2000; 456(1997):1069–1085.

Zhang, and Glotzer SC. "Self-Assembly of patchy particles." *Nano Letters* 2004; 4(8):1407–1413.

Zhang J, Wang X, Wu D, Liu L, and Zhao H. "Surface-Initiated free radical polymerization at the liquid-liquid interface." *Langmuir* 2009; 25(11):6431–6437.

Zhao YP, Ye DX, Wang GC, and Lu TM. "Novel nano-column and nano-flower arrays by glancing angle deposition." *Nano Letters* 2002; 2(4):351–354.

Zhong K, Peabodya G, Glicksmana H, and Ehrman S. "A spray pyrolysis approach for the generation of patchy particles." Aerosol Science and Technology, accepted in Oct 2012.

Zhong K, Peabodya G, Glicksmana H, and Ehrman S. "Particle generation by cosolvent spray pyrolysis: Effects of ethanol and ethylene glycol." *Journal of Materials Research* 2012; 27(19):2540-2550.

Zhu YJ, Qian YT , Zhang MW, Li YJ, Chen ZY, Zhou G. "Preparation and characterization of ultrafine powders of the yAg-Cu alloys by [gamma]-radiation method." *Journal of Alloys and Compounds* 1995; 221(1-2):L4–L5.